

STATUS OF THESIS

Title of thesis

Tribological Studies of Brake Pad Materials: Effect of Contact Pressure, Sliding Speed, and Relative Humidity

I

ABDUL MUNIR HIDAYAT SYAH LUBIS

hereby allow my thesis to be placed at the Information Resources Center (IRC) of Universiti Teknologi PETRONAS (UTP) with the following conditions:

1. The thesis becomes the properties of UTP.
2. The IRC of UTP may take copies of the thesis for academic purposes only.
3. The thesis is classified as

Confidential

Non-Confidential

If this thesis is confidential, please state the reason:

The contents of this thesis will remain confidential for ____ - ____ years

Remarks for disclosure:

Endorsed by:

Signature of Author

Permanent address:
Kompleks Ira Hampanan Permai
No D-15, Hampanan Perak
Sumatera Utara – Indonesia

Date : _____

Signature of Supervisor

Name of Supervisor:
A. P. Dr. Mustafar Sudin

Date : _____

UNIVERSITI TEKNOLOGI PETRONAS

Approval by Supervisor (s)

The undersign certify that they have read, and recommended to The Postgraduate Studies Programme for acceptance, a thesis entitle “**Tribological Studies of Brake Pad Materials: Effect of Contact Pressure, Sliding Speed and Relative Humidity**” submitted by **Abdul Munir Hidayat Syah Lubis** for the fulfillment of the requirements for the degree of Master of Science in Mechanical Engineering.

Signature : _____

Supervisor : A. P. Dr. Mustafar Sudin

Date : _____

UNIVERSITI TEKNOLOGI PETRONAS

Tribological Studies of Brake Pad Materials: Effect of Contact Pressure, Sliding
Speed, and Relative Humidity

By

Abdul Munir Hidayat Syah Lubis

A THESIS

SUBMITTED TO THE POSTGRADUATE STUDIES PROGRAMME AS A
REQUIREMENT FOR THE DEGREE OF MASTER OF SCIENCE IN
MECHANICAL ENGINEERING

BANDAR SERI ISKANDAR

PERAK

2009

I hereby declare that the thesis is based on my original work except for quotations and citations which have been duly acknowledge. I also declare that it has not been previously or concurrently submitted for any degree at UTP or other institutions.

Signature : _____

Name : Abdul Munir Hidayat Syah Lubis

Date : _____

ACKNOWLEDGEMENTS

First and foremost, I would like to give my sincere thanks to Allah S.W.T, the almighty god, the source of my life and hope for giving me the strength and wisdom to complete this thesis.

I am most grateful to my supervisor Assoc. Prof. Dr. Mustafar Sudin for giving me opportunity and guidance to accomplish my master degree. His patience and encouragement has steered me to the right direction for many times.

I would like to express my appreciation to AMREC-SIRIM and all people involved in IRPA Project No. 03-01-01-0056PR0066/04. I also would like to thank En. Muhd Anuar Muin, En. Faisal Ismail, En. Shairul, En. Zamil, En. Jani and En. Irwan Othman for their assistance and exceptional cooperation during the laboratory works together with other Mechanical Engineering Department staffs headed by Dr. Ahmad Majdi Abdul Rani.

Special thanks to postgraduate office staffs, Pn. Norma, Pn. Haslina, Pn. Kamaliah, and En. Fadhil for their assistance during my study. My warmest thank to my postgraduate friends for their encouragement and friendship.

At last and most importantly, I would like to thank my wife and family for their love, open mindedness and endless support which always being great strength in my life.

ABSTRACT

A study on the friction and wear properties of brake pad materials under nominal contact pressure, sliding speed and relative humidity was carried out in order to understand the phenomena related to friction and wear processes at the contact surface of brake pad. Three LRT brake pads were employed and their compositions were examined using three x-ray techniques; (i) energy dispersive x-ray (EDX), (ii) x-ray fluorescence (XRF) and (iii) x-ray diffraction (XRD). The friction and wear studies were carried out using a three pins-on-disc apparatus over wide ranges of contact pressure, sliding speed and relative humidity. The worn surface morphology was examined by electron scanning microscopy and x-ray analysis. The results of friction curve analysis shows that friction took place by several stages and form six friction curve shapes, where each curve was influenced by the test parameters. The test parameters were also found influencing the duration of the friction stage. This phenomenon is affected by composition and thermal degradation of the samples. The appearance of friction curve shape also considered to be related to formation and destruction of friction layer process on the contact surface. X-Ray analysis of the friction layer at the mating surface indicated that the friction layer mostly consist of iron oxides. Wear of the sample show increasing wear with contact pressure and sliding speed. This factor is concluded due to increasing of plastic deformation, frictional heating and fatigue effect. Only wear of Pad-3 was found increase with relative humidity. This difference is considered affected by hardness, porosity and thermal degradation of the sample. Friction curve analysis and micrograph of wear debris indicated that wear process of the sample was taken place by three modes: (i) surface fracture, (ii) abrasion by wear debris and hard particles, and (iii) material transfer. The micrograph of the worn surface show that wear of the sample was taken place by combination of four mechanisms: (i) adhesion, (ii) abrasion, (iii) fatigue, and (iv) delamination

Key words: Brake Pad, coefficient of friction, wear, contact pressure, sliding speed, humidity, pin-on disc.

ABSTRAK

Satu kajian sifat geseran dan haus pada bahan pad brek di bawah tekanan sentuh namaan, kelajuan gelangsar dan kelembapan nisbi telah dijalankan untuk memahami fenomena berkaitan proses geseran dan haus pada permukaan sentuh pad brek. Tiga pad brek untuk LRT telah digunakan dan komposisi mereka telah dikaji menggunakan tiga teknik sinar-X; (i) sinar-X tenaga terserak (EDX), (ii) pendarfluor sinar-X (XRF) dan (iii) pembelauan sinar-X (XRD). Kajian geseran dan haus telah dijalankan menggunakan radas tiga pin-atas-cakera dalam pelbagai julat tekanan sentuh, kelajuan gelangsar dan kelembapan nisbi. Morfologi permukaan terhakis telah dikaji dengan menggunakan kemikroskopan elektron imbasan (KEI) dan analisis sinar-X. Keputusan dari analisis garis lengkungan geseran menunjukkan geseran berlaku melalui beberapa tahap dan membentuk enam bentuk garis lengkungan, yang mana setiap garis lengkungan dipengaruhi oleh parameter ujian. Parameter ujian juga dijumpai mempengaruhi masa tiap tahapan geseran. Fenomena ini dijejaskan oleh kandungan dan pudar haba dari sampel. Rupa bentuk garis lengkungan juga dianggap berkait rapat dengan proses pembentukan dan pemusnahan lapisan geseran di permukaan sentuh. Analisis sinar-X dari lapisan geseran pada kedua-dua pasangan permukaan menunjukkan lapisan geseran kebanyakannya terdiri dari oksida besi. Haus pada sampel menunjukkan peningkatan haus dengan tekanan sentuh dan kelajuan gelangsar. Faktor ini disimpulkan kerana peningkatan ubahbentuk plastik, pemanasan geseran, dan pengaruh lesu. Hanya haus Pad-3 bertambah dengan kelembapan nisbi. Perbezaan ini dipertimbangkan terjejas oleh kerana kekerasan, keporosan, dan pudar haba sampel. Analisis garis lengkungan geseran dan mikrograf serpihan haus menunjukkan bahawa proses haus sampel berlaku atas tiga cara: (i) retak permukaan, (ii) lelasan serpihan haus dan partikel haus, dan (iii) pemindahan bahan. Mikrograf permukaan terhakis menunjukkan bahawa haus sampel terjadi dengan penggabungan empat mekanisme: (i) rekatan, (ii) lelasan, (iii) lesu, dan (iv) nyah lapisan.

Kata kunci: Pad brek, geseran, haus, tekanan sentuh, kelajuan gelongsor, kelembapan, pin-atas cakera.

Dedication

For My Passed Mom and Dad

TABLE OF CONTENTS

Title Page	i
Declaration	ii
Acknowledgments	iii
Abstract	iv
Table of Contents	vii
List of Tables	xi
List of Figures	xii
CHAPTER ONE: INTRODUCTION	
1.1. Background of Study	1
1.2. Problem Statement	2
1.3. Objectives and Scope of Study	3
1.4. Thesis Overview	4
CHAPTER TWO: THEORY AND LITERATURE REVIEW	
2.1. Introduction to Friction and Wear	5
2.2. Brake System	10
2.2.1. Disc Brakes	11
2.2.2. Drum Brakes	11
2.3. Brake Pad Materials	13
2.3.1. Organic Friction Material	15
2.3.2. Metallic Brake Friction Material	16
2.3.3. Carbon-Based Brake Friction Material	17
2.4. Ingredient Functionality	17
2.5. Friction and wear of Brake Pad Material	19
2.6. Wear mechanism in the Brake Pad Material	24
2.6.1. Adhesive Wear	25
2.6.2. Abrasive Wear	27
2.6.3. Thermal Wear	29
2.6.4. Macroshear	30
2.6.5. Fatigue Wear	30

2.7. Effect of load and Speed to Friction and Wear of Brake Pad Material	31
2.8. Effect of Humidity to Friction and Wear of Brake Pad Material	36

CHAPTER THREE: EXPERIMENTAL DESIGN

3.1. Introduction	38
3.2. Determination of Material Composition	38
3.2.1. Scanning Electron Microscope-Energy Dispersive X-Ray (SEM_EDX)	39
3.2.2. X-Ray Fluorescence (XRF)	40
3.2.3. X-Ray Diffraction (XRD)	41
3.2.4. Thermogravimetric Analysis	42
3.3. Tribological Test	42
3.3.1. Equipment	42
3.3.2. Sample Material	45
3.3.3. Experimental Procedure	45
3.3.4. Calibration	47
3.4. Surface Characterization	44
3.4.1. Surface Profile	44
3.4.2. Surface Morphology	44

CHAPTER FOUR: RESULTS AND DISCUSSION

4.1. Material Characterization	50
4.1.1. EDX Analysis	50
4.1.2. XRF Analysis	56
4.1.3. XRD Analysis	57
4.1.4. Thermogravimetric/Derivative Thermogravimetric (TG/DTG) Analysis	61
4.2. Effect of Test Parameters to Coefficient of Friction	63
4.2.1. Effect of Contact Pressure to Coefficient of Friction	64
4.2.2. Effect of Sliding Speed to Coefficient of Friction	74
4.2.3. Effect of Relative Humidity to Coefficient of Friction	78

4.3. Effect of Test Parameters to Wear	85
4.3.1. Effect of Contact Pressure to Wear	85
4.3.2. Effect of Sliding Speed to Wear	86
4.3.3. Effect of Relative Humidity to Wear	88
4.4. Morphology of Worn Surface	89
4.5. Generation of Friction Layer	105
CHAPTER FIVE: CONCLUSIONS	110
REFERENCES	113
APPENDIX A: EXPERIMENTAL FLOW CHART	122
APPENDIX B: ASTM G-99	123
APPENDIX C: PHYSICAL AND MECHANICAL PROPERTIES OF THE SAMPLES	127
APPENDIX D: MICROSTRUCTURE OF GRAY CAST IRON PIN	128
APPENDIX E: ELEMENTAL COMPOSITIONS OF THE SAMPLES DETERMINED BY EDX TECHNIQUE	129
APPENDIX F: TGA RESULT OF THE SAMPLES, CONTINUED TO APPENDIX G	130
APPENDIX G: TGA RESULT OF THE SAMPLES, CONTINUED TO APPENDIX H	131
APPENDIX H: TGA RESULT OF THE SAMPLES, CONTINUED FROM APPENDIX G	132
APPENDIX I: SUMMARY OF SAMPLE ELEMENTAL COMPOSITIONS DETECTED BY EDX/XRF/XRD TECHNIQUE	133
APPENDIX J: INITIAL SURFACE PROFILES OF THE SAMPLES, CONTINUED TO APPENDIX K	134

APPENDIX K: INITIAL SURFACE PROFILES OF THE SAMPLES, CONTINUED TO APPENDIX L	135
APPENDIX L: INITIAL SURFACE PROFILES OF THE SAMPLES, CONTINUED FROM APPENDIX K	136
APPENDIX M: SURFACE ROUGHNESS OF THE SAMPLES BEFORE AND AFTER TEST	137
APPENDIX N: ELEMENTAL COMPOSITIONS EDX ANALYSIS OF THE GRAY CAST IRON PIN BEFORE AND AFTER TEST	138

LIST OF TABLES

Table No.		Page
2.1.	Factors influencing friction behavior	9
2.2.	Brake friction ingredient function	17
4.1	Pad-1 SEM-EDX analysis result	51
4.2	Pad-2 SEM-EDX analysis results	53
4.3	Pad-3 SEM-EDX analysis results	55
4.4	Oxide elements in the sample formulation by XRF analysis	57
4.5	Compounds in the samples detected by XRD technique	61
4.6	Organic and inorganic contents	62
4.7	Elemental composition after test	72
4.8	EDX analysis of Pad-1 at different experimental humidity	82
4.9	EDX analysis of Pad-2 at different experimental humidity	83
4.10	EDX analysis of Pad-3 at different experimental humidity	84
4.11	Initial elements and EDX spectra of gray cast iron pin	107
4.12	Elements and EDX spectra of gray cast iron pin after sliding with Pad-1	108
4.13	Elements and EDX spectra of gray cast iron pin after sliding with Pad-2	108
4.14	Elements and EDX spectra of gray cast iron pin after sliding with Pad-3	109

LIST OF FIGURES

Figure No.		Page
2.1	Illustration of friction, (a) two body slid against another, and (b) two body rolled against another	6
2.2	Typical friction force curve	6
2.3	Parameters influence friction and wear process	8
2.4	Brake system component	11
2.5	Disc brake (a) Automotive disc brake, (b) PUTRA LRT disc brake	12
2.6	Drum brake (a) simplex drum brakes, (b) Duplex drum brakes, and (c) Duo servo drum brakes	12
2.7	Schematic illustration of friction layer of brake pad	21
2.8	Formation of contact plateau on the surface of an organic brake pad	21
2.9	Brake pad structure	22
2.10	(a) – (f) Growth process of contact patches, (g) – (i) Destruction	23
2.11	Schematic diagram of adhesive transfer process (a) flake-like wear particle (b) wedge-like wear particle	26
2.12	Micrographs of adhesive wear	27
2.13	SEM micrograph of the experimental investigation to (a) cutting mode, (b) wedge-forming mode, and (c) ploughing mode during abrasive wear	28
2.14	Thermogravimetric (TG)/Derivative thermogravimetric (DTG) curve showing thermal decomposition of organic material/resin	29
2.15	Brake pad material wear as function of temperature	29
2.16	Micrograph of macroshear	30
2.17	Micrograph of fatigue wear	31
2.18	Effects of load and speed to coefficient of friction of brake pad material	32
2.19	Variation of coefficient of friction at different applied force and sliding speed	33
2.20	Changes of coefficient of friction as function of speed; (a) NAO, (b) Low-steel friction material	34
2.21	Effects of load and speed to wear of brake pad material	35
2.22	Effect of humidity to friction of brake pad material	37

3.1	SEM-EDX Machine	39
3.2	S4 Pioneer XRF Machine	40
3.3	XRD Machine	41
3.4	Multi-specimen wear tester	43
3.5	Three pins-on-disc test configuration used in this research work	43
3.6	Humidity controller	44
3.7	Sample materials	45
3.8	Surface Profilometer	48
4.1	Surface topography and elemental mapping of Pad-1	52
4.2	Surface topography and elemental mapping of Pad-2	54
4.3	Surface topography and elemental mapping of Pad-3	55
4.4	Figure 4.4 XRD Diffractogram of Pad-1	58
4.5	Figure 4.5 XRD Diffractogram of Pad-2	59
4.6	Figure 4.6 XRD Diffractogram of Pad-3	60
4.7	Friction variation level interpretations; (a) tendencies for pull-out or sudden surface fracture, and (b) tendencies for transfer or seizure	64
4.8	Effect of contact pressure to friction characteristic of Pad-1	65
4.9	Friction curve of Pad-1, (a) contact pressure of 1 MPa, (b) contact pressure of 1.5 MPa – 3 MPa	65
4.10	Effect of contact pressure to friction characteristic of Pad-2	66
4.11	Friction curve of Pad-2, (a) contact pressure of 1 MPa, (b) contact pressure of 1.5 MPa and 2.5 MPa, (c) contact pressure of, 2 MPa, and 3 MPa	67
4.12	Effect of contact pressure to friction characteristic of Pad-3	68
4.13	Friction curve of Pad-3, (a) contact pressure of 1 MPa and 3 MPa, (b) contact pressure of 1.5 MPa, (c) contact pressure of 2 MPa and 2.5 MPa	68
4.14	SEM micrograph of friction layer form on the contact surface	70
4.15	EDX analysis after test; (a) Pad-1, (b) Pad-2, (c) Pad-3	70
4.16	SEM-EDX analyses of hard thin layer and compacted debris	71
4.17	SEM micrograph featuring typical well developed friction layer (Pad-3, 2 MPa, 600 rpm)	74
4.18	Debris layer feature on the contact surface (Pad-2, 2.5 MPa, 600 rpm)	74

4.19	SEM micrograph show friction layer consist of patch covered by another patch (Pad-1, 3 MPa, 600 rpm)	74
4.20	Effect of sliding speed to friction characteristic of Pad-1	75
4.21	Effect of sliding speed to friction characteristic of Pad-2	76
4.22	Effect of sliding speed to friction characteristic of Pad-3	76
4.23	SEM micrograph of plateau formed on contact surface at high sliding speed (1500 rpm, 1 MPa); (a) Pad-1, and (b) Pad-3	77
4.24	Skecth of schallamach waves during sliding	78
4.25	Effect of relative humidity to COF of Pad-1	79
4.26	Effect of relative humidity to COF of Pad-2	79
4.27	Effect of relative humidity to COF of Pad-3	80
4.28	SEM micrograph of Pad-1 surface rubbing at different RH; (a) low RH, (b) medium RH, and (c) high RH	81
4.29	SEM micrograph of Pad-2 surface rubbing at different RH; (a) low RH, (b) medium RH, and (c) high RH	83
4.30	SEM micrograph of Pad-3 surface rubbing at different RH; (a) low RH, (b) medium RH, and (c) high RH	84
4.31	Effects of contact pressure to wear	85
4.32	SEM micrograph of several types of wear debris collected from samples, (a) fiber pulled out type, (b) flake debris type, (c) flake debris type with bigger size, (d) spall debris type	87
4.33	Effects of sliding speed to wear	87
4.34	Effect of relative humidity to wear	89
4.35	Adhesive wear feature on Pad-1 at different contact pressure and sliding speed; (a) 1 MPa, (b) 1.5 MPa, (c) 2 MPa, (d) 2.5 MPa, (e) 3 MPa	90
4.36	Adhesive wear feature on Pad-1 at different sliding speed; (a) 300 rpm, (b) 600 rpm, (c) 900 rpm, (d) 1200 rpm, (e) 1500 rpm	91
4.37	Adhesive wear feature on Pad-2 at different contact pressure (a) 1 MPa, (b) 1.5 MPa, (c) 2 MPa, (d) 2.5 MPa, (e) 3 MPa	92
4.38	Adhesive wear feature on Pad-2 at different sliding speed; (a) 300 rpm, (b) 600 rpm, (c) 900 rpm, (d) 1200 rpm, (e) 1500 rpm	93
4.39	Adhesive wear feature on Pad-3 at different contact pressure (a) 1 MPa,	94

	(b) 1.5 MPa, (c) 2 MPa, (d) 2.5 MPa, (e) 3 MPa	
4.40	Adhesive wear feature on Pad-3 at different sliding speed; (a) 300 rpm, (b) 600 rpm, (c) 900 rpm, (d) 1200 rpm, (e) 1500 rpm	95
4.41	Delamination wear feature on Pad-1; (a) 2 MPa, (b) 2.5 MPa, and (c) 3 MPa	96
4.42	Delamination wear feature on Pad-2 at 2 MPa	97
4.43	Delamination wear feature on Pad-3 at different contact pressure; (a) 2.5 MPa, (b) 3 MPa	97
4.44	Abrasive wear feature on Pad-1 at different contact pressure and (a) 1 MPa, (b) 3 MPa	97
4.45	Abrasive wear feature on Pad-1 at 900 rpm	98
4.46	Abrasive wear feature on Pad-2 at different contact pressure; (a) 1 MPa, (b) 2.5 MPa, (c) 3 MPa	98
4.47	Abrasive wear feature on Pad-2 at different sliding speed; (a) 300 rpm, (b) 600 rpm, (c) 900 rpm, (d) 1200 rpm, (e) 1500 rpm	99
4.48	Abrasive wear feature on Pad-3 at different contact pressure; (a) 1 MPa, (b) 1.5 MPa, (c) 2 MPa, (d) 2.5 MPa, (e) 3 MPa	100
4.49	Abrasive wear feature on Pad-3 at different sliding speed; (a) 300 rpm, (b) 600 rpm, (c) 1200 rpm, (d) 1500 rpm	101
4.50	Fatigue wear feature on Pad-1 at different contact pressure; (a) 1 MPa, (b) 1.5 MPa, (c) 2 MPa, (d) 2.5 MPa	101
4.51	Fatigue wear feature on Pad-3 at different sliding speed; (a) 300 rpm, (b) 600 rpm, (c) 1200 rpm, (d) 1500 rpm	102
4.52	Fatigue wear feature on Pad-2; (a) 300 rpm, (b) 900 rpm, (c) 1200 rpm, (d) 1500 rpm	103
4.53	Fatigue wear feature on Pad-3 at different load; (a) 1.5 MPa, (b) 2 MPa	104
4.54	Fatigue wear feature on Pad-3 at different sliding speed (a) 300 rpm, (b) 900 rpm	104
4.55	Micrograph of pin surface; (a) the rough groove on the surface before tribological test, (b) formation of transfer layer after tribological test	106
4.56	Micrograph showing transfer layer has been generated on the pin surface using; (a) secondary electron and (b) backscattered electron	106

CHAPTER ONE

INTRODUCTION

1.1 Background of Study

Brake friction materials have been widely used in vehicles as part of their safety device. These materials have been used since the first vehicle was invented. Together with the intensive research and development of vehicles today, the requirement of suitable brake friction materials are increasing as well.

The development and improvement of a suitable brake pad material is still being considered as an extensively difficult task to carry out. The difficulties are generally due to many factors and parameters that influence brake pad performance. In order to get optimized function of braking force, it is important to have a good friction between brake friction material and the brake disc. This in turn means that the material must have stable coefficient of friction (COF, denoted as μ) in any working condition. Another difficulty in the formulation of a commercial brake pad material is manufacturer copyrights. To meet all of these demands, brake pad material is formulated not only by a single material but rather by composing more than ten constituents [1, 2]. Although the exact composition of commercial brake pad is still being confidential, polymer matrix composite are widely known to be used in automotive, air plane and railway transportation systems as brake pad material. They represent a replaceable (sacrificial) element in the friction couple and are typically rubbed against cast iron, steel, or aluminum matrix composite [3, 4].

Railway has been an important means of transportation since long time ago. Its capability to transport a large number of passengers has significant advantages compared to automobile or bus. In urban transportation system, train system has been modified into light rail transit (LRT) system, which has less capacity but easier to move around the city. Like any other vehicles, LRT cars is equipped with brakes in the safety system which is required to decrease the speed of moving cars, stopping, and holding the cars when parked.

In LRT braking system, the friction brake system is used in addition to the electrical braking system. The friction brake usually used when the speed reaches a certain point after the electrical braking system worked. However, in the case of emergency the friction brake system must able to stop moving cars at any speed within a minimum stopping distance in a relatively short period of time. Generally, this will cause very high energy levels to be dissipated in each brake disc in relatively short time [5]. Although the importance of this material to railway has been recognized, only few literatures on LRT brake pad material were found.

1.2 Problem Statement

Tribological studies of brake pad materials have been done extensively in the past several decades in order to understand the unique characteristics due to their operational function as a part of vehicle safety system. The role and mechanism of this special material in stopping the vehicle is still not fully exposed. Moreover, since the development of these materials is still relying on trial and error basis, the research on brake pad materials is still an open opportunity.

The tribological knowledge is crucial for identification, development, and improvement of brake pad materials. Improving the quality and performance of friction materials will certainly increase their efficiency.

It is common knowledge that braking retards the moving vehicles by transforming kinetic energy to heat. This job is performed by frictional action between the brake pad material and brake disc. However, the basic knowledge of gripping and contact mechanisms between the brake pad and brake disc is still relatively limited [6].

The requirement for faster but safer vehicles nowadays has increased the demands to improve brake pad performance as part of the vehicles' safety system. It has become a common knowledge that the operator/driver expects relatively constant level of friction at various braking conditions by applying less pressure on the brake pad. In addition, the brake pad material must be reliable, has a low wear rate, not affected by environment, have less noise and vibration.

In the development of a brake pad material, it is important to understand the role of contact pressure, sliding speed and relative humidity on friction and wear performance. Rhee [7], Pogosian *et.al* [8], and Castelli [9] stated that coefficient of friction and wear has inverse relationship with normal load and sliding speed. Blau *et.al* [10] found that moisture content also have significant effects to coefficient of friction. However, data of friction coefficient and wear of brake pad material at different range of load, sliding speed, and environment are seldom provided by manufacturer [11]. Furthermore, the phenomena at contact surface in microscopic level are also not fully understood.

When braking action is applied, friction will take place at the surface of the pads and the discs. Theoretically, the pads will rub against the disc surface and cause wearing, which will decrease the pad's thickness. Although the brake pad material is a sacrificial material in the braking system, it will incur high cost if several replacements are required during short period of usage time. Brake pad manufacturers would not be able to retain customer's trust with their product if the product worn easily even if it has good friction.

1.3 Objectives and Scope of Study

In the research and development of brake pad materials, laboratory scale test is usually required in order to obtain tribological properties of brake pad material, which will be used as a benchmark before a prototype of the brake pad formulation is tested on full scale. This research covers the laboratory scale test that forms the preliminary study in the development of brake pad material. The objectives of this project are:

- i. To study the friction interaction on brake pad material of various formulation under different contact pressures, sliding speed and relative humidity.
- ii. To understand the phenomena related to friction and wear process on the contact surface.

The scope of this study includes the examination of material composition in brake pad materials, mechanisms of friction and wear, and their relationship to

friction and wear, as well as surface morphology. The information obtained from this study will provide some understanding of tribological behavior of dry friction material in brake system, which in this case, light rail transit (LRT) brake material was used. The friction and wear tests were performed under low temperature condition. The experimental flow chart is attached in Appendix A.

1.4 Thesis Overview

This thesis is divided into five chapters. A brief introduction of friction and wear of brake pad materials, problem statement and, the objectives and scope of study are presented in chapter one.

Chapter two of this thesis presents the literature review on the concept and development of brake pad materials, role of base material to friction and wear of brake pad materials and, the mechanism of friction and wear of brake pad materials. The experimental methods are discussed in chapter three. The methodology is divided into assessment of the contents of the samples and, surface characterization and tribological experiments on the samples.

Chapter four presents the experimental results and the detailed explanation of those results, which are presented in the form of tables, graphs and figures. Finally, chapter five gives the conclusions found from the experimental works and the recommendations for future works. The important issues and results that arise from this research are addressed in relevance to the original aim and objectives.

CHAPTER TWO
LITERATURE REVIEW

2.1. Introduction to Friction and Wear

Tribology is the science and technology of the interactions between surfaces in relative motion and of related subjects and practices [12]. This subject covers the study of friction, wear, and lubrication of mating material, which designate to understand the interactions between surfaces and solving the technological problem associated with the interfacial phenomena. Various incidents may come up in these interactions: forces are transmitted, mechanical energy is converted, and physical and chemical natures including surface topography of the interacting materials are changed. Thus, it related to many disciplines, from physics and chemistry to mechanical engineering and material science, and also the technological importance [12].

The concept of friction was first introduced by Da Vinci in late 1400s, Amonton in 1699, and Coulomb in 1785. Friction is the resistance to motion during sliding or rolling that is experienced when one solid body moves tangentially over another with which it is in contact. When two solid bodies tangentially slid or rolled against each other, there will be a resistance force occur which oppositely to direction of the motion. This tangential resistance force is known as friction force, where friction force, F , usually defines as a non dimensional factor called coefficient of friction, μ , times applied force, P . This relationship mathematically expressed as:

$$F = \mu P \dots\dots\dots(1)$$

Figure 2.1 illustrates typical friction between two solid bodies. When two solid bodies relatively moving each other are loaded with a vertical force, P , the value of the tangential force that is required to initiate motion is acknowledged as the static friction force, F_{static} or F_s and the tangential force required to maintain relative motion is known as the kinetic (or dynamic) friction force, F_{kinetic} or F_k . From this type of force, two types of friction coefficients can also be distinguished: static coefficient of friction, μ_s , and kinetic coefficient of friction, μ_k .

Figure 2.2 illustrates typical friction force curves. Figure 2.2.a and 2.2.b show typical normal friction characteristics. Friction force a and c are used to determine the static coefficient of friction, μ_s , whereas force b is used to determine the kinetic friction of friction, μ_k . When the friction force curve shows trend as figure 2.2.c, this means that the friction shows a stick and slip behavior. The stick slip behavior commonly caused vibration at the sliding system. As consequence, the squeal and chatter noises are occur where in most braking system, squeal noises are consider undesired [13].

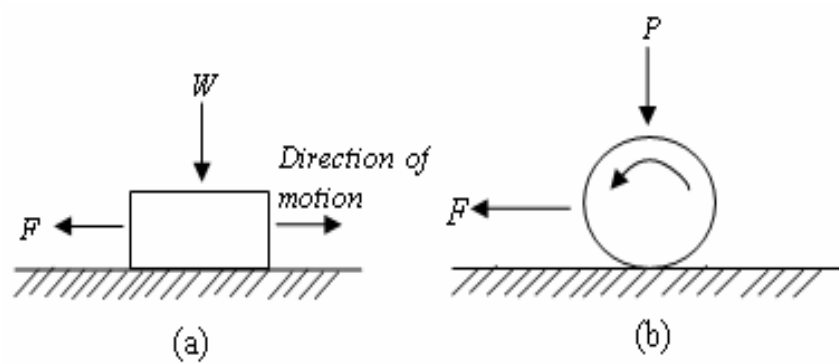


Figure 2.1 Illustration of friction; (a) two body slid against another, and (b) two body rolled against another [12]

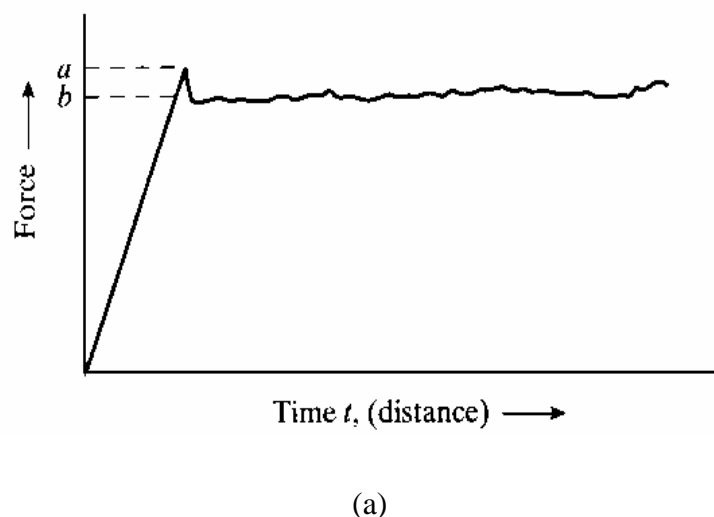


Figure 2.2 Typical friction force curve [14]

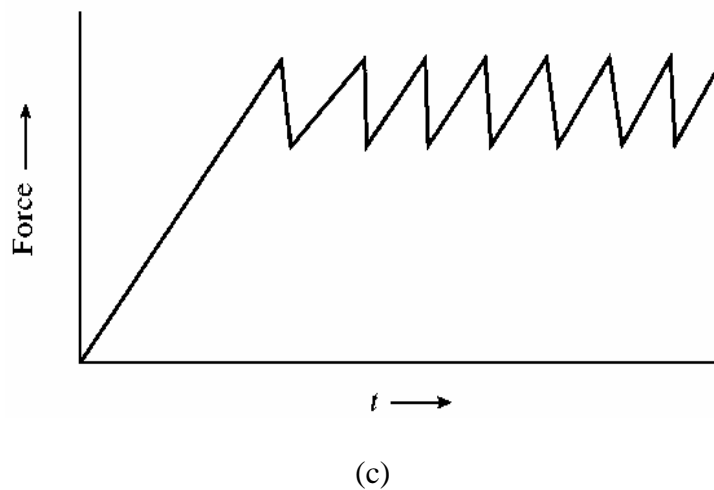
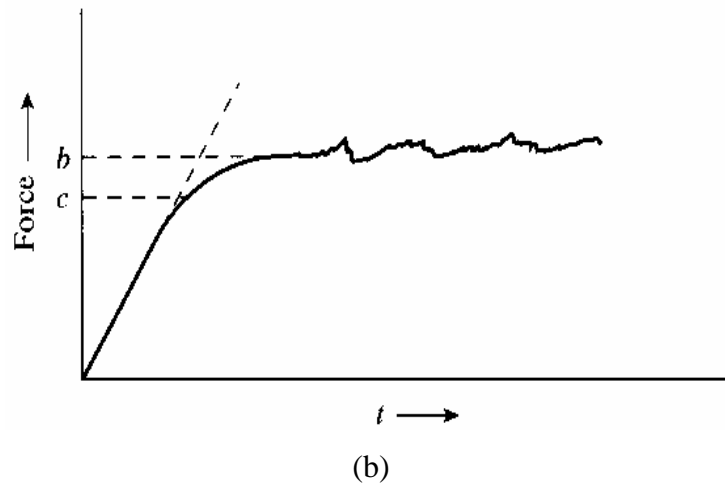


Figure 2.2 Typical friction force curve (*continued*)

Generally, friction is not a material property but rather a system response which depends on several parameters as shown in Figure 2.3. The parameters which influence friction of material pair are [15, 16]:

- i. Structural parameters, which characterize the components such as material, lubricant, and environment including their physical, chemical, and technological properties that involved in the friction and wear process.
- ii. Operating parameters, such as loading, kinematics, temperature conditions, and functional duration.
- iii. Interaction parameters, which characterize particularly operating parameters on the structural components of the tribological components of the system and define its contact and lubrication modes.

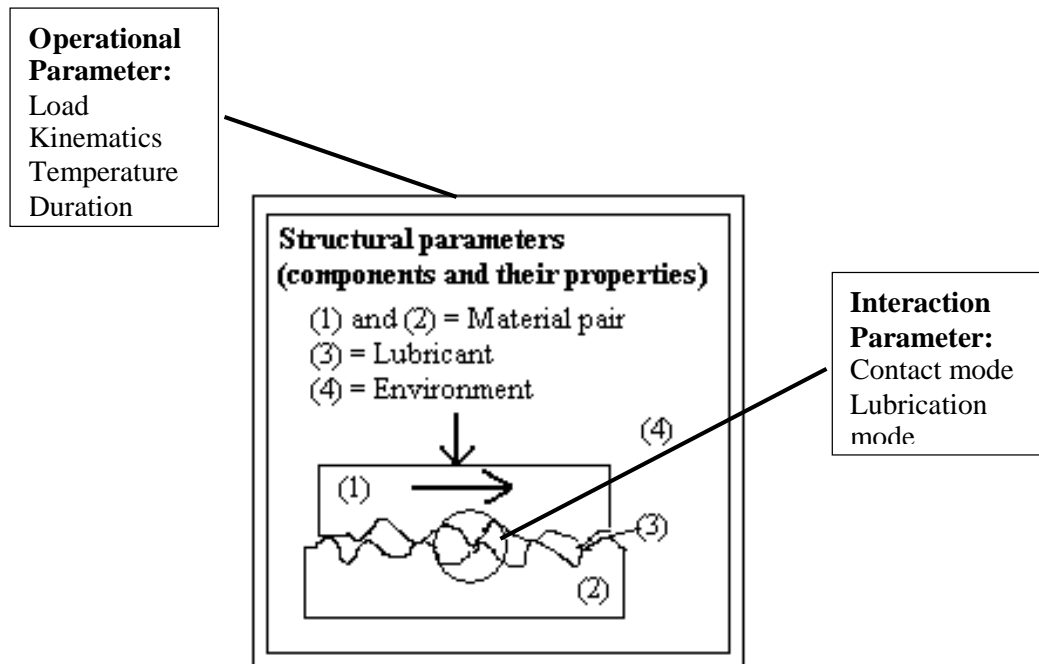


Figure 2.3 Parameters influence friction and wear process [15, 16]

There are two main types of friction that are commonly encountered: dry friction and wet friction. Dry friction describes the tangential component of the contact force that exists when two dry surfaces move or tend to move relative to one another. Wet friction describes the tangential component of the contact force that exists between adjacent layers in a fluid that are moving at different velocities relative to each other as in liquid or gas between bearing surfaces.

These considerations lead us to taking care of any possible factors that influence the frictional behavior of sliding materials. Several examples of the factors that influence the frictional behavior are tabulated in Table 2.1.

Friction cannot be avoided in normal life. It will always occur as long as relative motion between two components exists. It has productive and desired outcomes such as friction at brake systems, clutches, belts, wheels of cars and trains, bolts and nuts, *etc.* It also has non-productive and undesired outcomes like friction in internal combustion engines, bearings, gears, seals, and cams.

Table 2.1 Factors influencing friction behavior [16].

Category	Factor
Contact geometry	<ul style="list-style-type: none"> - Conformity of the components (macro-scale mating of shapes) - Surface roughness (micro-scale features-asperity shapes, size distribution) - Surface waviness - Surface lay (directionality) with respect to relative motion
Fluid properties and flow	<ul style="list-style-type: none"> - Lubrication regime (boundary, mixed, hydrodynamic, elastohydrodynamic) - Viscosity and characteristics of the fluid as its affect Newtonian or non-Newtonian flow - Temperature and pressure effects on viscosity - Shear thinning effects on viscosity in ultra thin films
Lubrication chemistry	<ul style="list-style-type: none"> - Formation of friction-altering films - Stability of friction-modifiers over time - Oxidation and acidification of lubricants
Relative motion	<ul style="list-style-type: none"> - Unidirectional or reciprocating motion - Constancy of motion (acceleration, pauses, start-stop) - Magnitude of relative surface velocity
Applied force	<ul style="list-style-type: none"> - Magnitude of the normal force (contact pressure) - Constancy of applied forces
Third bodies	<ul style="list-style-type: none"> - Characteristics of particles entrained in the lubricant - Characteristic of particle assemblages contained within interface (e.g., wear particles, external contaminants, lubricating powder layers)
Temperature	<ul style="list-style-type: none"> - Thermal effects on material properties (thermoelastic instabilities) - Thermal effects on lubricant properties (viscosity, flow, possibility for cavitation)
Stiffness and vibration	<ul style="list-style-type: none"> - Contact compliance (stick slip) - Damping of frictional or external vibrations - Feedback between frictional stimulus and structural response

As the result of friction, wear also will be occurring on those two components and affecting its useful life. According to ASTM G-40, wear is defined as damage to a solid surface, generally involving progressive loss of material, due to relative motion between the surface and a contacting substance or substances. Like friction, wear also a system response which occurs not as a single process but rather in the several mechanisms such as: adhesive, abrasive, fatigue, impact by erosion and percussion, chemical or corrosive, and electrical-arc-induced wear [12].

2.2. Brake System

The brake is a mechanism which is used to absorb the kinetic energy of the vehicle with the aim to stop or retard the motion [17]. Friction between the brake friction material and the rotor will generate heat. This heat generated caused of the brakes transform kinetic energy to heat while it working through the structure of the brake system.

Brake system is one of main component in a vehicle. This component is subjected to decelerate the vehicle by rubbing the brake friction material to the rotor part i.e. brake pad to disc brake, brake shoe to drum brake. Not only to decelerate, brake system also meant to hold the vehicle steadily when it parked. All of these actions are maintained by friction between the brake lining and brake rotor. The friction between brake lining materials and the rotor will convert kinetic energy to heat and dissipate the heat through its system surrounding.

The brake system also required to provide sufficient friction level and maintain stable in the changes of speed, applied load, and sliding temperature during braking operation. This system also should be able to operate in good and safe in all conditions such as wet and dry road. For example when applying brake on slippery or coarse road, whether using old or new brake linings material, when vehicle was driven by a new or experience driver, when brake on the straight or corner road [18, 19, 20, 21]. Generally, the brake system can be categorized into four major components [18, 19]:

- i. Power supply is component of the brake system which provides and control the energy required during braking.
- ii. Control device is component act on the operation and control the brake system
- iii. Transmission device
- iv. Brake pad/shoe

Figure 2.4 shows a typical brake system and its components commonly found in automotive vehicles. When the driver apply braking force by pressing the brake pedal, brake fluids inside the cylinder will push pistons at the caliper through the

transmission device. This operation then will force brake pad or brake shoe against the rotating brake disc or drum and generate friction.

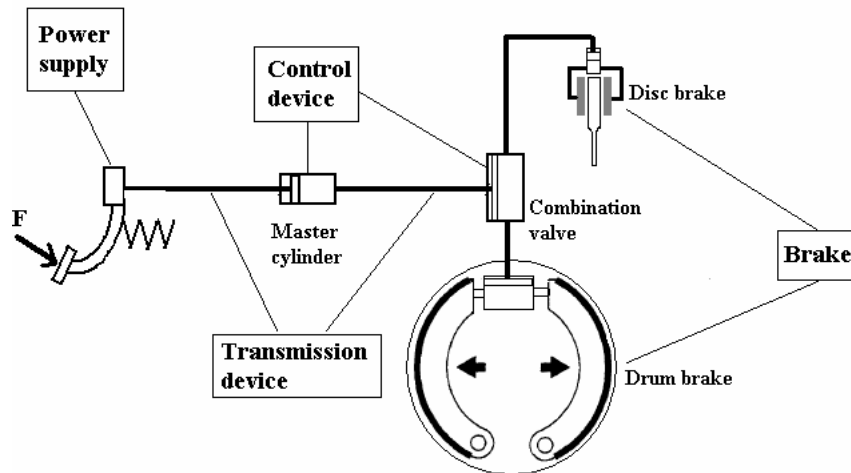


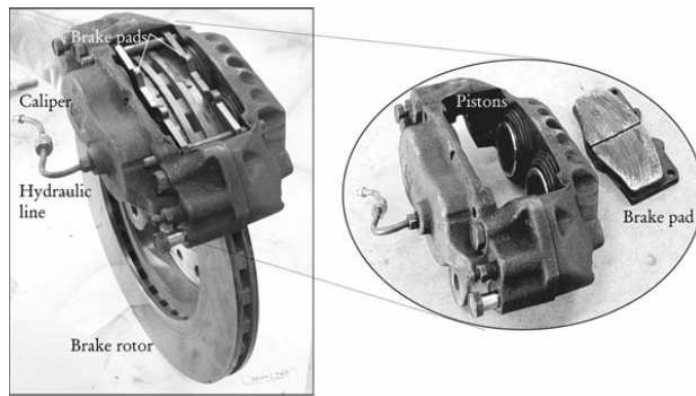
Figure 2.4 Brake system components.

2.2.1. Disc Brakes

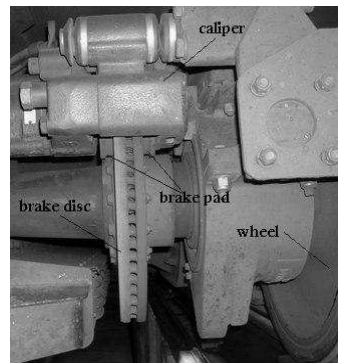
Disc brakes use a rotor disc slid against a pair of friction pad (Figure 2.5). This type of brake has advantages in offering faster cooling, with their larger exposed surface areas and better cooling geometry, but are more vulnerable to either liquid or solid particulate contamination [22].

2.2.2. Drum Brakes

Drum brakes system mainly using internal expanding shoes with brake linings that load the majority of the drum rubbing surface (typically 50 – 70 % of the load) [22]. This system has advantages in their high effectiveness because of the self amplification. Contrary with disc brake system, this system not so capable to dissipate the heat generated from friction. Thus it has disadvantages due to its sensitivity to brake fade [17]. Generally drum brake system have 3 types in their application; simplex drum brake, duplex drum brake, and duo servo drum brakes (Figure 2.6).

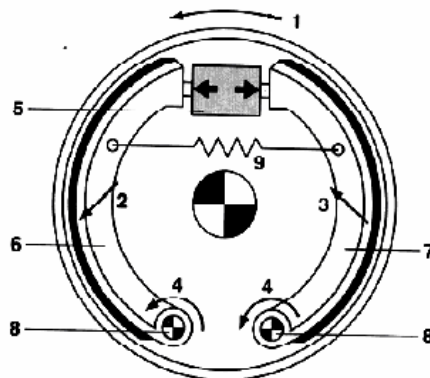


(a)



(b)

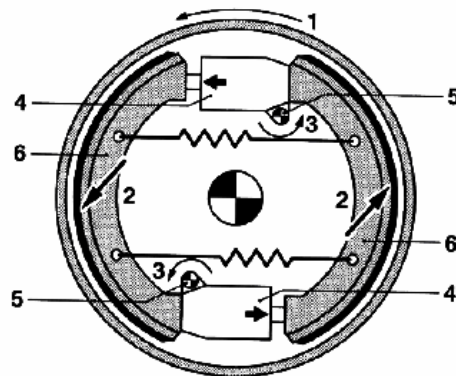
Figure 2.5 Disc brakes (a) automotive disc brake [23], (b) PUTRA LRT disc brake



1. direction of motion 2. self-energization of the brake force 3. self-reduction of the brake force 4. torque
5. wheel cylinder 6. leading shoe 7. trailing shoe 8. pivoting point 9. return spring.

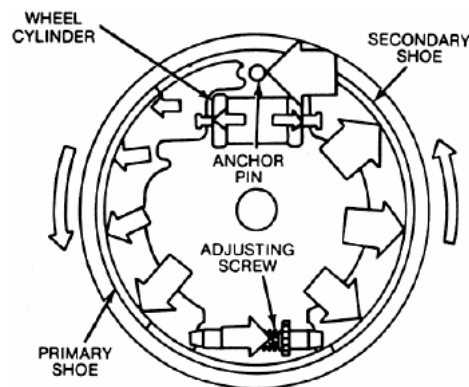
(a)

Figure 2.6 Drum brakes; (a) simplex drum brakes, (b) duplex drum brakes, and (c) duo servo drum brakes [17]



1. direction of motion 2. self-energization of the brake force 3. torque 4. wheel cylinder 5. pivoting point 6. leading shoe

(b)



(c)

Figure 2.6 Drum brakes; (a) simplex drum brakes, (b) duplex drum brakes, and (c) duo servo drum brakes (*continued*)

2.3. Brake Pad Materials

Historically, many kinds of materials had been used for brake since vehicle was found. At the earlier time, wagon brakes used wood and leather as brake material. Current brake materials are commonly contains organic-based materials, like polymers and plant fibers.

The research activity in the developments and improvements of the brake pad materials are open widely since the optimum formulation of brake pad materials are not fully documented yet. In addition, the role of each element in the formulation to friction and wear of the brake pad are still not clear yet too. Thus, it is still being a difficult task to performed because different element will give different result.

Moreover the formulation of industrially manufactured friction materials is still being company proprietary information [24].

In general, components consisting in the formulation of brake pad materials able to classify into five groups [6, 19, 25]:

- i. Binder (matrix) materials; used to hold all components together and determine the thermal stability, common binder materials used in the brake pad formulation are: phenolic resin; rubber; metallic; and carbon.
- ii. Reinforcing fibers; usually subjected to provide and improve the mechanical strength. Some reinforcing fibers usually used are: asbestos; glass fiber, ceramic fiber, metal fibers (steel, copper, brass, aluminium, etc.), para-aramid (kevlar), wollastonite, potassium titanate.
- iii. Fillers; used to maintain the overall composition, improve manufacturability and reduce cost. Several materials typically used as fillers are: mineral fillers (like mullite, kyanite, silliminate, alumina, and crystalline silica), barium sulfate or barite, calcium carbonate, cashew nut shell oil, cotton, lime, sea coal, zinc oxide, vermiculite, molybdenum trioxide.
- iv. Solid lubricants; these materials are functioned to lubricate, raise and stabilize the friction, or react with oxygen to help control interfacial films. Several material usually used are: carbon (graphite), brass powder (62% Cu-38% Zn); copper powder, friction dust (commonly consist of processed cashew resin), metal oxides such as ZnO, Fe₃O₄, Cr₂O₃, and metal sulfide such as Cu₂S, Sb₂S₃, PbS, and MoS₂.
- v. Abrasive materials, meant to help maintaining the cleanliness of mating surfaces by removing the iron oxides and control the build up of friction films. They also increase friction, particularly when initiating a stop (i.e. they increase “bite”). Materials usually used as abrasive are: aluminum oxide (Al₂O₃), Iron oxide, quartz or silica, and Zirconium silicate (ZrSiO₄).

As the development of brake pad materials has become more intensively conducted by researchers and manufacturer, Anderson [22] has classified three abroad

classifications of the friction material: organics, metallic, and carbon. This classification was made based on the binder bind all element and compound composed in the brake pad material.

2.3.1. Organic Friction Material

This type of friction material is composites of one or more binder resins blended together with reinforced fiber and some additives which is to modified friction, improve wear, reduce cost, aided processing, changed color, and so on. There are three subclasses of these resin-bonded friction materials:

i. Asbestos brake friction material

Asbestos brake friction materials are composed from chrysotile asbestos material bind with phenolic resins and additives. The usage of asbestos widely used as basic fiber material before the early 1980's. It has advantages due to its fibrous nature that combine strength, flexibility, heat and chemical resistance [26, 27]. It thermally stable up to 500 °C, able to regenerate the friction surface during used, it wears well, and most important is available at reasonable cost [26, 27]. However it was found that asbestos fiber is dangerous to health if inhaled. It was prohibited to use asbestos fiber since 1985 in Europe, 1993 in US and Japan, and 2003 in Australia. The major diseases resulting in the long term of asbestos exposure are asbestosis, lung cancer, and mesothelioma [28].

ii. Non asbestos organic (NAO) brake friction material

Although the usage of asbestos fiber in the formulation of brake pad materials has been prohibited in many countries due to health reason, it can generally replaced by other fiber/fiber blends [27]. Generally non asbestos organic brake friction material is composed of non asbestos organic material and some additives. This brake lining has been rapidly evolved and continuously developed. There over 1200 different fibers, acicular materials, and other reinforcing agents have been tested to date [22]. This factor affected the number of the potential combination in the formulation become stunning because of most NAO materials use a blend of different fibers and other

reinforcing agents. The most commonly used fibers are glass (including chopped glass fibers, mineral wool, and many proprietary species), metal, ceramic, para-amid (Kevlar), cellulosic, and other organics forms. Acicular materials, such as wollastonite, and plate like-material, such as attapulgite, are also used as reinforcing agents in NAO linings. Beside its potential to be improved, this type of friction material shows better performance in terms of friction stability and comfort [29,30]. However there are still many concern about brake induced problem such as noise, judder, and excessive wear of the rotor and friction materials regardless of the type of friction material [30].

iii. Semi metallic (semimet) brake friction material

Semimet linings are generally consist of about 65 wt% total irons content, 10 – 25 wt% steel wool, and bind with heat resistance phenolic resin about 10 % wt., and the remainder is commonly a porous iron powder. Graphite, usually synthetic, as addition, is about 15 wt%. The semimet brake pad material has advantage due to its high temperature performance and wear resistance [31], excellent disc compatibility, improved energy absorption, possibility of smaller brake sizing, and premium price [32]. However it cannot be used universally for various reasons for example corrosion [24].

2.3.2. Metallic Brake Friction Materials

Metallic brake linings can be based on either copper or iron. Most of are solid-state sintered, often with inorganic additives to improve performance. These have been developed for very high power input densities. For example, solid-state-sintered bronze and mullite linings are used in the race car and high speed railroad brakes. Sintered iron with graphite is used on some heavy duty brakes; both disk and drum, as well as on a few production passenger cars drum brakes.

Another metallic friction material is cast iron. Although this venerable material is used on some old railroad tread brakes, no new automotive applications are known to use cast iron as brake lining. However it is the predominant counter-surface material used for automotive drum and disk brakes. Therefore it remains a friction element, although not a brake lining.

2.3.3. Carbon-Based Brake Friction Materials

Carbon based brake lining such as carbon-carbon is commonly developed for military and commercial aircraft disk brakes. Some are now used on racing cars where weight is critical, performance is demanding and cost is secondary. Carbon-carbon friction materials are made from carbon fiber (also called graphite fiber) that is bonded with amorphous carbon. Organic resins are either baked at high temperatures or a chemical vapor deposition process is applied to generate this amorphous carbon binder. After further processing, the resultant friction material is essentially pure carbon with a very low porosity. A 2000°C operating temperature and a high specific heat property permit carbon-carbon materials to provide weight savings of nearly 85% when replacing cast iron in suitable applications.

2.4. Ingredient Functionality

Brake material ingredient serves a variety of functions. Each ingredient has its own role in the friction material characteristics and changes in the type and weight percentage of the ingredients may result in changes in physical, mechanical, thermal, and chemical properties of the developed formulation. Table 2.2 shows several material ingredients and its functions.

Table 2.2 Brake friction ingredient function

Material	Nominal Function
Phenolic Resin	Most common binder used in friction materials and control friction [22, 23, 24, 27,28, 33, 34]
Rubber	Additional binder; modify flexibility [24, 35, 36] and improve thermal resistance [24]
Asbestos	Reinforcing fiber as well as filler; Common filler before found as dangerous material to health; posses good strength, flexibility, heat and chemical resistance, as well as wear resistance [26, 27, 32, 37, 38]
Steel fiber/steel wool/ steel chips	Reinforcing fiber; improve fade resistance at elevated temperature [39,40]; reduce wear as well as control formation of friction film [4], but in large amount may cause high disc/drum wear [23]
Potassium titanate (K ₂ O.6(TiO ₂))	Reinforcing fiber; high thermal resistance and good wear resistance [23], posses good fade resistance as well as provide strength to maintain friction film [34, 41]

Table 2.2 Brake friction ingredient function (*continue*)

Material	Nominal Function
Aramid Fiber	Reinforcing fiber; enhance mechanical strength [34,36], has low fade resistance [34], reduce thermal conductivity [36], improve wear resistance and friction stability [41], used as asbestos replacement [42]
Copper fiber	Reinforcing fiber; improve high temperature fade resistance [39], has capability to reduce friction [34]
Glass fiber	Reinforcing fiber; a proper content of glass fiber prevent swelling [4]
Copper sulfide (Cu ₂ S)	Solid Lubricant; causes gradual lost of friction [35]
Antimony trisulfide (Sb ₂ S ₃)	Solid Lubricant; stabilize the friction [1, 2, 35], has lower thermal conductivity [23]
Molybdenum disulfide (Mo ₂ S)	Solid lubricant; effective to build up friction film on the disk surface [43].
Graphite	Solid Lubricant; show unstable friction [1] but able to form self sustaining lubricant layer [23, 43]
Zinc oxide (ZnO)	Filler as well as lubricant; lubricates, improve wear resistance but also can cause drum polishing [26, 27]
Vermiculite	Fillers; improve low-frequency brake noise, but has low high temperature resistance [23]
Barium sulphate (BaSO ₄)	Filler; inert material, improve heat stability [23], aid friction characteristics [23], increase wear resistance [26],
Calcium carbonate (CaCO ₃)	Filler; substitute to barium sulphate, improve fade properties but not as stable as barium sulphate at high temperature [23, 26]
Lime (Ca(OH) ₂)	Filler; used to avoid corrosion in Fe-additives, help raise fade temperature [26, 27]
Wollastonite (CaSiO ₃)	Filler; offer similar performance characteristic like asbestos [3, 26, 27]
Quartz (SiO ₂)	Abrasive; cleaning drum/disk surface and control formation of friction film [27, 42, 44]
Iron Oxide (Fe ₂ O ₃ or Fe ₃ O ₄)	Abrasive; improve cold friction [26, 27]
Zirconium Silicate (Zr ₂ SiO ₄)	Abrasive; affect friction torque [2], proper combination with antimony trisulfide has synergetic effect to control the formation of friction film [2], improve wear resistance but intensify friction-induced noise [34]
Magnesium oxide (MgO)	Abrasive; increase friction as well as intensify friction-induced noise [34]
Alumina (Al ₂ O ₃)	Abrasive; sufficient percentage of alumina able to improve friction and wear [45, 46]

2.5. Friction and Wear of Brake Pad Material

Braking is much depending on how friction between the friction material and the rotor works which represented by the coefficient of friction, μ , to retard speed of the vehicle. Generally brake pad material is required to fulfill several requirements such as:

- i. The mean coefficient of friction, μ , possess around 0.45 for passenger cars and 0.35 for trains [47].
- ii. The coefficient of friction, μ , should be stable at any ranges of temperature, vehicle speed, load or pedal pressure, relative humidity, and other parameters as mentioned before.
- iii. Wear rate of the friction pair should be low. Although the brake pad is a sacrificial material in brake system it should have good resistance. This consideration is necessary in order to replace them on a regular basis. In addition, damage to rotor also must be as minimal as possible [42]. If the attack of brake pad material to disc is high, it will increase surface roughness of the disc, thus increase the wear rate of the brake pad too. Damage to the brake disc also will causing disc thickness variation (DTV) and judder.
- iv. Noise and judder must be avoided for comfortability.
- v. Thermal conductivity shall be low.
- vi. Strength and durability shall be high.
- vii. The raw material used should be cheap and not hazardous to the environment.

Jang *et.al* has been conducting several researches to investigate the role of raw materials to friction and wear of brake pad material [1, 2]. In the study of role several solid lubricant such as graphite, Sb_2S_3 , and MoS_2 , they concluded that anti-fading was not dependent on the type of solid lubricant used in the friction material and addition of Sb_2S_3 or MoS_2 improve friction stability but on the other hand an addition of graphite showed worse stability. However, they also suggested that addition of solid lubricants such as Sb_2S_3 or MoS_2 mixed with graphite might aggravate the rotor disc thickness variation (DTV) during service. By comparing friction materials using two different novolac resins, unmodified and modified resins in powder forms [33, 34], Kim and Jang concluded that; (i) the wear rate of the friction materials was dependent

on the friction level, porosity, heat resistance and mechanical strength of binder resin, and temperature profile, (ii) friction materials containing modified resin showed a good thermal stability and could be burnished (stabilized) in a shorter period of time. Kim *et.al* [34] found that aramid pulp improved friction stability due to its capability to improve heat resistance of the friction material. They also concluded that a stable coefficient of friction is related to the formation of heat affected layers on sub-surface of the friction material. This layer is produced incessantly by maintaining a certain thickness while the material at the top surface is removed during sliding.

As aforementioned, the formulation of the brake pad material has important influences to meet those brake material requirements. This factor is believed to affect the formation of friction film, friction layer or third body which play important role to friction and wear characteristics of brake pad material. Cho *et.al* concluded that the thickness of the transfer layer was strongly affected by temperature and the relative amount of ingredients, in particular, solid lubricants and iron powders were effective for developing a thick transfer layer [43, 48]. They also concluded that coefficient of friction and wear rate was independent of transfer layer thickness but intensity of friction oscillation was reduced when the transfer layer was thick. This phenomenon was also postulated by Jacko *et.al* that a stable friction level and low wear rates can be maintained at various temperatures when stable friction films are readily formed for a given friction couple as long as the friction film not destroyed [49, 50].

Godet suggested that wear particle compaction play important role for third body formation [51]. This suggestion was also revealed by Filip *et.al* [3]. They revealed that the friction process is typified by the development of friction debris which adheres to the friction surface and forms a friction layer. The friction layers are representing a newly formed matter, heterogeneous and consist of several different phases. On the other hand, Oesterle *et.al* concluded that friction layers is comprises of a nanocrystalline microstructure and the friction layer on the pads are not continuous, but interrupted either by carbon constituent or by wear troughs [47, 50, 52, 53]. A typical friction layer of brake pad is illustrated in Figure 2.7.

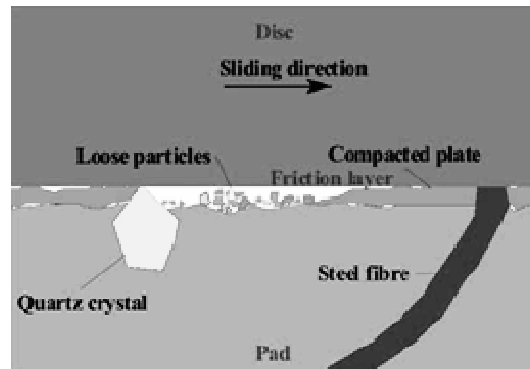


Figure 2.7 Schematic illustration of friction layer of brake pad [50]

Jacobson *et.al* found that the friction layers are consisting of primary and secondary plateaus [6, 54, 55, 56, 57]. There are only limited fraction of pad surface is in contact with the disc. Thus, the real contact area is confined within a number of contact plateaus and scattered over the pad surface. These plateaus often can observe by naked eye as a shiny spot against a dark background as shown in Figure 2.8.

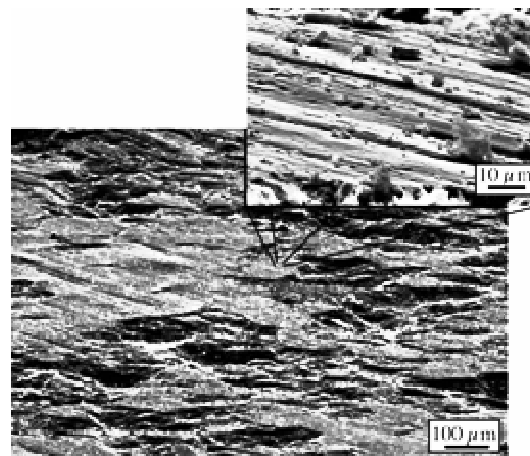


Figure 2.8 Formation of the contact plateau on the surface of an organic brake pad [54]

The primary plateaus are formed due to lower removal rate of the mechanically stable and wear resistant ingredient of the brake pad. The friction increase during the run-in of a ground brake pad is primarily correlated to the formation of primary plateaus. Between the contact spots, there are gaps that enough for wear debris, in the form of small particle, from both disc and pad to fit in and make way. These wear particles then occasionally hit a contact spot and trapped in its way through the contact between the pad and the disc. There is only a small fraction

of wear particle trapped at first, but because of the continuous flow of the particle, more particle jammed together. The combination of normal pressure, shear forces and frictional heat then compact this particles and further forms the secondary plateau. The build up of compacted areas requires supply of wear debris, a limited space between pad and disc, friction energy, and normal load. Thus, the formation of the secondary plateaus is a gradual process.

Another study similar with this matters also conducted by Oestermeyer [43, 58, 59]. In order to explain dynamics wear in brake system, Oestermeyer suggests an approach to a structure of brake pad shown in Figure 2.9. For simplicity, he splits the functional structure of a brake pad by two components: a rather soft polymer matrix and the hard particles; like SiO_2 particles.

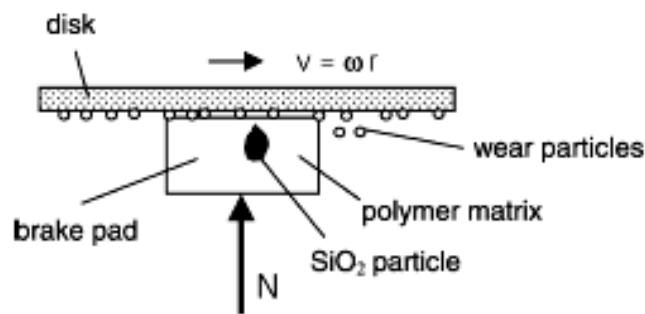


Figure 2.9 Brake pad structure [43]

Figure 2.10 shows the formation and destruction process of contact patches. As the normal load N applied to the brake pad, the contact between metallic disk and soft polymer matrix will produce wear particles. These wear particles move rather homogeneously through the contact zone and partially they adhere to disk surface, and then show again coming into the contact zone some time later from the other side. When the SiO_2 particle reaches the surface by wear of the pad matrix, the wear particle flow will be disturbed at this location because they are harder than the soft polymer matrix (Figure 2.10 (c)).

The SiO_2 particle will be more and more pressed down in the soft matrix because the polymer matrix around this hard particle will be lowered by wear, but this particle itself shows nearly no wear. The growing normal pressure will result in the increasing of temperature. This will result in the growing effects of the SiO_2 particle

by the wear particles. Further the load on the SiO_2 particle causes wear of the brake disc, so now the wear debris from the pad matrix and disc is to be found in the wear material flowing through the contact zone. There are formed hard thin patches by mechanical alloy or even melting processes of the wear particles (Figure 2.10 (d)–(e)).

The thermal and mechanical load lead the destruction of the patches (Figure 2.10 (g)–(i)). After certain time, the patches will become unstable and cracks will arise. Hard part of them flow out the contact zone together with other wear particles and the other part will integrate directly with other patches or initiate the growth of another patch at another place. This event can be concluded to a theory that friction not only causes the wear, but wear rather also modulate the friction power and as the result the coefficient of friction.

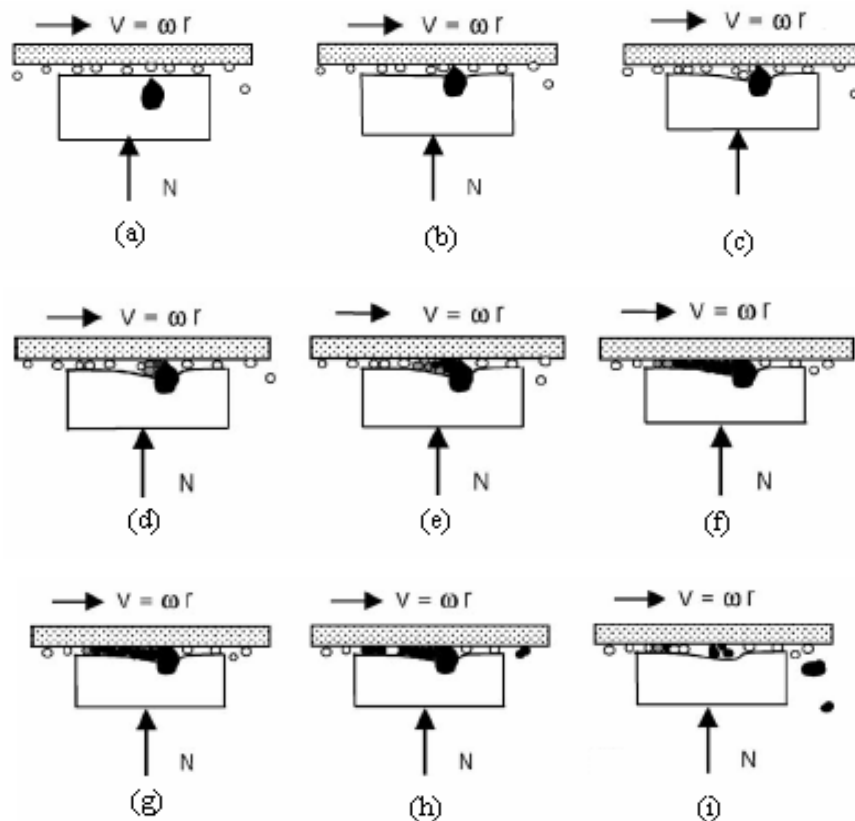


Figure 2.10 Formation and destruction process of contact patches; (a) – (f) Growth process of contact patches, (g) – (i) Destruction process of contact patches [43]

2.6. Wear Mechanism in the Brake Pad Material

Friction brakes are inherently energy dissipating devices, so wear is unavoidable [22]. The friction materials are widely used simply because they are smaller, lighter, simpler, and less expensive than the counterpart. Wear is one of the main causes to the lifetime limitation of a brake pad material. Although brake pad is the sacrificial material in the braking system, from economical point view, it will take a lot of cost if the brake pad frequently replaced.

Friction and wear are complex phenomenon that depends on the material composition, manufacturing process, microstructure, mechanical and physical properties, environment, and temperature [19]. However, wear is more complicated than friction because it involves plastic deformation as well as localized fracture [19, 60]. As the coefficient of friction increased at the onset of braking, then it will decrease with braking time and thereafter reached a steady state. This was thought to be due to the ploughing and shearing of the peak asperities, the formation of a transfer layer, and the decomposition of organics materials, micro-structural and physical changes and transition in wear mechanism.

Wear mechanism act not as a single process, it is combination of several other wear mechanism. According to Rhee [61], when a polymer of polymer bonded friction material slide against a metal surface, the friction material wears out by any one or combination of the following wear mechanism:

- i. Adhesion wear
- ii. Abrasive wear
- iii. Thermal wear
- iv. Macroshear
- v. Fatigue wear

He also stated that each of these mechanisms can reasonably be expected to be dependent on the conditions of sliding, *i.e.* load, speed, and time. If the system does not reach a steady state, but goes through a transient state such as rising temperature due to friction, the relative contribution to the total wear of the individual wear

mechanism may vary with temperature. The relationship between the parameters is shown as:

$$\Delta W = kF^a V^b t^c \dots\dots\dots (2)$$

Where: ΔW = weight loss of a friction material
 K = wear factor (or wear coefficient)
 F = Load
 v = Sliding velocity
 t = time
 a, b, c = parameters

This equation can also be rewritten as:

$$\log \Delta W = \log K + a \log F + b \log v + c \log t \dots\dots\dots (3)$$

The parameters a, b and c can be determined experimentally by varying only one variable at a time and keeping the other two variables constant. The value of a is the slope of line $\log W$ vs. $\log P$, value of b is the slope of line $\log W$ vs. $\log v$ and value of c is the slope of line $\log W$ vs. $\log t$.

From several studies conducted on the brake friction material wear mechanism, it was found that wear mechanism is related to temperature. Rhee concluded that at low temperature (less than 230 °C), adhesion and shear mechanisms were occurred [62]. He also concluded that three body abrasive wear mechanism occurred which the wear caused by hard particle entrapped between the rotor and friction material. At temperature more than 230 °C, it was found that pyrolysis mechanism dominantly caused the wear [35, 36, 62, 63]. Another conclusion by Jacko *et.al* [32] stated that at temperature below 230 °C shear mechanism was dominant and thermal wear at temperature more than 230 °C.

2.6.1. Adhesive Wear

Adhesive wear occurs if adhesion takes place at the asperity contact interface when two nominally flat bodies contacted in sliding contact. Adhesion is generally recognized as the principal mechanism by which matter may be transferred from one tribosurface to another and vice-versa, although such transfer may result from

mechanical interlocking adhesion as well as by adhesive bonding [64]. The sliding shear the asperity contact and result in the detachment of a fragment from one surface and attached to another surface.

There are several basic of adhesive wear mode [65]. The tangential shear under compression at the contact interface of strong adhesive bonding generates slips along slip planes in the contact region. As result, flake-like shear tongues are formed and are followed by a crack initiation and propagation in the combined fracture mode of tensile and shear in the leading region of contact. The large plastic deformation in the contact region sometimes forms a wedge-shape which is followed by crack initiation and propagation in the combine fracture mode of tensile and shear in the trailing region of the contact. Both modes of wear that produce this flake-like and wedge-like wear particle are consider as basic of adhesive wear (Figure 2.11).

In adhesive wear process transfer and retransfer of from one surface to another take place in many cases resulting relatively large wear particles composed of two surfaces are formed. This mode also considered as another basic of adhesive wear.

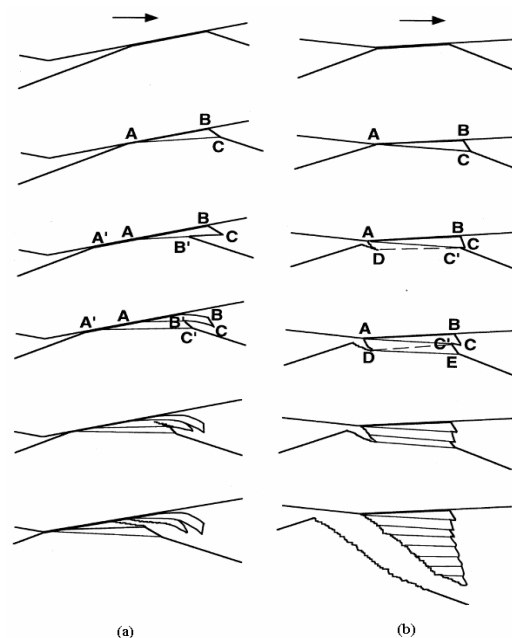


Figure 2.11 Schematic diagram of adhesive transfer process (a) flake-like wear particle (b) wedge-like wear particle [56]

Another aspect of basic mode is in the process of repeated sliding, the wear particles leave the contact interface as free particles or stay on either surface and form prows to scratch the counterface. Even if the contact is made between flat surfaces of similar materials and the contact interface is at first parallel to the sliding direction, the interface rotates and becomes inclined and wavy as a result of the combined effect of normal and tangential forces in sliding.

In the case of friction material, it is difficult to predict the rate at which friction material constituents probably stick on the cast iron counterface. Self-mating metal contact, such as that which might be experienced between the rotor substrate and steel wool protruding from the friction material provides an extremely strong bond comparable to that of the bulk material and frequently leads to severe wear regimes. Contact between dissimilar metals may also be significant because of interatomic diffusion and depends upon the two metal's alloying compatibility. Ionic or covalently bonded materials, such as ceramics, are unlikely to form strongly adhesive bonds with metals but may bond to each other if lattice parameters and orientations coincide [64]. The micrograph of adhesive wear symptom is shown in Figure 2.12.

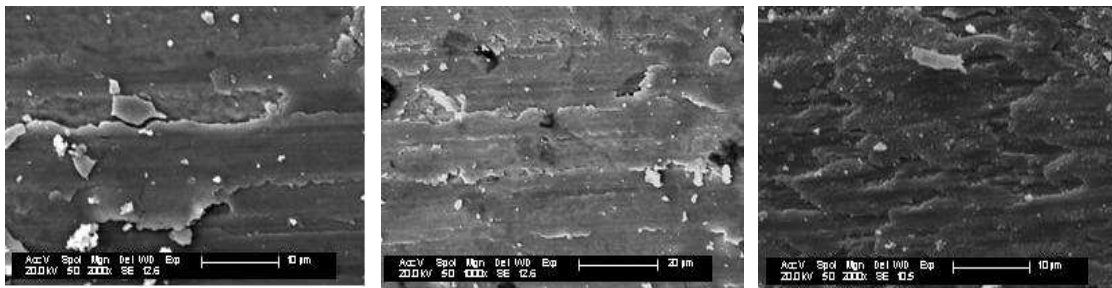


Figure 2.12 Micrographs of adhesive wear [19]

2.6.2. Abrasive Wear

Abrasive wear occurs when asperities of a rough, hard surface or hard particles slide on a softer surface and damage the interface by plastic deformation or fracture. There are two general situations for abrasive wear: (1) the hard surface is the harder of two rubbing surfaces (two body abrasion), (2) three body abrasion; the hard surface is a third body generally a small particle of abrasive, caught between the two

other surfaces and sufficiently harder that it is able to abrade either one or both of the mating surfaces.

There are three different modes of abrasive wear take place: microcutting, wedge forming, and ploughing [65]. Figure 2.13 shows typical modes of abrasive wear. In microcutting, a tip of abrasive material with large attack angle plough a groove and removes the material in a form of discontinuous debris particle similar like chips in the metal cutting process. In wedge forming mode, a tip of abrasive material plough a groove and a wedge-like wear particle is formed at the tip of the grooving asperity and stays there working as a kind of built-up wedge to continue grooving. This wear mode appears as a combined effect of adhesion at an inclined or curved contact interface and shear fracture at the bottom of the wedge. In ploughing process, material is displaced from a groove to the sides without removal of the material. In this mode, a wear particle is not generated by a single pass of sliding and only shallow groove is formed. However, after the surface has been ploughed several times, material removal can occur by a low-cycle fatigue mechanism. This resulted in occurrence of series of grooves as a result of the plastic flow of the softer material.

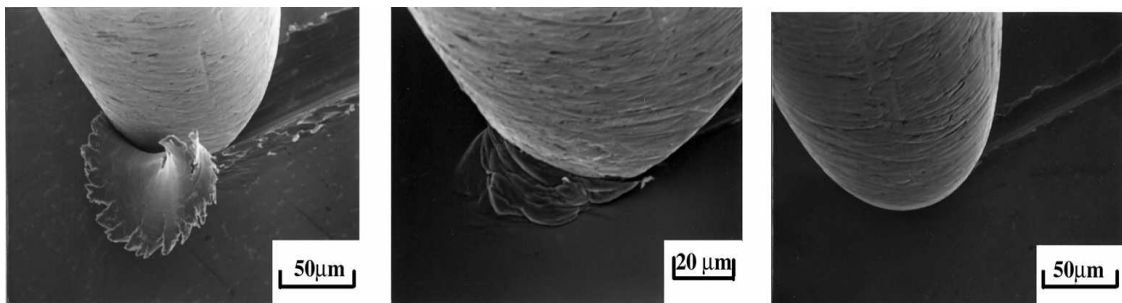


Figure 2.13 SEM micrograph of the experimental investigation to (a) cutting mode, (b) wedge-forming mode, and (c) ploughing mode during abrasive wear [65].

The types of abrasive contact that are encountered during friction braking are described as closed two-body, i.e. two opposed surfaces in contact, and closed three-body, i.e. the action of trapped interfacial debris between two opposed surfaces [64]. The abrasive wear component of the friction material acting at the rotor countersurface is clearly of critical importance for numerous reasons. However, since an oxidized ferrous surface exhibits a higher Mohs hardness than > 95 volume %

constitution of a typical NAO friction material, it is not difficult to see why it is the pad that is considered the sacrificial triboelement.

2.6.3. Thermal Wear

Thermal wear is occur when material removal is governed by surface melting caused by frictional heating or by surface cracking caused by thermal stress. In friction material, thermal wear occurs upon thermal decomposition of the organic material in the brake friction material (Figure 2.14). Unlike the other mechanisms taking place at the friction interface, thermal wear takes place at a predictable rate, increasing exponentially with interfacial temperature [64], as can be seen in Figure 2.15.

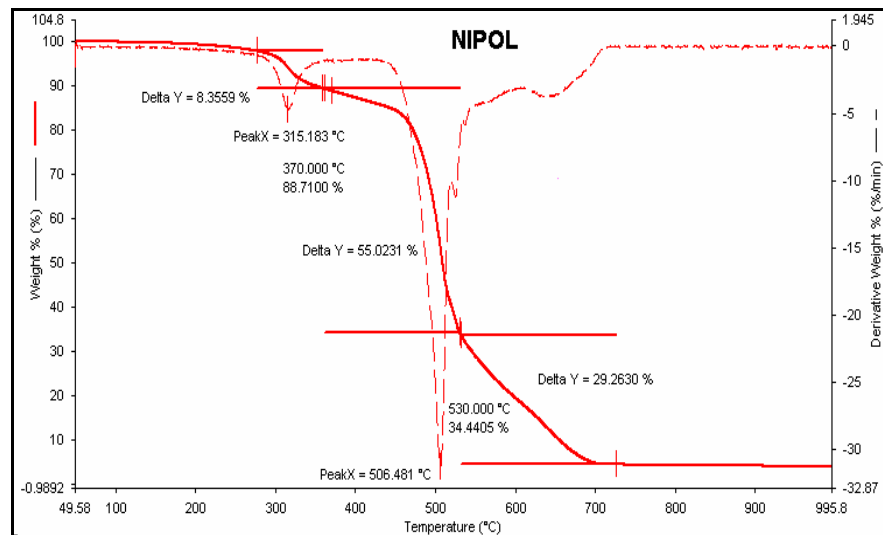


Figure 2.14 Thermogravimetric (TG)/Derivative thermogravimetric (DTG) curve showing thermal decomposition of organic material/resin [66].

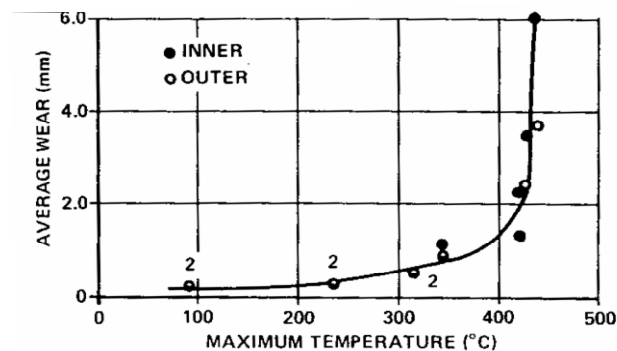


Figure 2.15 Brake pad material wear as function of temperature [67]

2.6.4. Macroshear

The removal of relatively large quantities of matter from the friction material surface is involved in this type of mechanism. Macroshear wear tends to be most distinct at the interface periphery but may also occur due the high temperature delineation of the pad surface such as that experienced during the final stages of metallization when foliate ferrous accretions, which have transferred to the friction material surface, become dislodged (Figure 2.16). Ultimately, macroshear wear is simply a descriptive mechanism of large-scale delineative adhesive wear [64].

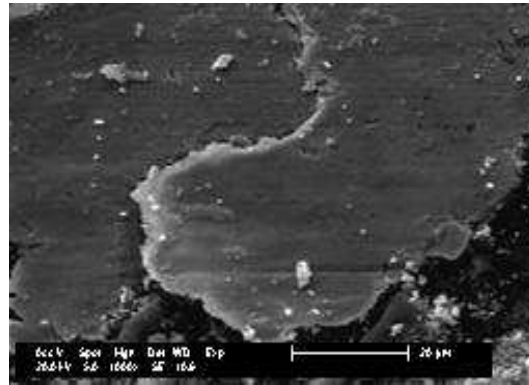


Figure 2.16 Micrograph of macroshear [19]

2.6.5. Fatigue Wear

Fatigue wear is the process by which material may become fractured and detached from its original surface via a fatigue mechanism in response to cyclic stress variations [64]. Such cyclic stress variations are manifold in the friction brake system where thermo-mechanical cycling and thermal shock situations abound. The natural upshot of such effects is the loss of material by the interconnection of surface fatigue cracks. It is important to note that if similar fatigue effects were observed to affect the rotor, this would not be considered the onset of a wear mechanism, rather as the onset of potential catastrophic failure via thermal rupture necessitating immediate replacement of the offending component.

When sliding surfaces make contact via asperities, wear can take place by adhesion and abrasion. However, it is conceivable that asperities can make contact without adhering or abrading and can pass each other, leaving one or both asperities

plastically deformed from contact stresses. As the surface and subsurface deformation continues, cracks are nucleated at and below the surface. Once the cracks are present (either by crack nucleation or from pre-existing voids or cracks), further loading and deformation causes cracks to extend and propagated. After a critical number of contacts, an asperity fails due to fatigue producing a wear fragment. In sliding contact, maximum shear stress occurs at the surface due the high friction which leads to surface fatigue [64]. Figure 2.17 shows SEM micrograph of fatigue wear.

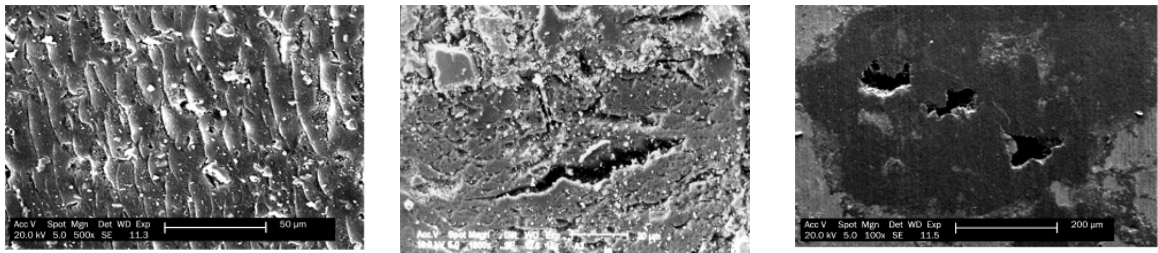


Figure 2.17 Micrograph of fatigue wear [68]

2.7. Effect of Load and Speed to Friction and Wear of Brake Pad Material

According to Orthwein [11], curves of the coefficient of friction as a function of load and speed between friction material and their mating surface are no longer available from many manufacturers. However, it was considered in braking system the coefficient of friction shows a decreasing behavior when the tangential velocity or normal load on the brake pad is increased [7, 8, 9], as shown in Figure 2.18. Other studies by Mahmoud [17] as well as Tanaka *et.al* [69] also found decreasing trend of coefficient of friction with incremental of load.

In his study, Mahmoud [17] show effect of load and sliding speed effect to the friction characteristic as shown in Figure 2.19. He was found that the increasing of normal force accompanied with three zones: (i) the first zone is oxide influence the coefficient of friction decreases to the minimum value and then increases, (ii) the second zone is metal deformation and plowing are prominent that the coefficient of friction still to increase to the maximum value and still at constant value, and (iii) the third zone is hydrostatic stress-enhanced plasticity that the coefficient of friction reduces with the increase of normal load. He also concluded that friction variation depends on the applied force. He stated that difference between the maximum and

minimum values increases with the increases of applied force, result in the increasing generated temperature which leads to reduce the coefficient of friction. Furthermore, Mahmoud also stated that high normal force tends to reduce the coefficient of friction to more than 20 %. However, there is no significant dependency of friction to speed found from both of the studies.

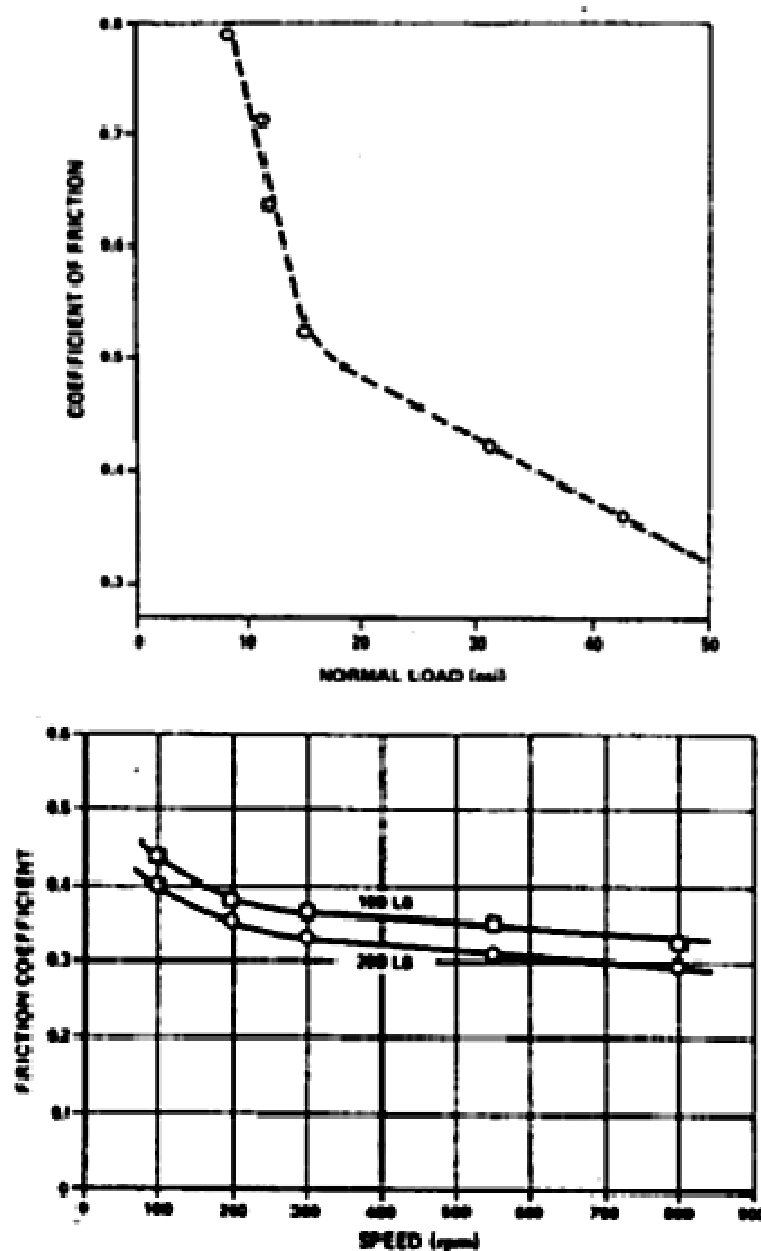


Figure 2.18 Effects of load and speed to coefficient of friction of brake pad material [7].

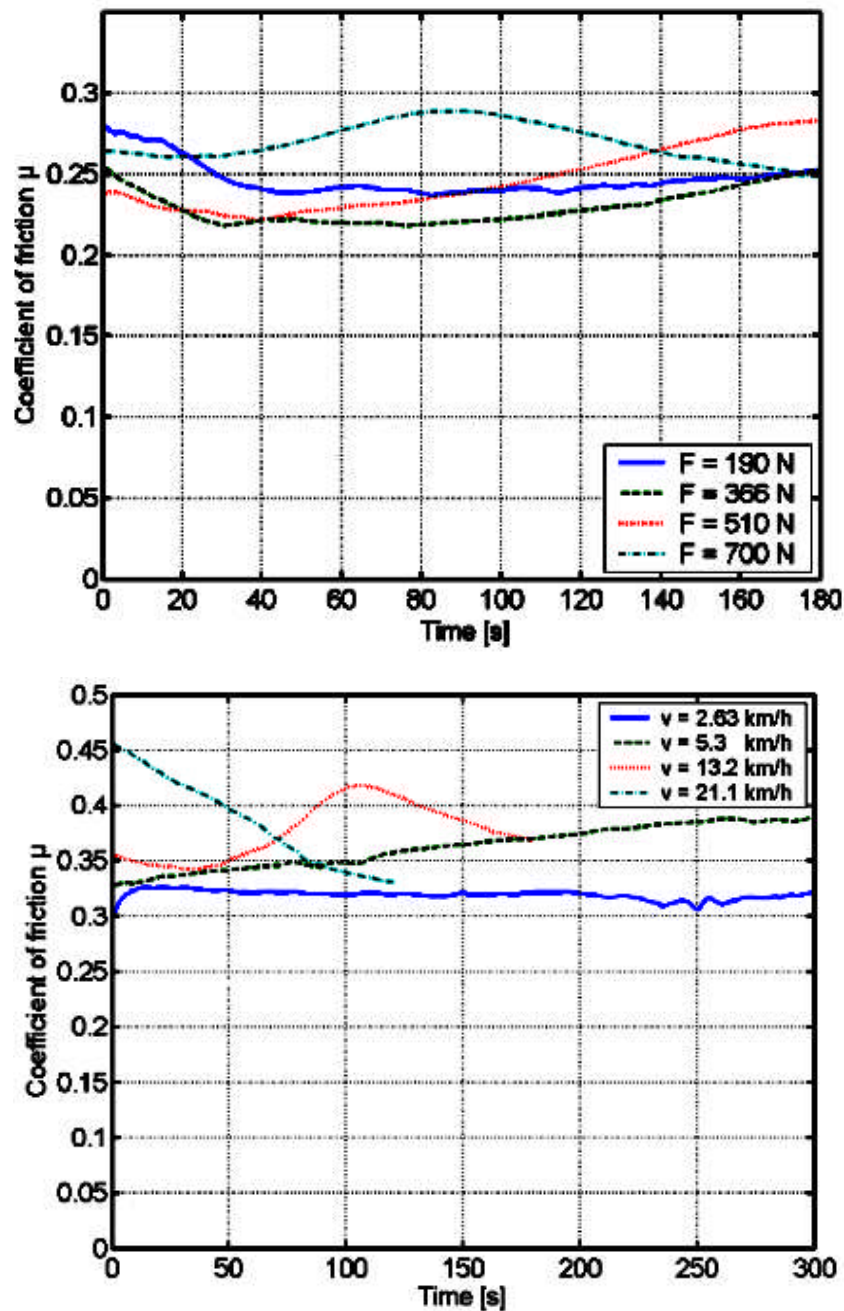
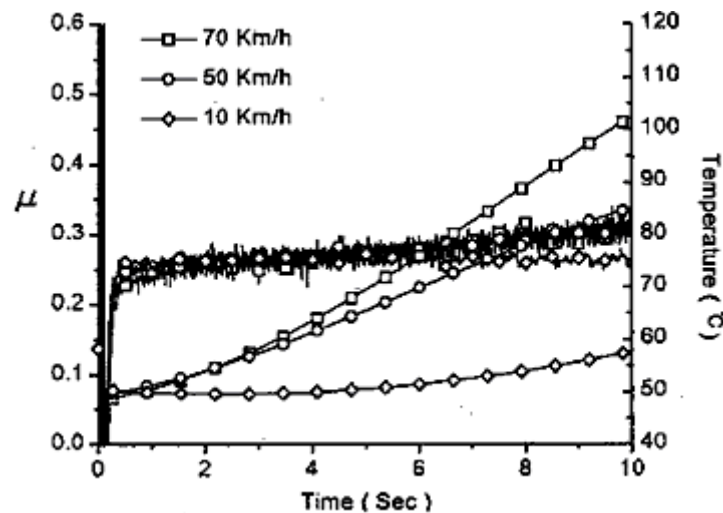


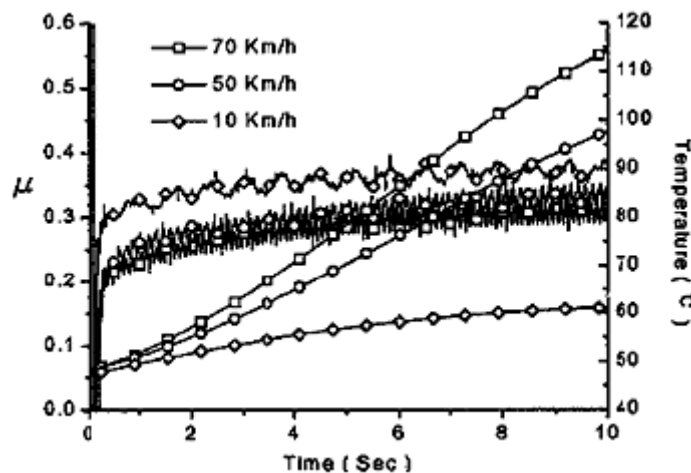
Figure 2.19 Variation of coefficient of friction at different applied force and sliding speed [17]

On another occasion, Kim and Jang [30] study of speed sensitivity to friction characteristic of NAO and low-steel friction materials. They found that the low-steel friction material was strongly affected with sliding speed and showing stick slip behavior at low speed. On the other hand, NAO materials showing less sensitivity to the sliding speed as shown in Figure 2.20. Blau *et.al* [70] recently reported that

working environment also affect the dependency of sliding speed to friction. They found that friction coefficient tends to decreased linearly with sliding speed at dry condition but behaved as power law under wet condition.



(a)



(b)

Figure 2.20 Changes of coefficient of friction as function of speed; (a) NAO, (b) Low-steel friction material [30]

Wear of brake pad material was found increase with incremental of load [8, 61, 63], but it shows little variation with braking speed [8, 22]. Figure 2.21 shows effect of load and braking speed to wear rate of brake pad material. According to Andersson [22], there typically a slight rise of wear below a rubbing speed of 2 m/s.

Brake asperity “flash” temperature are known to vary with speed. It was presumed that the variation of the lining wear rate and associated variation of friction level are related to flash temperature transition. At very high rubbing speed, the linings wear increase. This increase is greater when the initial brake drum or disk temperature is high. It is presumed that this speed effect is simply result of higher interfacial temperatures.

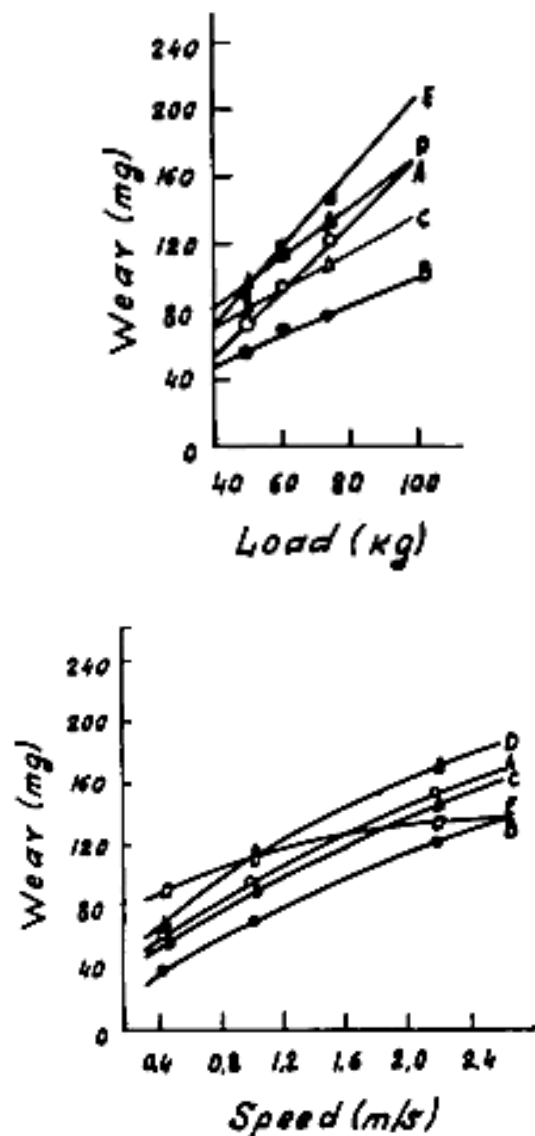


Figure 2.21 Effects of load and speed to wear of brake pad material [8]

Sataphathy and Bijwe [71] stated that wear performance of friction material also depends on material properties such as chemical and physical nature of the ingredients as well as operating parameter such as pressure, speed, temperature, *etc.*

By varying amount and nature of four abrasives (SiC, SiO₂, ZrO₂, and Al₂O₃) in their formulation, they confirmed that brake pressure is the most influencing operational parameter to wear, but they also found that composition and concentration of abrasive influencing dependency of wear to sliding speed. They reported that the braking pressure affected the wear of their friction material in order of SiC>>ZrO₂>Al₂O₃>SiO₂, whereas that of speed was in the order ZrO₂>>SiO₂>Al₂O₃>SiC. They also concluded that contribution of the abrasive content tended to abate the effects of operating variable such as pressure and speed.

2.8. Effect of Humidity to Friction of Brake Pad Material

A vehicle is designed not only to operate at a certain environment atmosphere but also designed to able to operate at any different type of environment and climate. Sometimes dry and sometimes wet, at some area has high humidity but another area has low humidity. In order to assure the braking system work well, brake pad materials demanded to maintain its stability at any environment.

According to Eriksson *et.al* [72], humidity has stabilizing effect on the coefficient of friction as shown in Figure 2.22. They assumed it might be correlated to the propensity to form tribofilms at different humidity. However, Blau *et.al* [10] found that; (i) the average coefficient of friction of brake pad material deviate under both dry and wet condition, (ii) high lubricant contents had high friction under dry conditions, and (iii) hand high abrasive content had high friction under wet condition.

Kim *et.al* [73] study the effects of humidity on friction characteristics of friction material related to solid lubricant contents (graphite, MoS₂, and Sb₂S₃) and friction materials without solid material but using barite and potassium titanate to replace the solid lubricant. They found that friction material containing graphite was strongly affected by the humidity and had lower friction at high humidity than the other, whereas the fillers materials (barite and potassium titanate) were not affected by humidity.

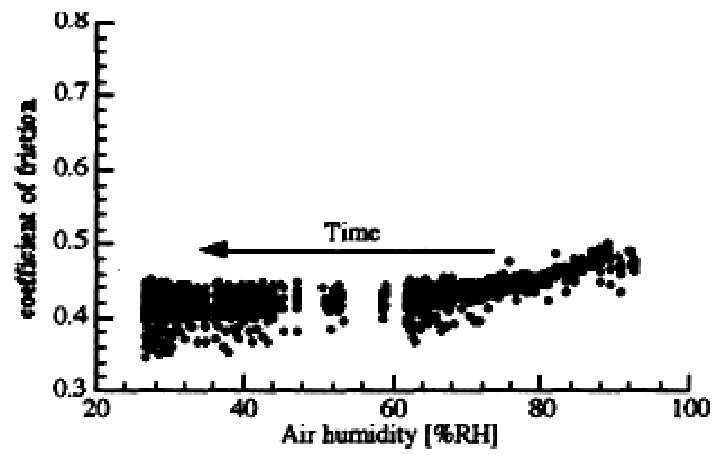


Figure 2.22 Effect of humidity to friction of brake pad material [72]

CHAPTER THREE

EXPERIMENTAL DESIGN

3.1. Introduction

Three LRT brake pad materials were used in this research, named as Pad-1, Pad-2, and Pad-3, respectively. According to its manufacturer, these brake friction materials are categorized as semi-metallic brake pad material. Pad-1 was brake pad material manufactured by foreign manufacturer; while Pad-2 and Pad-3 were locally developed brake pad materials. These friction materials were tested on a pin-on-disk apparatus complying with ASTM (American Society for Testing Material) G99-95a entitled “Standard Test Method for Wear Testing with a Pin on Disc Apparatus” (see Appendix B).

According to Czichos [74] the diagnosis of the friction and wear data corresponding to the laboratory test configurations and the test specimens requires special attention. This is due to the friction and wear are not materials properties, but related to material pairs and interfacial lubricant. Thus, inasmuch as brake pad material is commonly slid against gray cast iron disc, the counterpart of the brake pad material used in this research work was manufactured from the actual car gray cast iron brake disc. These material pair was experimentally tested under different contact pressures, sliding speeds, and relative humidity as experimental parameters. The results obtained from the tribological tests were mean coefficient of friction obtained from WINDUCOM V3 software and average weight losses from three readings for each set of tests condition. In addition, the microstructure of the surface of each sample was examined to study the wear mechanism in operation on the sliding surface.

3.2. Determination of Material Composition

Elements and compounds composed in the brake pad material used in this research were examined by Scanning Electron Microscope – Energy Dispersive X-Ray (SEM-EDX), X-Ray Fluorescence (XRF) and X-Ray Diffraction (XRD) before going through the friction and wear assessment. The combination of XRF and XRD

results not only improve the accuracy of the analysis result but also the range of samples that can be measured, including the samples which little or nothing unknown in advance [75].

3.2.1. Scanning Electron Microscope – Energy Dispersive X-Ray (SEM-EDX)

This technique is mostly used to study the morphology and composition of the brake pad material. Usually a SEM machine is equipped with Energy Dispersive X-ray (EDX), see Figure 3.1. The combination of SEM/EDX is known as a strong tool to get an overview of both topography and main composition of the surface of large number of the sample in relatively shorter time [76]. This feature has capability to do simultaneous non-destructive elemental analysis of the sample as well as quantify the detected elements. It also possible to map the elements found in SEM image by X-ray analysis.



Figure 3.1 SEM-EDX Machine (with courtesy of Universiti Teknologi Petronas)

Both brake pad and gray cast iron samples were analyzed by this technique. The sample for brake pad material was prepared by releasing the brake pad material from its backing plate and then was cut to a size of 40 mm × 40 mm × 5 mm whereas for gray cast iron material, the sample was prepared by machining the brake disc to

form a pin with a dimension of 6 mm diameter and 12 mm length. The brake pad sample was coated with gold or platinum by sputtering to avoid charging during examination in the SEM. This procedure is necessary due to the non-conductive behavior of the phenolic resin as matrix material. Sample was then mounted on the sample holder in SEM-EDX chamber for examination of the microstructural changes on the worn surface and EDX analysis

3.2.2. X-Ray Fluorescence

This technique is widely used for elemental analysis and chemical analysis of a material. X-ray fluorescence (XRF) works by comparing intensities of unknown sample with the intensities of standard sample. XRF measurements on the samples were performed with the Bruker-AXS S4 PIONEER and the SPECTRA^{plus} software, see Figure 3.2.

The composite brake pad and gray cast iron samples were cut to a dimension of 5 cm diameter and 5 mm thickness. The surface of the sample was ground with 320 grit number of SiC paper in order to flatten the surface. It was then placed into the oven and kept for 24 hours at temperature of 50 °C to ensure removed moisture in the sample. The samples were then put into the X-ray chamber for further analysis.



Figure 3.2 S4 Pioneer XRF Machine (with courtesy of Universiti Teknologi Petronas)

3.2.3. X-Ray Diffraction (XRD)

XRF provides highly accurate information about the elemental composition of a sample, but it cannot deliver direct phase information [75]. To confirm the phase identification results, and to obtain semi-quantitative phase amount estimates consistent with the actual elemental composition of the sample, combination of XRD-XRF analysis was performed. XRD analysis was performed using Bruker-AXS D8 Advance (Figure 3.3) where phase identification and quantification were analyzed with DIFFRACplus software packaged with EVA. According to Berhan *et.al* [76], combination of EDX and XRD analysis is required since the brake pad material consisting of several materials with different phase, including crystalline (metals graphite, silicates, oxides, and sulfide), and non-crystalline or semi-crystalline (plastics, rubber, and resins).

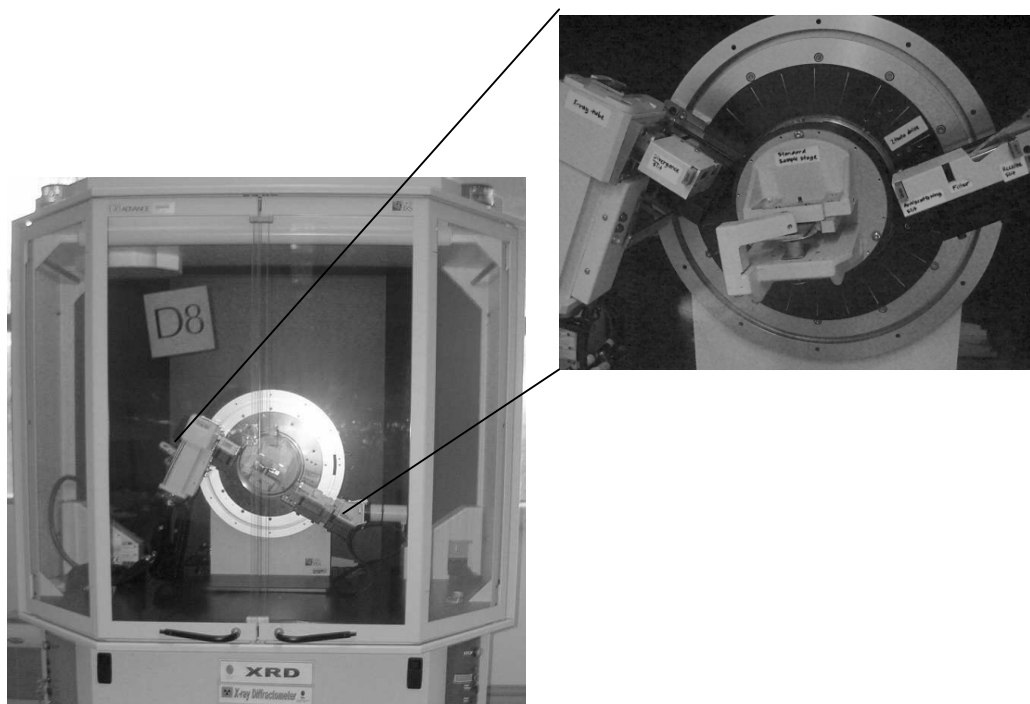


Figure 3.3 XRD Machine (with courtesy of Universiti Teknologi Petronas)

The brake pad sample was cut into a sample with a dimension of 5 cm diameter and 5 mm thickness. The surface of the sample was ground with 320 grit number of SiC paper in order to flatten the surface. It was then placed into the oven and kept for 24 hours at temperature of 50 °C to remove moisture in the sample. In

order to get a good peak of the phases present in the brake pad material formulation, the scan was chosen from 20 degree to 70 degree in 2θ of diffraction angle.

3.2.4. Thermogravimetric Analysis

Thermogravimetric analysis is a method of detecting changes in weight as function of temperature under defined atmospheric condition [66]. Friction material powders were taken from the each sample by drilling and then sample was placed in the cup which is then heated by the heater coil at the rate of 10°C per minute. Samples were measured in an open aluminum standard crucible of 70 μ l volume. The TGA temperature program ran dynamically from 30 °C to 600 °C at a heating rate of 10 °C/min. Nitrogen gas was employed as reactive gas with flow rate of 50 mL/min. The samples were heated under a nitrogen controlled atmosphere. The operation of this equipment will automatically stop when the temperature reaches 900 °C. The equipment used was a TG machine model METTLER TOLEDO TGA/SDTA851^e. The results were evaluated with the V8.10 STAR^e software package.

3.3. Tribological Test

3.3.1. Equipment

Ducom Multi Specimen Wear Tester MS- TR-706 was used to evaluate the friction and wear characteristics of the sample materials. A photograph of this equipment is shown in Figure 3.4. This equipment has a lot of capability to conduct tribological test such as: pin on disk, four ball test, cylinder on disc, and thrust washer on disc. Pin-on-disk apparatus was chosen to determine tribological characteristic of brake pad material in this work for the following reasons;

- i. Its capability as laboratory scale of testing materials under a wide range of loads and sliding speeds [77].
- ii. It is one of the most frequently used test systems for sliding friction and wear studies in the literature [10, 78, 79]
- iii. Flat-to-flat contact geometry provided by this apparatus similar to flat-on-flat geometry of disc brake system [77].

Three pins-on-disk configuration was used in this research. This configuration is shown in Figure 3.5. According to Elliot *et.al* [80], tribological results from three-pin-on-disk wear apparatus are often different from those of single pin types. A single pin is more prone to stick slip phenomena and preferential wear of the leading edge of the pin. Thus by using three pins-on-disc, it is expected the effect of stick slip phenomena could be reduced.

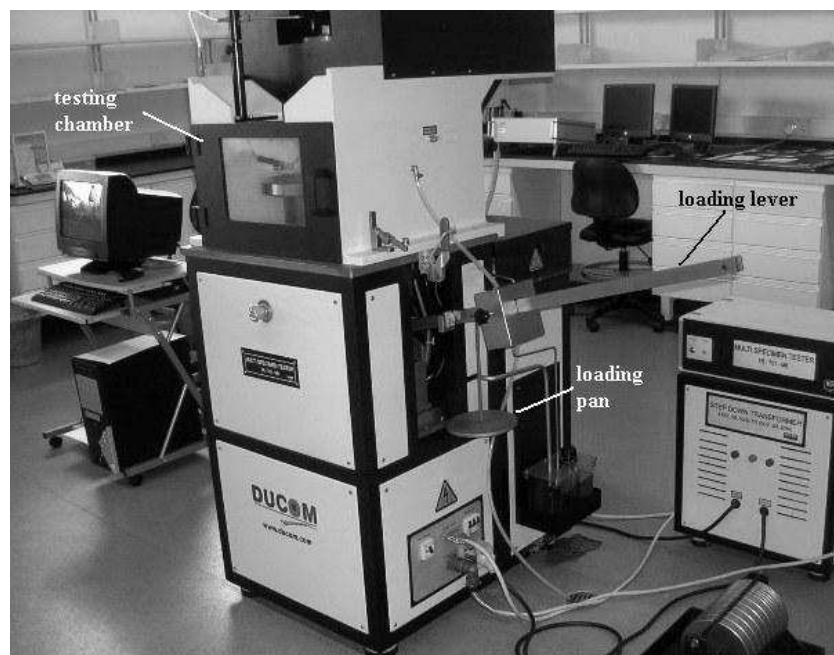


Figure 3.4 Multi-specimen wear tester

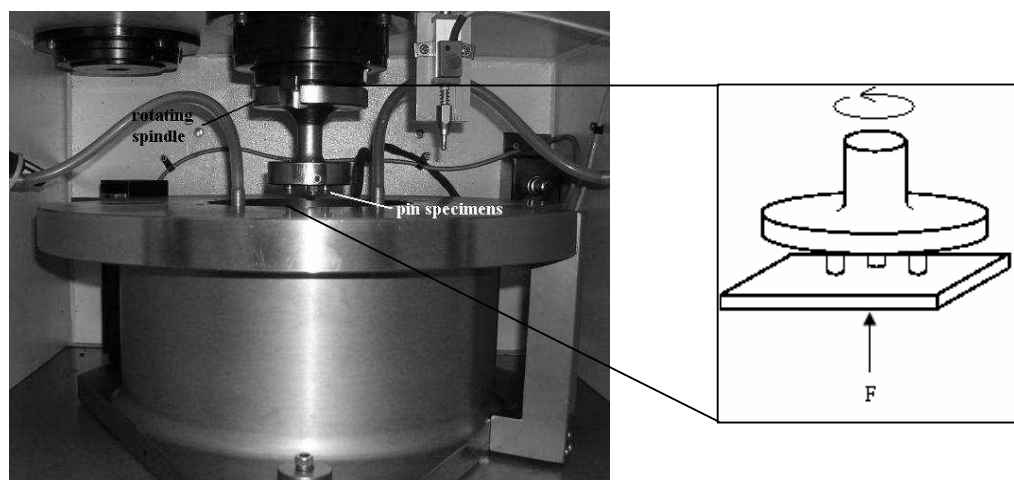


Figure 3.5 Three pins-on-disc test configuration used in this research work

In this apparatus, the pins are rotating against a stationary disc. The rotating pin is attached to a spindle driven by a servo motor with speed range 0 – 7200 rev/min. The wear track diameter of this pin on disk configuration was set at 30 mm. The normal load was applied by a loading lever, where a loading pan is hanging to place dead weights at one end of the lever. The loading lever is freely supported on a pivot and rests below the loading pin under the disc specimen holder. When the weight was placed on the loading pan, the lever lifted the loading pin and pushed it against load cell. The force exerted was measured by a load cell. When sliding occurs between friction surfaces, the frictional torque was measured by a beam type load cell. The frictional torque then divided by the radius of the contact point/circle to calculate frictional force. Thus, the coefficient of frictions of the sample was calculated from the ratio of frictional force and normal load. All of these actions were monitored by WINDUCOM 2006-v3 software, the supplied Windows-based data acquisition software program and data acquisition was acquired by National Instrument PCI 6221.

To control the environmental effect, the test area surrounding the spindle was enclosed on all sides in a chamber with a door in the front for placing and removing the specimen. It provided with a humidity sensor and ports as inlet and exhaust of the air from humidity chamber. The humidity was controlled by a humidity controller by blowing pressurized air passed a jar contained of distilled water and a jar contained Al_2O_3 , as shown in Figure 3.6.

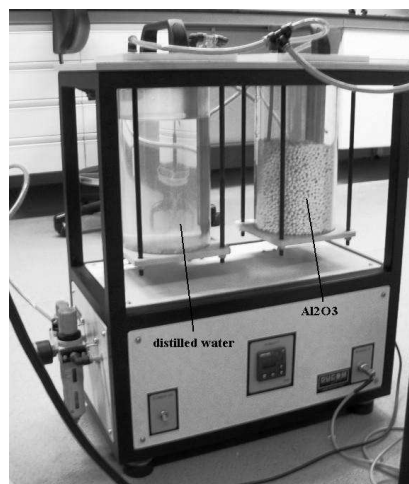
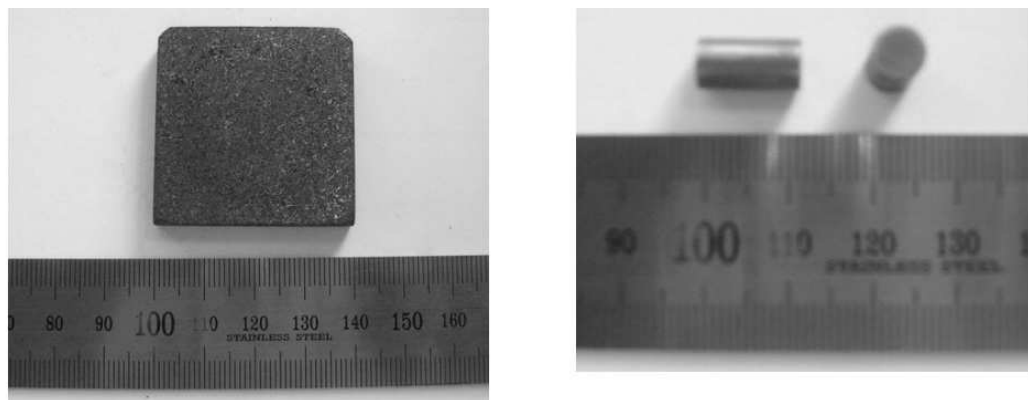


Figure 3.6 Humidity controller

A PID senses the present of the humidity value and sends suitable solid state relay's (SSR) to control the required humidity. To increase the humidity, the solenoid of jar contained distilled water is opened to increase its value. On the other hand, for decreasing the humidity value, the solenoid of Al_2O_3 jar is opened. Thus by continuous opening and closing operation automatically, the required humidity is achieved.

3.3.2. Sample Materials

Three semi metallic LRT brake pad materials were used in this work. The physical and mechanical properties are as per Appendix C. All of these materials were arranged to be the disc or pad in the testing configuration. The brake pad materials were released from backing plate by using a hacksaw, then cut to a size of $40 \text{ mm} \times 40 \text{ mm} \times 5 \text{ mm}$. Subsequently, the sample was ground using 320 grit number SiC paper to ensure each sample is having similar a surface roughness. This sample material was then weighted and mounted on the sample holder. Gray cast iron was chosen to be a pin material which is commonly used as a brake disc in the brake system. The pin was machined from the brake disc for passenger car to a diameter 6 mm and length 12 mm. The microstructure of the pin is shown in Appendix D. Figure 3.7 shows the sample materials.



(a) Brake pad

(b) Pin

Figure 3.7 Sample materials

3.3.3. Experimental Procedure

The tests were consisted of three modes; the first mode was to determine the effect of the contact pressure to friction and wear on sample at standard room

temperature (23 – 25 °C) and humidity (60 – 65 %RH). The experiments were carried out at five different contact pressures 1 MPa, 1.5 MPa, 2 MPa, 2.5 MPa and 3 MPa whereas the sliding speed and duration was kept constant at 600 rpm and 12 minutes, respectively.

The second mode was to determine the effect of the sliding speed to friction and wear of the sample at standard room temperature (23 - 25 °C) and humidity (60 – 65 %RH). However, the samples were slid at five different sliding speeds, 300 rpm, 600 rpm, 900 rpm, 1200 rpm, and 1500 rpm whereas, the contact pressure and duration was kept constant at 1 MPa and 12 minutes, respectively.

The last mode was meant to determine the effect of relative humidity to friction characteristics of the materials. The samples were tested under 3 types of relative humidity, low humidity (10-15 %), medium humidity (55-65%), and high humidity (85-90 %). The tests were carried out at constant contact pressure of 2 MPa and sliding speed of 600 rpm as suggested by [10, 73]. At each humidity level test, the samples were kept in the chamber for 1 hour to make sure that the required humidity level had stable in the chamber. The entire tests were conducted within 12 minutes with initial temperature of 25 - 30 °C. The weight of the sample before and after test was measured using an electronic balance model Metler Toledo AX 540.

The experimental procedures basically following ASTM G99 standard procedure:

- i. Prior to tribological test, the sample was cleaned, dried and weighted to nearest 0.0001 g
- ii. The sample was positioned into the holding device and then pin was securely inserted into its holder. This procedure is to ensure that the disk is fixed perpendicular to the axis of the rotation.
- iii. The balancing mass was added to the lever system to develop the selected force, so that the pin is pressed against sample.
- iv. Close the experimental chamber.

- v. Pushes the power on multi specimen tester and set the speed to the desired value while the pin in contact with the sample.
- vi. Set the experimental time to the desired time.
- vii. Begin the test with the specimens in contact under load. The test is stopped when the desired experimental time is achieved. The test should not be interrupted or restarted.
- viii. The specimens were removed and cleaned off any loose wear debris. Note and record the existence of feature on or near the wear scar such as: protrusions, displace metal, discoloration, microcracking, or spotting.
- ix. Finally, the specimens were reweight to the nearest 0.0001g accuracy.

The experiment was repeated three times for each experimental parameter and the arithmetic mean of the three readings was taken as the average weight loss and coefficient of friction.

3.3.4. Calibration

Load sensor was calibrated using calibration unit consist of a calibrated 5000 N load cell with indicator. Load calibration was done by applying the death weight to the calibrated load cell. The percentage of error was calculated by comparing seven applied load shown in Winducom software and load cell indicator. The percentage of error was obtained was in the range of 0.09 – 0.2 %

Speed sensor was calibrated using an infrared calibrated tachometer. The percentage of error was calculated by comparing eight different speeds indicated on the Winducom software and calibrated tachometer. The percentage of error obtained was in the range 0.1 – 0.45 %.

Frictional torque was calibrated by applying 1 mV input voltage to the card from a calibrated voltage source, flat table with C clamp, loading pan, and dead weight. The friction torque was calculated from applied load multiplied by distance of frictional force sensor to spindle center (210 mm). The percentage of error was calculated by comparing friction torques indicated in the Winducom software and

calibrated card from five applied loads. The percentage of error obtained was in the range 0.19 – 0.97 %.

3.4. Surface Characterization

3.4.1. Surface Profile

A surface roughness tester model Mahr Perthometer PGK-120 was employed to measure surface profile (Figure 3.8). Surface profile was detected by tracing randomly selected cross-sectional areas of wear track. The get conviction data, at least three cross-sections in the wear track were measured. Ra (center line average) surface roughness was determined from the profilometer software directly. The mean average of Ra was calculated from three measurements.



Figure 3.8 Surface Profilometer

3.4.2. Surface Morphology

The surface morphology of the sample material was analyzed by SEM-EDX model LEO-1430VP OXFORD INCA instrument. The SEM technique has advantages due to its high resolution and large depth of field, which produce apparent three dimensional images, provide invaluable information about the surface over a wide range of magnification [77]. Moreover, the interaction of the electron beam with

the specimen surface provides different signal which can be monitored independently [81].

Operation of SEM is basically based on scanning the surface using a finely focused beam of electrons and detecting a signal associated with a point-by-point interaction and using it to modulate the brightness of a cathode ray tube (CRT), which is also scanned in synchronization with the beam. The changes in the brightness represent changes in particular property within the scanned area [81].

There are two kind of SEM signal commonly used in study tribological studies of brake pad material [82]: secondary electron (SE) and back scattered electron (BSE). The SE signal is operated at low voltage [81] and very useful in obtain the surface topography and morphology [3, 82, 83]. On the other hand, the back scattered electron signal is used in detecting compositional variation [81].

To optimize the quality of the image, the operational parameter such as accelerating voltage, beam diameter, beam current, angle of incidence, line and frame speeds should be adjusted [81]. In this research, worn surface of the brake pad material was observed by selecting the accelerating voltage in the range of 10–20 kV, beam current 100mA with walking distance 120 mm to give better focus to investigated area, and 500–1000× magnification scales. EDX analysis was performed using 20 kV accelerating voltage and 100mA beam current.

CHAPTER FOUR

RESULTS AND DISCUSSION

The data obtained from experimental studies of this research work are presented and discussed in this chapter. The results of material characterization in this work was presented and discussed in section 4.1. The material characterization was done by a combination of four methods that are commonly used; (i) energy dispersive X-ray (EDX), (ii) X-ray fluorescence (XRF), (iii) X-ray diffraction (XRD), and thermogravimetric analysis (TGA). The results from tribological test are presented and discussed in section 4.2 to section 4.3. The micrograph of the worn surface and wear mechanism are also presented and discussed in this chapter.

4.1. Material Characterization

4.1.1. EDX Analysis

The tribological properties of brake pad material are believed to be much affected by its composition [1, 2, 33, 34, 41, 43, 48]. Therefore, prior to the tribological studies, it is important to predict the elements and compound composed in the brake pad material.

The typical output of EDX analysis is EDX spectrum. The spectrum shows the peaks equivalent to the energy levels for which most X-rays are penetrable. The peaks are typical for each atom that matches up to a single element. The higher a peak in the spectrum indicates more concentration of the element in the specimen.

The elements and typical spectra of the EDX analysis of the samples (Pad-1, Pad-2, and Pad-3) are presented in Table 4.1 to Table 4.3. It was found that all the three samples were contained of same elements of carbon (C), oxygen (O), iron (Fe), barium (Ba), aluminum (Al), silicon (Si), and sulfur (S).

High amount of Carbon (C) was found in all sample materials. High carbon peaks in the EDX analysis is possibly due to the organic composition (resin, graphite, friction dust, and rubber) in the brake friction material and absorbed carbon in the

analysing chamber or the sample has been exposed to atmosphere during storage. Therefore, another analytical method such as XRD and TGA are required to provide more conclusive analysis for this element.

The SEM-EDX analysis result of Pad-1 is presented in Table 4.1. The content of each element found in Pad-1 are reported in %-wt. Iron (Fe) was found to be dominant in all samples, 20.77 %-wt, compared to other elements barium (Ba) 2.83 %-wt, magnesium (Mg) 1.23 %-wt, sulfur (S) 0.59 %-wt, aluminum (Al) 0.32 %-wt, and silicon (Si) 0.16 %-wt).

Table 4.1 Pad-1 SEM-EDX Analysis Result

Pad-1		
Element	Weight %	Atomic %
C K	62.75	81.47
O K	11.34	11.05
Mg K	1.23	0.79
Al K	0.32	0.19
Si K	0.16	0.09
S K	0.59	0.29
Fe K	20.77	5.80
Ba L	2.83	0.32
Totals	100	100

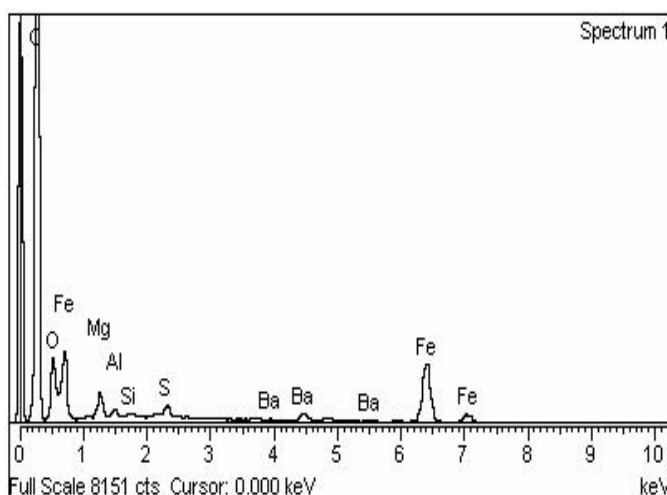


Figure 4.1 shows the surface topography and elemental mapping of the Pad-1. From the surface topography, the different constituents in the material can be identified from its color contrast. For example; the lightest represents the metallic constituents, whilst the darkest represents carbon.

Another advantage of SEM-EDX analysis is its capability to examine the elemental mapping. However, only view element with significant appearance able to be detected. The elemental mapping of Pad-1 is shown in Figure 4.1 as well. The presence of carbon, steel fiber, iron oxide or iron powder and magnesium oxide can be seen clearly in the elemental mapping. This elemental mapping suggests that short iron/steel fiber is used in the formulation. It is also observed that the iron/steel fibers as well as iron oxide are well distributed on the surface.

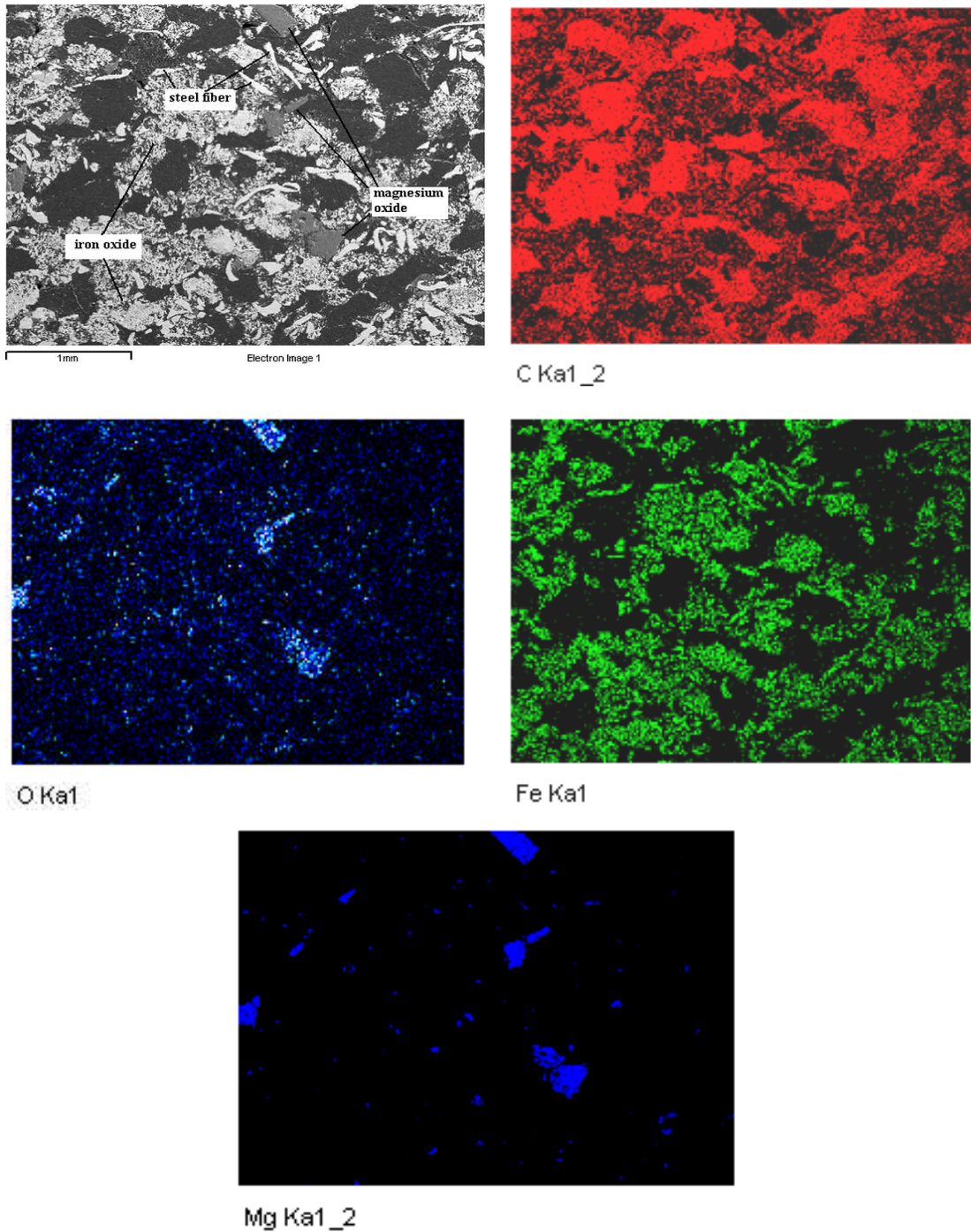


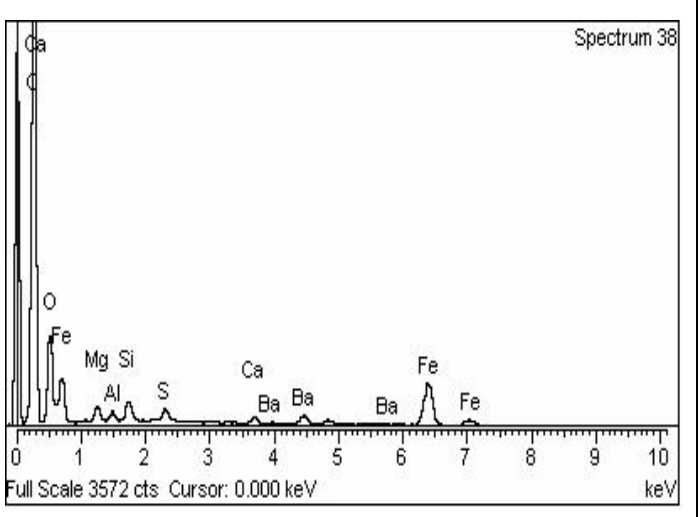
Figure 4.1 Surface topography and elemental mapping of Pad-1

The SEM-EDX analysis result of Pad-2 is presented in Table 4-2. Similar to Pad-1, iron is found to be dominant in Pad-2 as well. It is observed that Pad-2 contains the same element as in Pad-1 with the addition of calcium (Ca). The percentages of Ba and Si in Pad-2 material are higher than Pad-1 while the percentage

of Mg is lower. The content of other elements such as Al and S is about the same in both Pad-1 and Pad-2.

Table 4.2 Pad-2 SEM-EDX Analysis Results

Pad-2		
Element	Weight %	Atomic %
C K	62.29	78.66
O K	16.08	15.24
Mg K	0.65	0.41
Al K	0.34	0.19
Si K	0.84	0.46
S K	0.60	0.29
Ca K	0.54	0.20
Fe K	15.50	4.21
Ba L	3.14	0.35
Totals	100	100



The surface topography and elemental mapping of Pad-2 are shown in Figure 4.2. The elemental mapping indicates clearly the presence of carbon, steel fiber, iron oxide as well as barium oxide in Pad-2. However, the steel fibers are of different shapes and sizes, which seem to indicate that a combination of long and short fibers as well as granule type are used in the formulation of Pad-2. From the surface topography, it is also observed that the particles of iron powder/iron oxide are quite well distributed.

The SEM-EDX result of Pad-3 is presented in Table 4.3. Ten (10) elements were detected in the Pad-3. The significant difference observed in Pad-3 sample is the presence of copper (Cu). This indicates that copper-based material was used in this formulation. The existence of copper in the material could be in the form of copper sulfide, copper fiber, or copper oxides, which are commonly used as friction modifiers in brake pad materials [27]. Iron is still the dominant element and its content in Pad-3 is more or less equal to the content in Pad-2. It is also observed that the percentages of Mg, S, and Ca are also more or less equal in both Pad-2 and Pad-3 but their peak height are different. The Ba content in Pad-3 is about the same as in Pad-1 but less than Pad-2. However, Pad-3 shows higher peak than Pad-1 or Pad-2. The percentages of Al and Si are higher than those in Pad-1 and Pad-2.

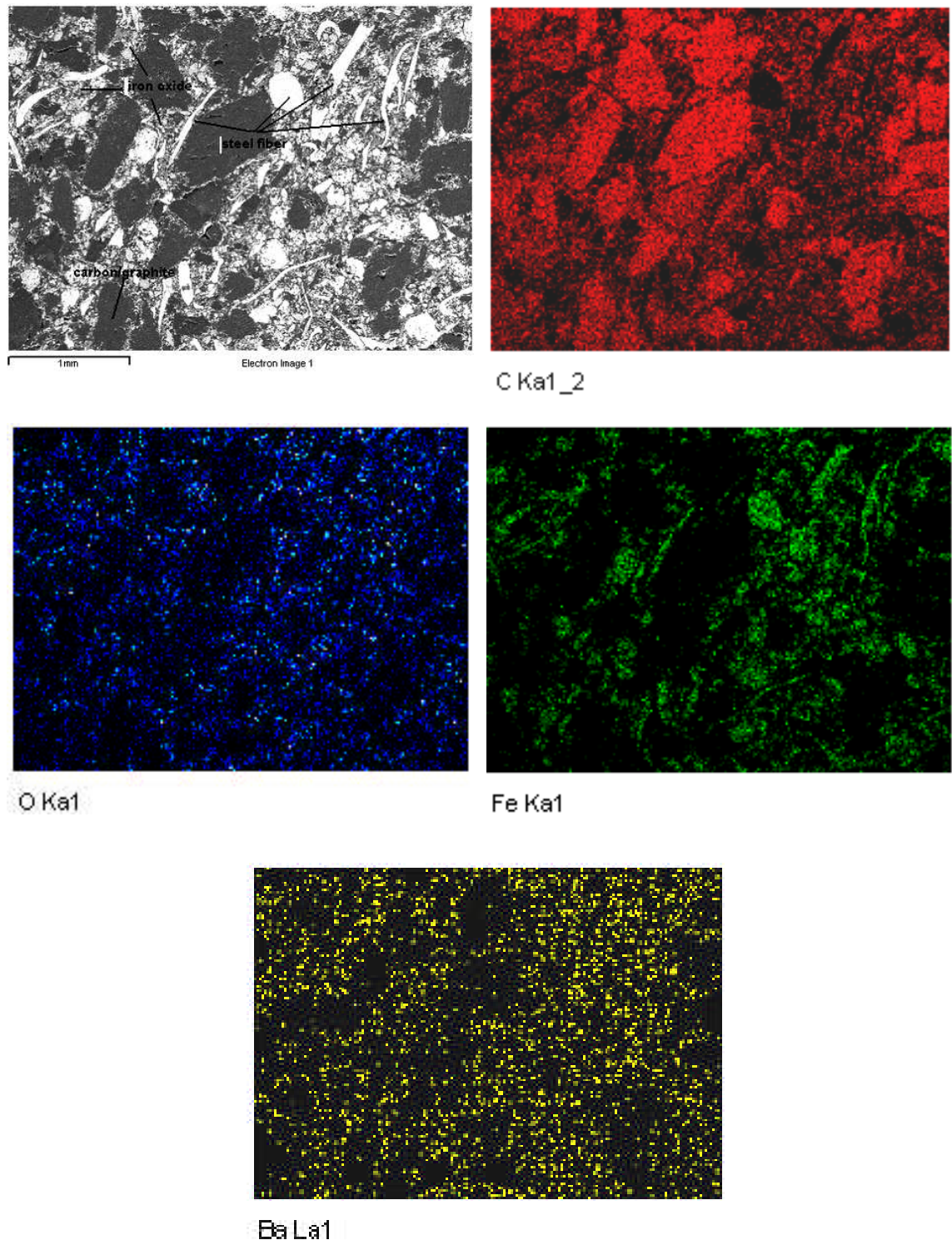
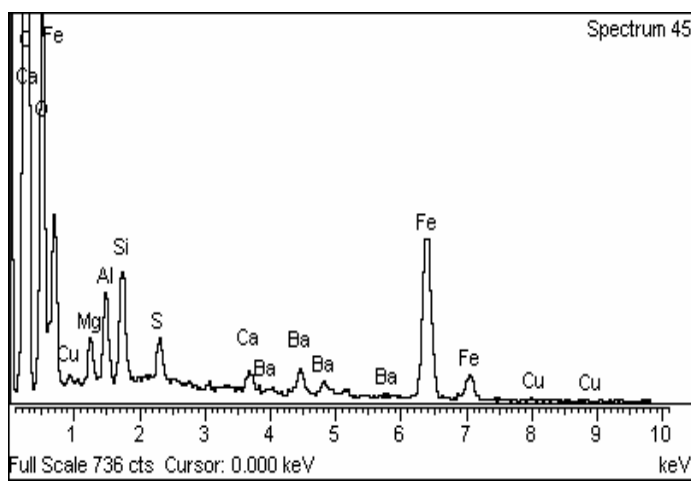


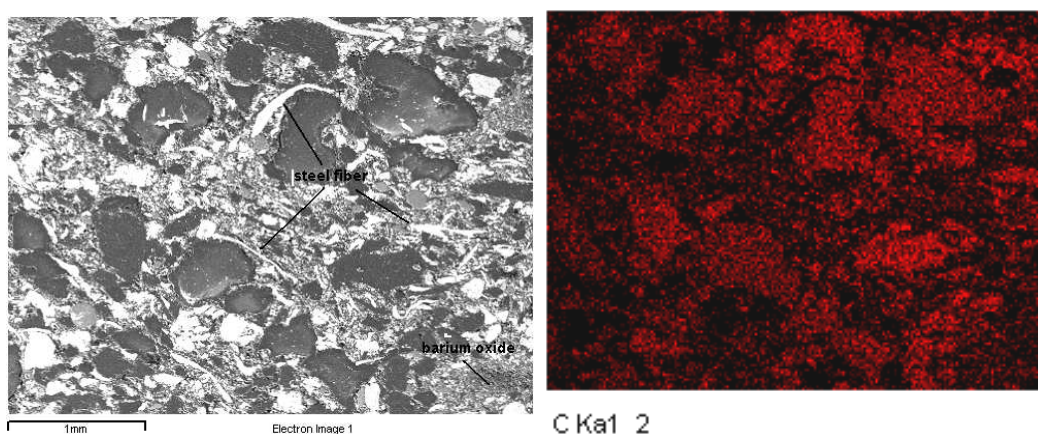
Figure 4.2 Surface topography and elemental mapping of Pad-2

Table 4.3 Pad-3 SEM-EDX Analysis Results.

Pad-3		
Element	Weight %	Atomic %
C K	59.35	75.94
O K	17.83	17.13
Mg K	0.58	0.37
Al K	0.96	0.55
Si K	1.41	0.77
S K	0.63	0.30
Ca K	0.42	0.16
Fe K	16.00	4.40
Cu L	0.43	0.10
Ba L	2.39	0.27
Totals	100	100



The surface topography and elemental mapping of Pad-3 is shown in Figure 4.3. Similar to Pad-2, the presence of steel fiber, iron oxides as well as barium oxide in the material can be clearly seen from the elemental mapping. However, steel fibers in fewer amounts compared to Pad-1 and Pad-2 were revealed. This indicates that different types and shapes of steel fibers are used in this material. However, the particle distribution of iron powder/iron oxide is less than previous samples. Comparison of the elemental composition of the samples detected by EDX technique are detailed in Appendix E.

**Figure 4.3** Surface topography and elemental mapping of Pad-3

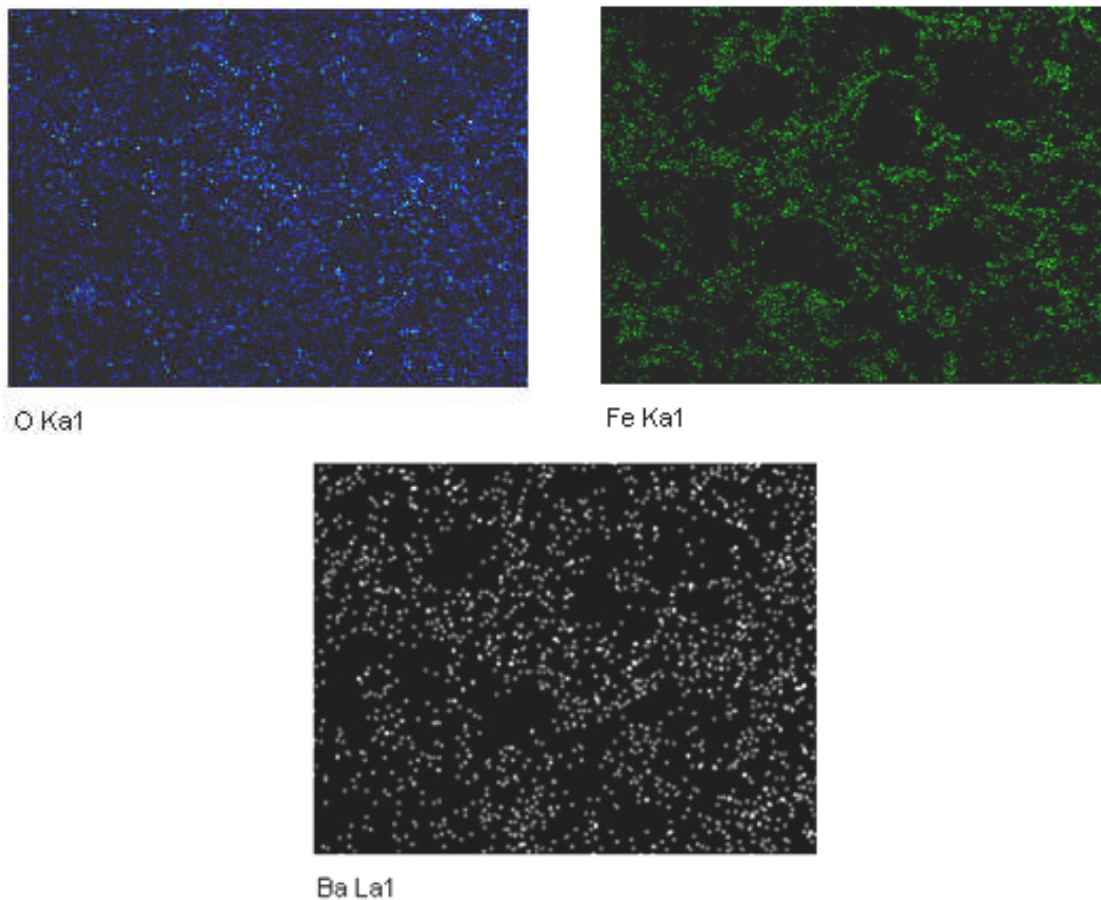


Figure 4.3 Surface topography and elemental mapping of Pad-3 (*Continue*)

4.1.2. XRF Analysis

The SEM-EDX results provide information pertaining to single element and elemental mapping but other information such as oxide could not be obtained. Therefore, XRF method was used to determine other elements which could not be found by SEM-EDX. Plenty of oxides were found by XRF, however only oxides which has percentage more than 0.5 % was taken into consideration. The results of the XRF characterization are presented in Table 4.4.

More than 60 %-wt. of iron oxide was found in all sample materials. However, the iron oxide content in Pad-2 is the highest among all the samples. This result shows that oxide element in the samples mainly consist of iron oxide. Iron oxide is usually used as an abrasive material, which is used to increase friction gripping at initial stop, maintains the cleanliness of mating surface and controls the build up of friction film [26, 27, 83]. The presence of aluminum oxide and silicon oxide is also possibly

related to the existence of abrasive material in the brake pad materials investigated in this study [23, 27]. Significant amount of sulfur trioxide/sulfite (SO_3) also detected. Filler materials such as calcium oxide (quicklime), magnesium oxide (magnesia), zinc oxide (ZnO) are also detected.

Table 4.4 Oxide elements in the sample formulation by XRF analysis

Elements	Pad-1 (%-wt.)	Pad-2 (%-wt.)	Pad-3 (%-wt.)
Fe_2O_3	65.8	68.3	61
SO_3	10.8	6.3	4.24
Al_2O_3	5.18	2.09	6.58
SiO_2	5.15	5.28	9.31
BaO	4.12	9.81	7.38
ZnO	3.76	0.0201	0.0275
CaO	1.64	1.95	3.49
Sb_2O_3	0.921		
K_2O	0.436	0.313	0.266
Na_2O	0.431	0.381	0.352
MgO	0.423	4.07	4.07
CuO	0.376	0.0402	1.77
MnO	0.361	0.349	0.566

4.1.3. XRD Analysis

As mentioned earlier, XRD analysis was carried out in order to determine the element and compound that are not detectable by SEM-EDX and XRF techniques. The XRD analysis result is shown in the form of phase spectrum of a compound. Only compounds with typical peaks that match the peak in the main spectrum will be reported. The phase spectra of pad-1, pad-2, and Pad-3 are shown in Figure 4.4 to Figure 4.6 and the compounds in the composition of samples is shown in Table 4.5.

Several similar compounds were found in all investigated materials. Graphite, silicon oxide (quartz), vermiculite, and wollastonite were found in all samples. The existence of graphite shows possibility used as a solid lubricant in this material. Vermiculite is typically used as a friction modifier [23, 48, 84]. Wollastonite (CaSiO_3) is a type of silicate material commonly used in friction material formulation (brake and clutches) as a replacement of asbestos fiber along with vermiculite [3, 26, 27].

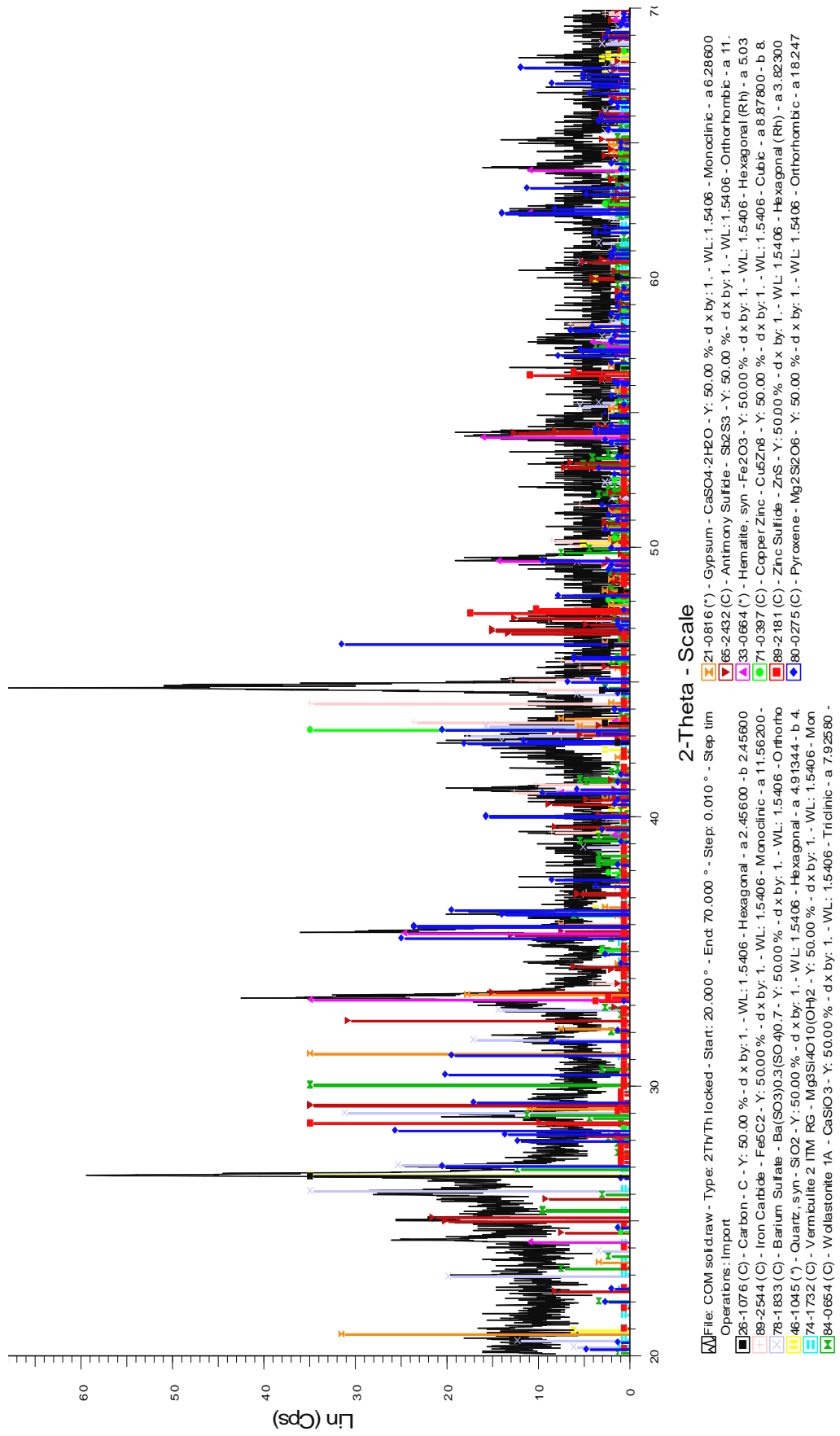


Figure 4.4 XRD Diffractogram of Pad-1

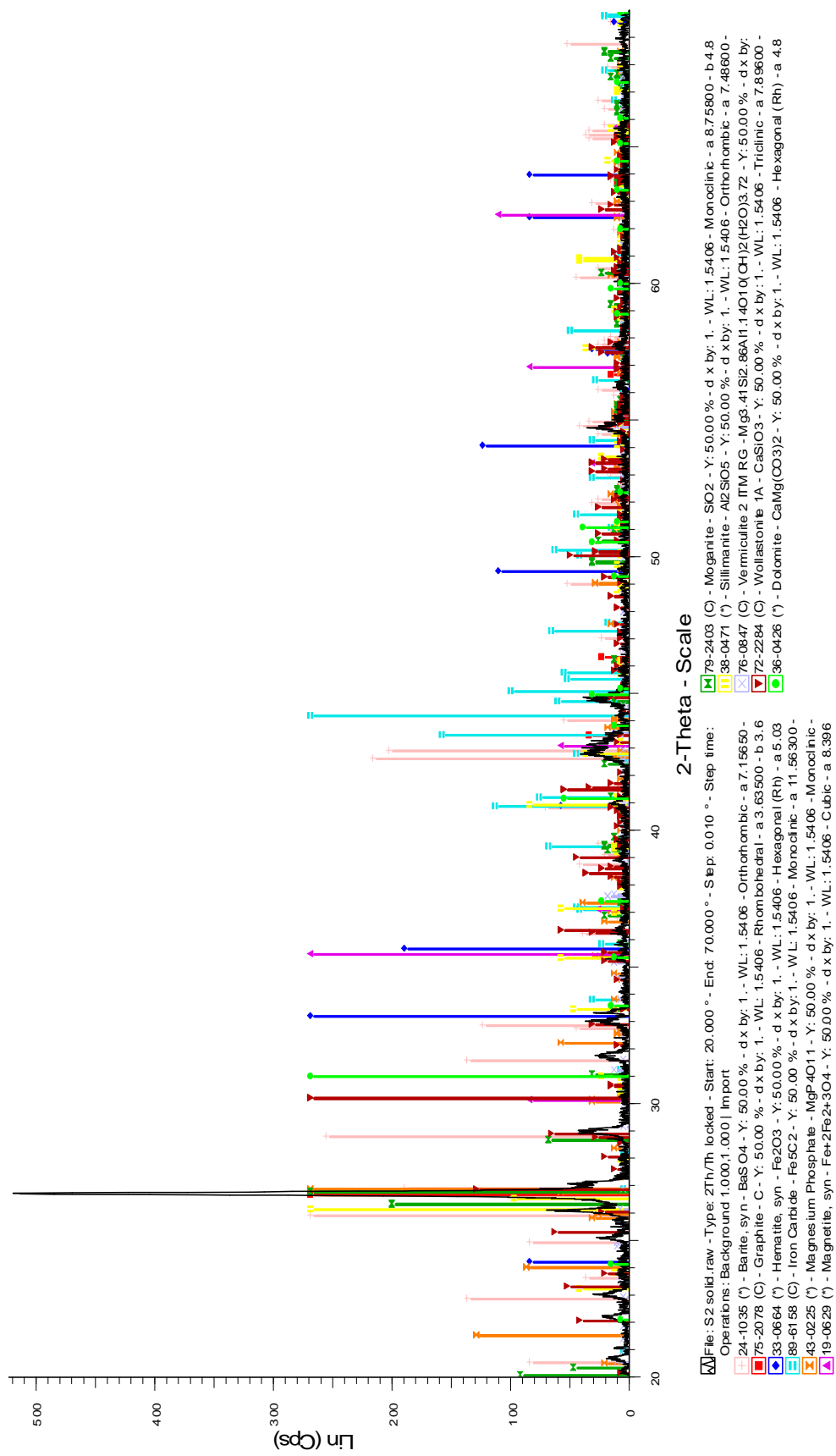


Figure 4.5 XRD Diffractogram of Pad-2

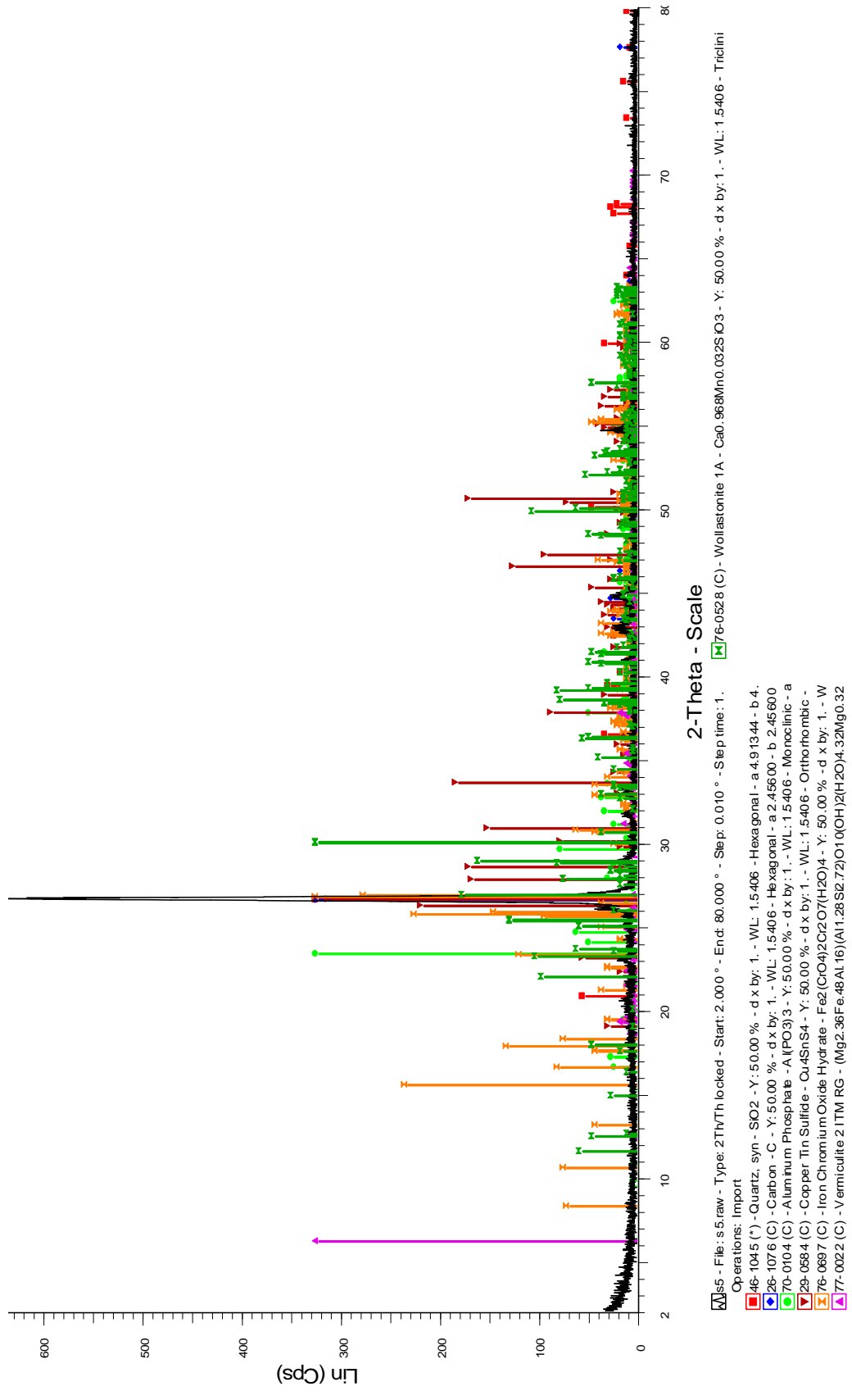


Figure 4.6 XRD Diffractogram of Pad-3

Table 4.5 Compounds in the samples detected by XRD technique

Pad - 1	Pad - 2	Pad - 3
Carbon	Graphite	Carbon
Barium sulphate, BaSO ₄	Barium sulphate	-
Quartz, SiO ₂	Quartz	Quartz
Vermiculite, MgSi ₄ O ₁₀ (OH) ₂	Vermiculite	Vermiculite
Wollastonite, CaSiO ₃	Wollastonite	Wollastonite
Gypsum, CaSO ₄ 2H ₂ O	-	-
Antimony sulphide, Sb ₂ S ₃	-	-
Hematite, Fe ₂ O ₃	Hematite	-
Copper zinc, Cu ₅ Zn ₈	-	-
Zinc sulphide, ZnS	-	-
-	Magnesium phosphate, MgP ₄ O ₁₁	-
-	Domolite, CaMg(CO ₃) ₂	-
		Copper tin sulphide, Cu ₄ SnS ₄

It was also observed that gypsum is contained in Pad-1. Gypsum might be used as a replacement for asbestos fiber too. Several other mineral such as dolomite, and magnesium phosphate were also detected. These minerals are probably used as fillers. Different types of copper alloys were found in Pad-1 (copper zinc) and Pad-3 (copper tin sulphide), which were probably used either as a solid lubricant or reinforcing fibers.

4.1.4 Thermogravimetric/Derivative Thermogravimetric (TG/DTG) Analysis

The curves of TG/DTG analysis of the samples are shown in Appendix F – Appendix H. TG curve of Pad-1 showed weight gained behaviour at early section before degraded associated to reaction of the material with atmosphere in the testing environment [85]. The initial weight lost of this sample was occurred around 80 °C. TG/DTG curve of Pad-2 shows its initial weight lost started at temperature around 60 °C and TG/DTG curve of Pad-3 show its initial weight lost started at around 60 °C. Generally all polymeric/organic materials will be evaporated at 600 °C [86] and its mass

decrease is due to production of gaseous products (carbon monoxide, water vapour and carbon dioxide). Whereas, other ingredients such as; antimony trisulfide start to decomposed at around 200 °C, molybdenum disulfide at around 300 °C [1], iron oxide start to decompose at around 220 °C [66], barium at 380 °C [66], and graphite at 800 °C [87].

Organic and inorganic contents can be determined from the TG/DTG curve as well. Table 4.6 shows organic and inorganic content in the samples. The percentage of the organic materials is calculated by dividing the weight lost of the organic material at 600 °C with the mass of the sample used.

Table 4.6 Organic and inorganic contents

Elements	Weight %		
	Pad - 1	Pad - 2	Pad - 3
Organic	2.11	8.10	5.48
Inorganic	97.89	91.90	94.52

Based on the results of SEM-EDX, XRF and XRD analyses, predictions on the composition of the sample could be made. The results of brake pad elemental composition detected by EDX/XRF/XRD technique are depicted in Appendix I. The large amount of iron in the composition of all samples suggests that the brake pad materials are a semi metallic type of friction material. It observed that Pad-1 and Pad-3 are having the highest content of metallic material and organic material, respectively (Table 4.6).

Pad-1 is considered to have a low organic component with high solid lubricant in its formulation. This assumption is based on the result of thermo-gravimetric analysis as well as XRF; which show a high percentage of sulfur trioxide/sulfite (SO_3), zinc oxide (ZnO), antimony oxide (Sb_2O_3) in this sample as compared with other samples. Furthermore, XRD result shows the presence of graphite, brass, antimony sulphide, and zinc sulphide (Figure 4.4) even these elements were not detected by SEM-EDX and XRF technique. Iron oxide, silicon oxide, aluminum oxide are used as abrasive material. The magnesium oxide, wollastonite, and vermiculite are used as a filler material in this sample.

Pad-2 is considered to use higher organic material and filler especially barium sulphate in its formulation. This could be due to the highest percentage of barium oxide in Pad-2 compared to other samples and the presence of some sulfur trioxide too. In addition, calcium oxide and magnesium oxide are also used as fillers. The low percentage of sulfur trioxide as shown on Table 4.4, indicates that this material contain less solid lubricant than Pad-1. However, SEM-EDX and XRD results show that graphite is contained in this material. This indicates that this material used graphite as its lubricant.

Pad-3 is considered to contain quite high organic material, but less than Pad-2, and abrasive material in its formulation. This can be seen from the highest percentages of SiO_2 and Al_2O_3 among all the samples (Table 4.4). It also has about the same amount of calcium oxide and magnesium oxide as Pad-2. The elemental mapping of this sample (Figure 4.3) also shows that this sample contains some barium oxide. The presence of copper tin sulphide and graphite detected by XRD analysis indicates that this material uses bronze sulphide and graphite as solid lubricant.

4. 2. Effect of Test Parameters to Coefficient of Friction

The results of tribological testing were mainly presented in terms of friction characteristic by WINDUCOM 2006 software. This friction characteristic is shown as friction variation with respect of time. There are three important aspects is used to analyze these results; (a) the general curve shape, (b) duration of certain transitional features of friction-time curve, and (c) level of variation of the friction force as function of time [88]. This variation is mainly as the result of the local friction coefficient, which is a function of the local shear strength at the local contact interface and the local contact geometry [78]. It is also reflect the stability of the microscale events which contribute to overall frictional behavior [89].

There are two kinds of variation level interpretation attributes to friction variation in the friction-time curve; (i) tendencies for pull-out or sudden surface fracture, and (ii) tendencies for transfer of seizure as shown in Figure 4.7.



Figure 4.7 Friction variation level interpretations; (a) tendencies for pull-out or sudden surface fracture, and (b) tendencies for transfer or seizure [88]

4.2.1. Effect of Contact Pressure to Coefficient of Friction

The friction characteristics of all sample materials at different contact pressures are shown in Figure 4.8 - Figure 4.13. It was observed that each sample has different friction characteristic with respect to contact pressure. All samples show gradual increasing of friction at the initial stage. This initial stages, also known as running-in period, appear in a relatively short period of time; not more than 0.01 hours (36 seconds). After the initial stage, different trend were observed indicate that different process possibly taken place.

The friction characteristics of Pad-1 are shown in Figure 4.8. This sample shows a rapid increased of COF at the early stage of sliding and after reaching a maximum value, the COF gradually decreased and thereafter reaching a steady state.

The friction curve of Pad-1 has two kind of general shape and can be divided into five different stages; namely stage I, stage II, stage III, stage IV, and stage V (Figure 4.9). Stage I or the initial stage is represented by gradually increasing of coefficient of friction. Stage II is represented by a concave parabolic curve. The stage III is represented by a decreasing coefficient of friction after the maximum value was reached and stage IV is represent by a steady state condition of the friction variation and stage V is represent by a raise of friction again [88, 89]. It was observed that the increase contact pressure affected the changes of general curve shape of Pad-1, where incremental of contact pressure tend to produce the stage V.

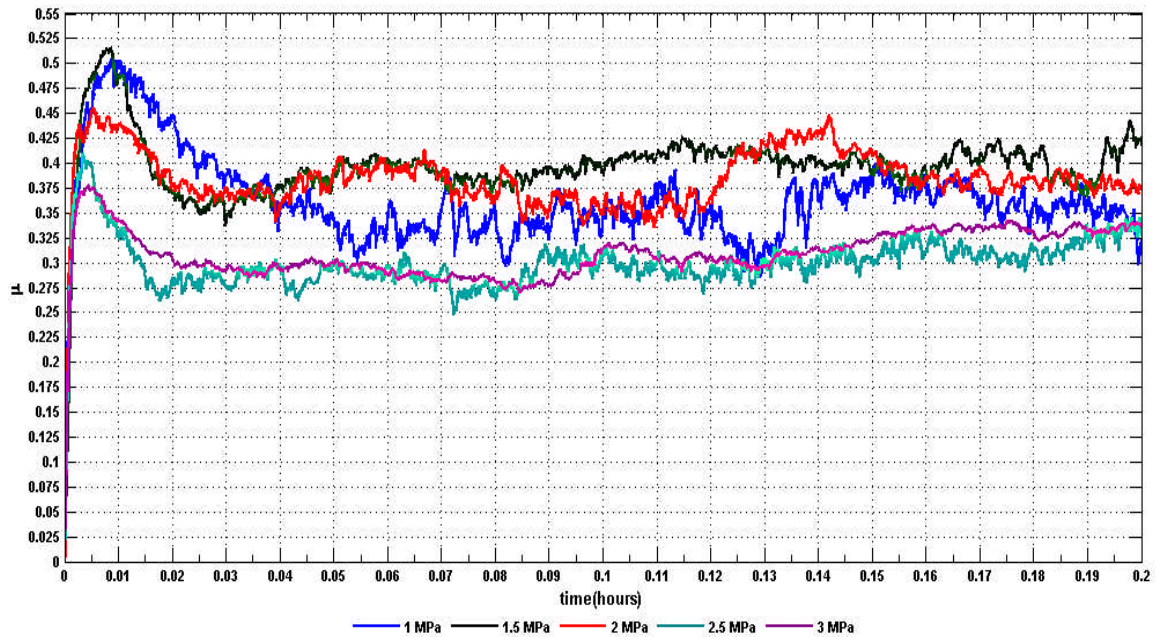


Figure 4.8 Effect of contact pressure to friction characteristic of Pad-1

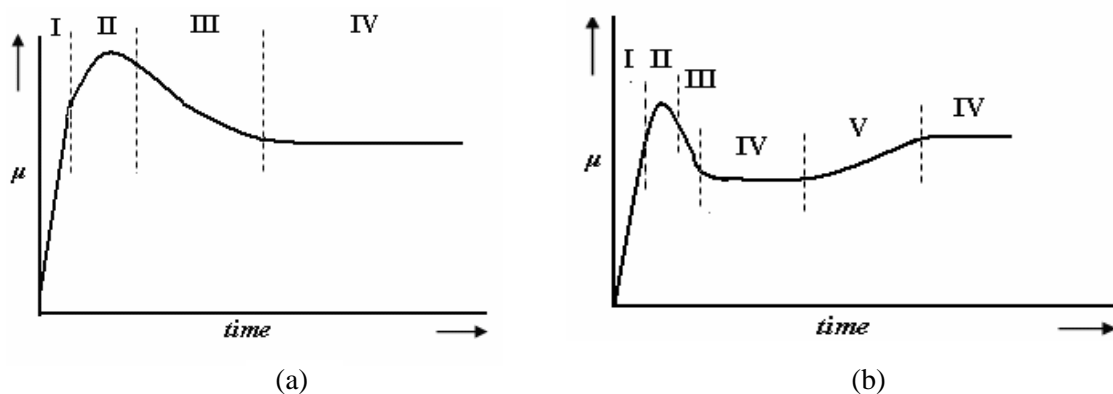


Figure 4.9 Friction curve of Pad-1; (a) contact pressure of 1 MPa, (b) contact pressure of 1.5 MPa – 3 MPa

The increasing of contact pressure was seemed to influence duration of each stage. At contact pressure of 1 MPa, the maximum value of COF was obtained around 36 sec. When the pressure was increased to 1.5 MPa, the maximum COF was obtained around 28 sec, 18 sec at 2 MPa, and 10 sec at 2.5 and 3 MPa. The different of duration was also observed at stage II, stage II, stage IV, and stage V at each applied contact pressure.

The friction variations evidently show that tendencies of different process to interchange happen during rubbing process (see Figure 4.7). In addition, such sudden increasing peak of COF was observed during this process (*e.g.* 0.068 – 0.072 hours at 1 MPa in Figure 4.8). These sudden rises of friction representing the three body abrasions during this stage [90]. It was also observed that the level of friction variation tends to getting smoother with the increasing of contact pressure.

The effect of contact pressure to friction characteristics of Pad-2 is shown in Figure 4.10. Different types of the general curve shape were observed (Figure 4.11). Similar to Pad-1, rapid increased of COF at the early stage of sliding was observed, however, the magnitude of stage II and III was not as clear as Pad-1. Similar curve feature as shown in Figure 4.9(b) was also occurred in this sample; however the maximum COF at stage V was higher than stage II. The duration and occurrence of the stage were also much affected by applied contact pressure. The variation level was observed to become smoother with the incremental of contact pressure.

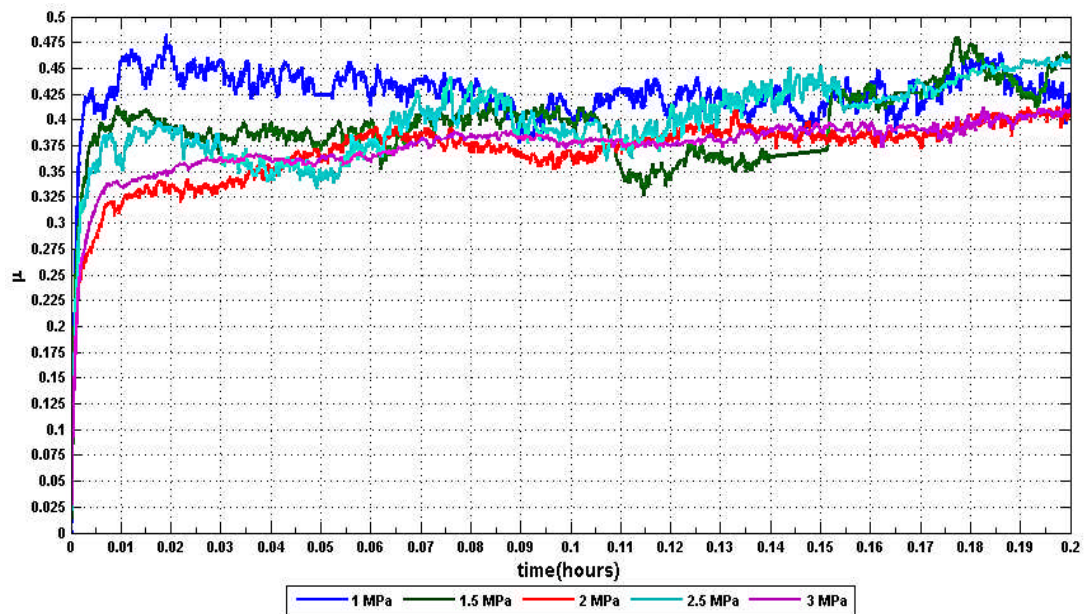


Figure 4.10 Effect of contact pressure to friction characteristic of Pad-2

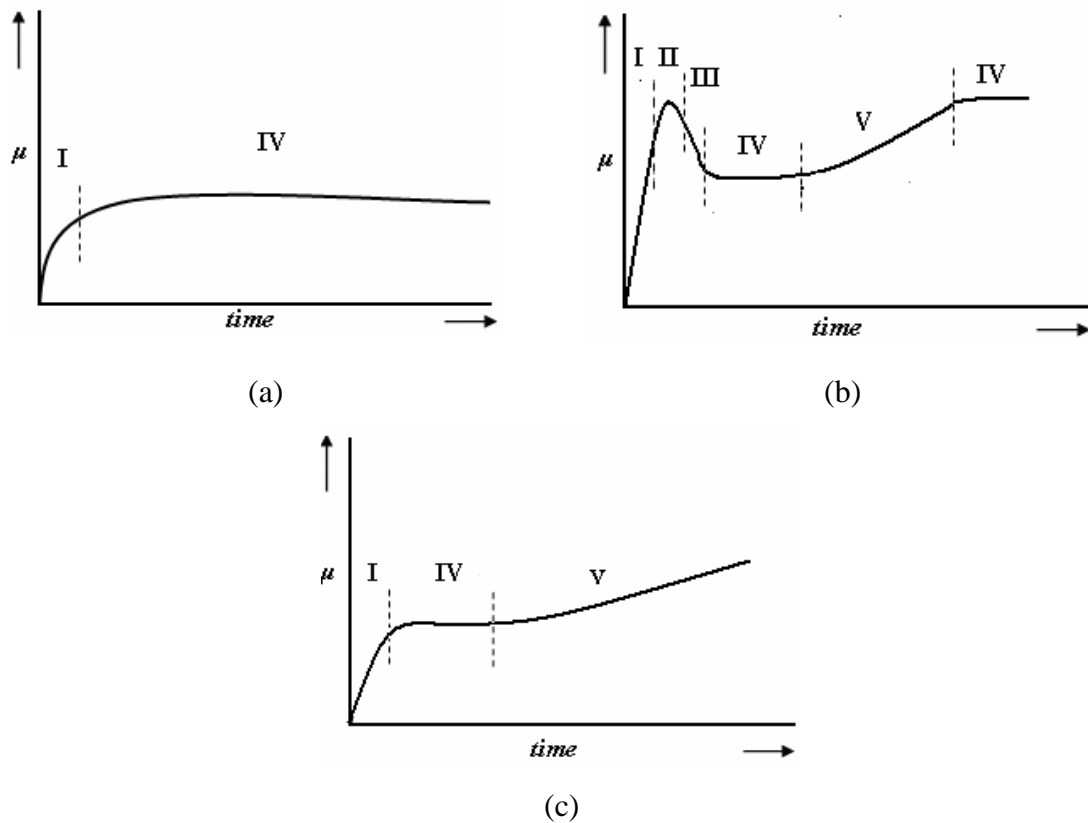


Figure 4.11 Friction curve of Pad-2; (a) contact pressure of 1 MPa, (b) contact pressure of 1.5 MPa and 2.5 MPa, (c) contact pressure of, 2 MPa, and 3 MPa

The effect of contact pressure to friction characteristics of Pad-3 are shown in Figure 4.12. Rapid increase of COF at initial sliding also observed, but time required to reach the next stage was quite longer than the previous brake samples. This sample has 3 general shapes (Figure 4.13). At contact pressure 2 and 2.5 MPa, stage II and III was not clearly observed. The duration and occurrence of the stage is affected by contact pressure and the variation of COF level become smoother with the incremental of contact pressure.

Many events could be taking place when the mating samples in sliding process. By using the friction curve, the friction and wear can be determined. Process such as material transfer, fiber pull out, surface scratch *etc.* could be possibly happen in rubbing process due to multifarious compound in brake pad material. Figure 4.8 – Figure 4.13 suggest that the shape of friction characteristics affected not only by materials involved, but also the applied contact pressure. These differences basically caused by; (i) oxide growth or removal, (ii) surface composition alteration due to

diffusional process, (iii) compositional temperature rise, (iv) mechanical disruption of surface oxide films with increasing metallic contact (v) contact geometry changes [90]

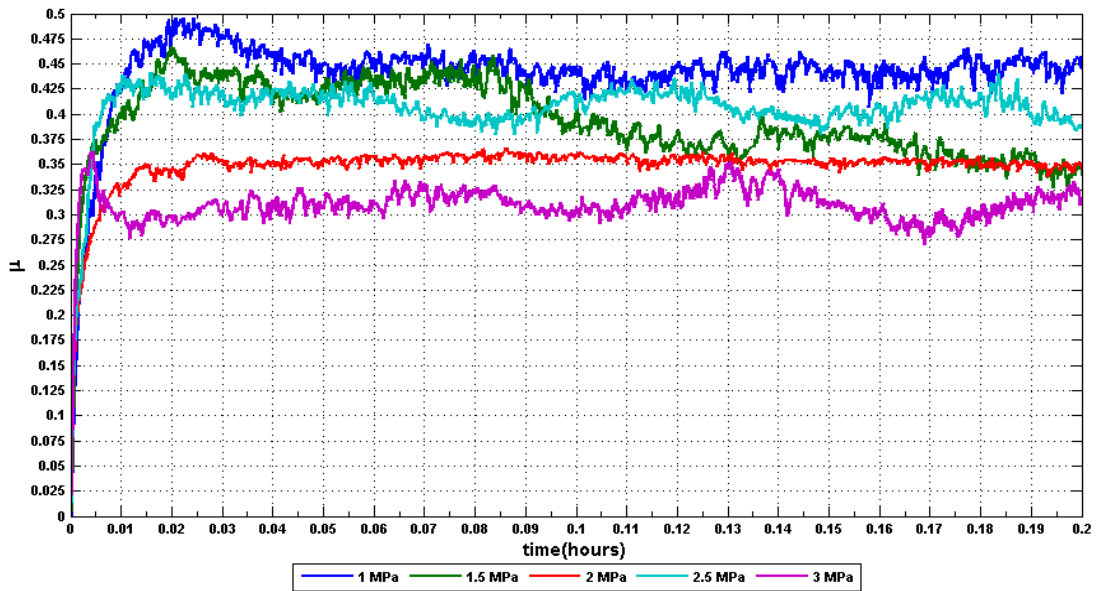


Figure 4.12 Effect of contact pressure to friction characteristic of Pad-3

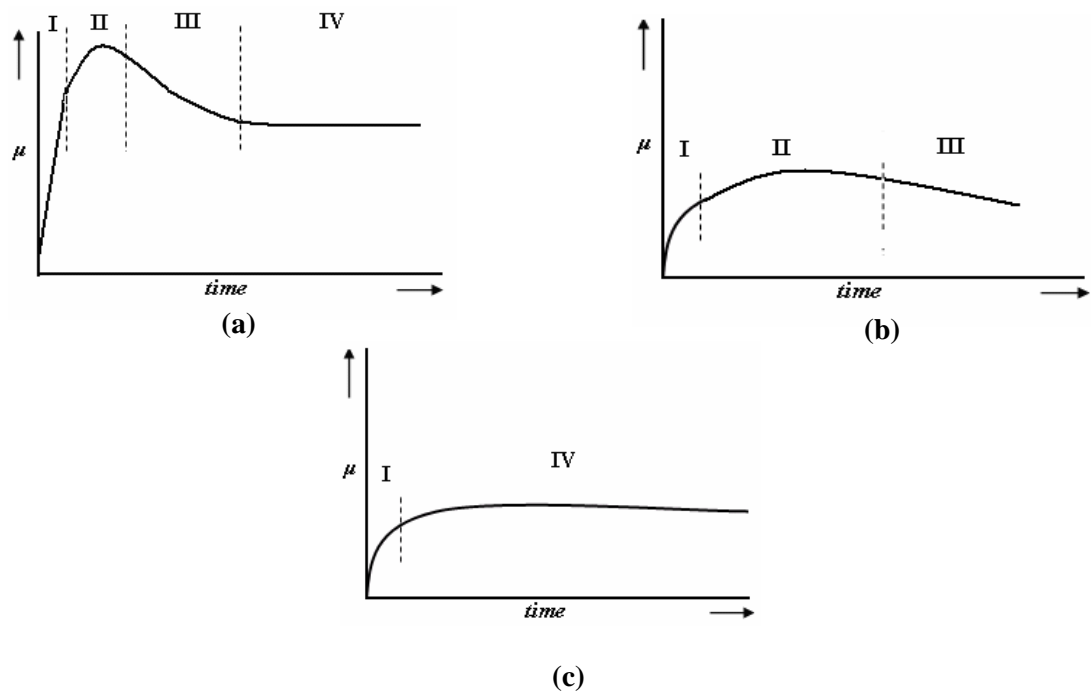


Figure 4.13 Friction curve of Pad-3; (a) contact pressure of 1 MPa and 3 MPa, (b) contact pressure of 1.5 MPa, (c) contact pressure of 2 MPa and 2.5 MPa

The general curve shape as shown by 4.9(a) and 4.13(a) is recognized as one of the most common curve in dry friction [89], however Blau also suggested other curve shapes as detailed in [88, 90]. These curve shape features indicate different process was taken place during the rubbing process.

When the rotating pin tangentially pressed against brake pad, resistance forces will occur against the motion. Because of surface irregularities of both mating surfaces (APPENDIX J – L), frictional shear will be generated at the contact asperities. If the frictional shears exceed the asperities tip strength, the tip will be plastically deformed and subsequently altered the surface profile (APPENDIX M).

Because of brake pad material is a phenolic resin based composites, deformation may effects the friction due to its viscoelastic properties [69]. The deformation results in produce loosen particles that could form metallic junction and adhered to another surface [91] as well as agglomerate forming wear debris [44] to form hard thin layer, namely friction layer, by mechanical alloy or even melting processes of the wear particles. Figure 4.14 show typical friction layer formed on the sample surface. Figure 4.15 and Table 4.7 shows the elemental composition of the samples after rubbing process. These results suggest that the rubbing surface has covered with thin iron oxide layer [92]. SEM-EDX analysis at a certain point on the contact surface (point A) and compacted debris (point B) indicate that mechanical alloy process has taken place during sliding process (Figure 4.16).

The rapid increase in coefficient of friction at the initial stage is believed due to the increasing interaction of the encountered asperities, contact area and adhesion [56, 89, 93]. Moreover, hard particles contained in the brake pads actively abrade the soft part of the brake surface as well [19, 44, 89]. Smearred and plowed mark on the sample surface in Figure 4.16 indicates both of these actions have taken place during the rubbing process.

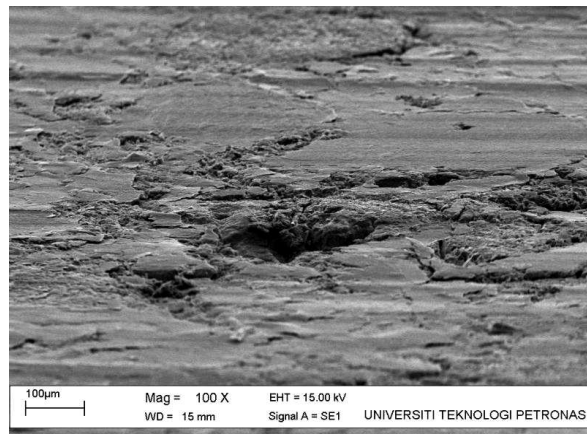


Figure 4.14 SEM micrograph of friction layer form on the contact surface

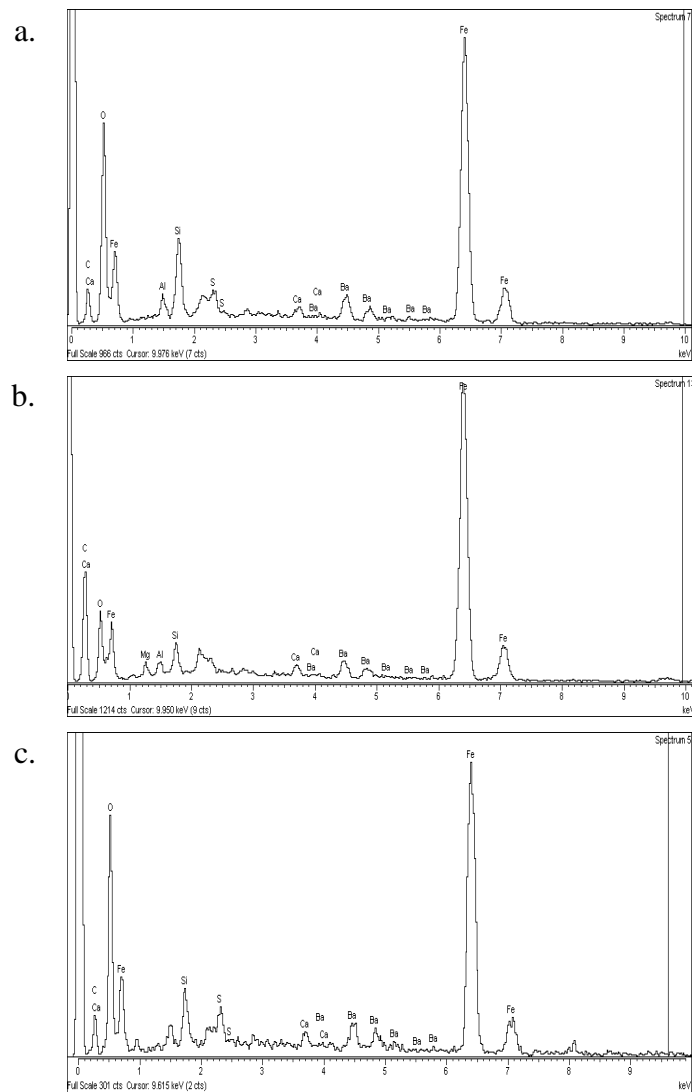


Figure 4.15 EDX analysis after test; (a) Pad-1, (b) Pad-2, (c) Pad-3

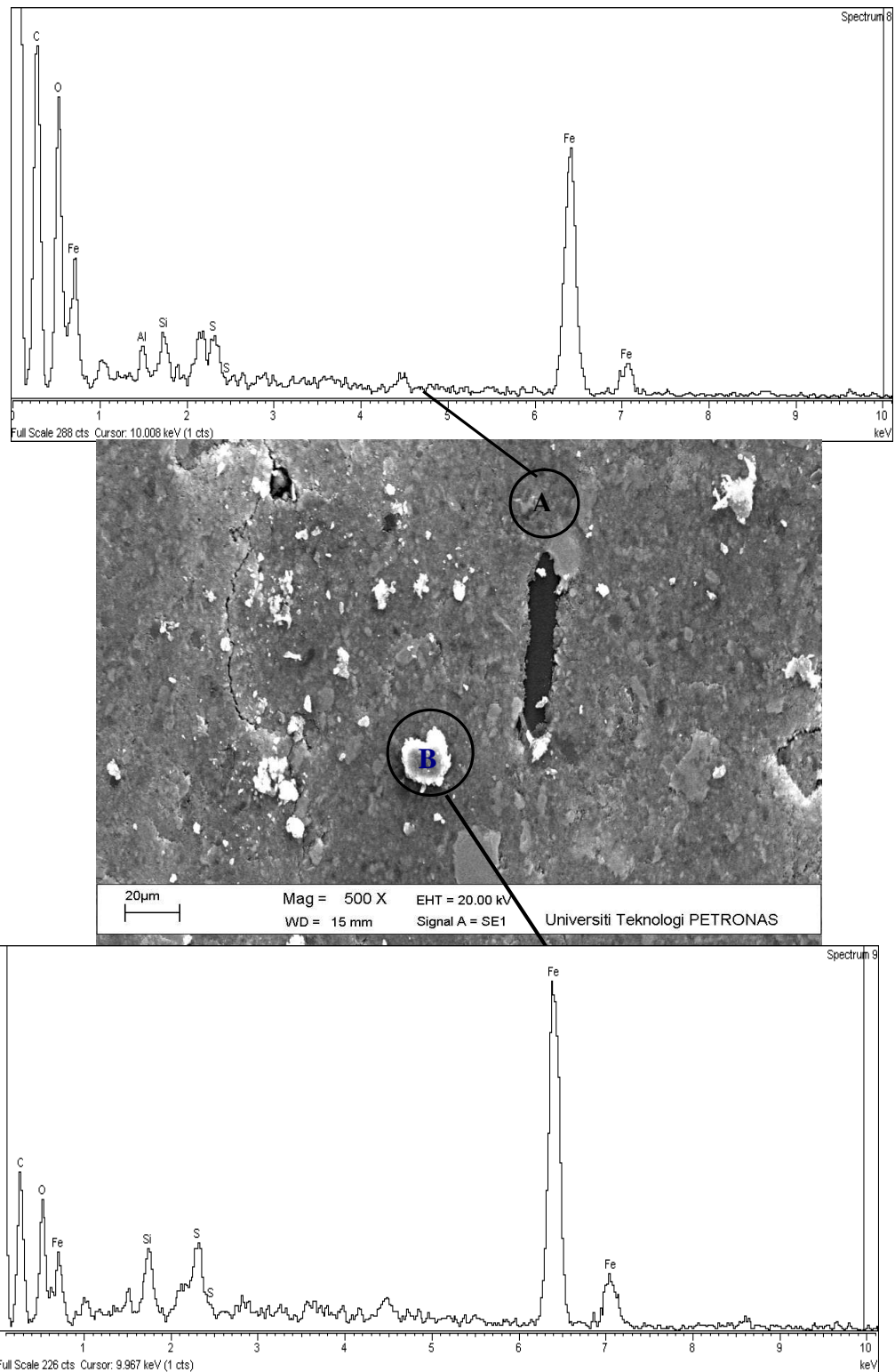


Figure 4.16 SEM-EDX analyses of hard thin layer and compacted debris

Table 4.7 Elemental composition after test

Pad-1			Pad-2			Pad-3		
Element	Weight (%)	Atomic (%)	Element	Weight (%)	Atomic (%)	Element	Weight (%)	Atomic (%)
C K	12.49	26.98	C K	40.10	62.68	C K	13.32	27.97
O K	26.82	43.48	O K	19.62	23.02	O K	28.91	45.58
Al K	1.36	1.31	Mg K	1.09	0.84	Si K	2.89	2.59
Si K	4.04	3.73	Al K	0.76	0.53	S K	1.43	1.12
S K	0.87	0.70	Si K	1.47	0.98	Ca K	0.87	0.55
Ca K	0.65	0.42	Ca K	0.55	0.26	Fe K	46.73	21.11
Fe K	47.96	22.28	Fe K	33.67	11.32	Ba L	5.86	1.08
Ba L	5.81	1.10	Ba L	2.74	0.38			
Totals	100.00		Totals	100.00		Totals	100.00	

The process of deformation, adhesion, as well as abrasion continuously taken place until the stage II. At the stage II, the maximum interfacial adhesion, plastic deformation, and wear particles entrapment was reached [89]. These events possibly caused by the continuous rubbing process that will actively shear and deform the contact asperities. As consequence, wear particles may formed between the contacting surfaces. At the beginning, small fraction of this wear particle may trap and attached together and then dense and adhere to other area. In concurrence with this process, the hard particles contained in brake pad will be pressed down in the soft matrix as well. The growing of wear debris by the hard particles will occur in this process. The wear debris from pad matrix and pin will be flowing through the contact zone and then form hard thin layer due to combination of normal pressure, shear forces and frictional heat.

Coefficient of friction was found to be decreased at stage III. There are three possible reasons may cause this behavior: (i) degradation of organic content, (ii) fine friction layer has been developed at the interfacial contact and (iii) a lot of tip of asperities has been sheared.

As the brake system is meant to absorb the kinetic energy to heat, it is generally understand that heat much affected brake pad performance. Since the rubbing process related to time, surface temperature will increase with rubbing time and result in degradation of organic content and furthermore produce liquid and gaseous product [19]. Frictional heating during the braking process will easily raises

the temperature at contact asperities beyond the glass transition temperature of the resin and often rises above the decomposition temperature resulting in the abrupt change of friction force during braking [33]. TGA results show onset thermal degradation of the samples was started below 80 °C (APPENDIX F – H). The decreasing of friction coefficient is postulate related to softening of matrix resin and degradation of other organic component [33, 94]. Furthermore, the degraded organic content together with the wear debris form fine friction layer [19, 22, 95, 96]. Another reason of the decreasing of friction if this stage is most of tip of the asperities contact has been sheared and blunting the surface [97, 98]. Thus, interlocking between the asperities tip will be reduced and then reduced the resistant to the motion [19].

In the case of Figure 4.11(a) and 4.11(c) in Pad-2 and Figure 4.13 (c) in Pad-3, stage II and III was not clearly observed. This behavior is possibly due to the formation of friction layer with fewer plastic deformations.

Because of the continuous process of rubbing, well developed and stable friction layer would possibly form. This factor is considered resulting in the occurrence of stage IV. At stage IV, steady state condition was reached and lower coefficient of friction was observed. Figure 4.17 show typical well developed friction layer which has covered most of the contact asperities.

Although the destruction of the friction layer has become more intensive due to increased contact pressure [44], the capability of the wear particles to initiate development of other friction layer has to be counted as well. The occurrence of stage V is considered caused by more wear debris abraded friction layer, which was previously formed at stage IV, and then initiates formation of another layer. Figure 4.17 evidently show several wear debris embedded on friction layer at stage IV.

Friction curve analysis was conduct to strengthen this assumption. Most of the stage V occurrence was initiated from sudden increase of friction peak, which suggest that three body abrasions was acted there. Thus, it validates Godet conclusion in [51], Jacko *et al.* [99], and Oestermeyer in [44] that wear particle compaction has significant influences the formation of friction layer. Figure 4.14 And Figure 4.18 reveal wear debris compacted and form layer on the contact surface. Another possible reason is high contact pressure able to produce more plastic deformation and an

excessive transfer material on the contact surface will happen and increase true contact area [69, 88]. Figure 4.19 shows patch covered another patch which indicates that intense adhesion mechanism has involved during the process.

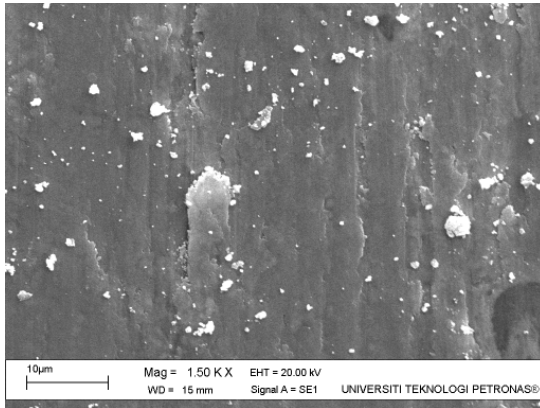


Figure 4.17 SEM micrograph featuring typical well developed friction layer (Pad-3, 2 MPa, 600 rpm)

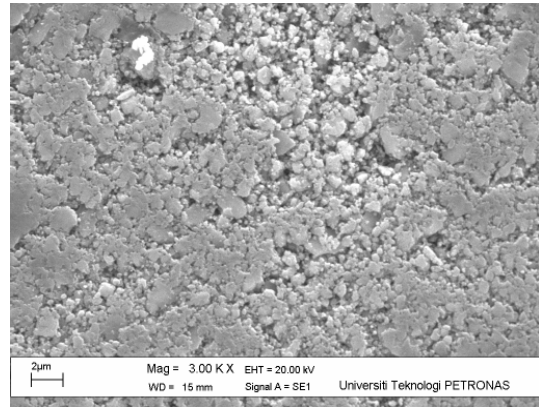


Figure 4.18 Debris layer feature on the contact surface (Pad-2, 2.5 MPa, 600 rpm)

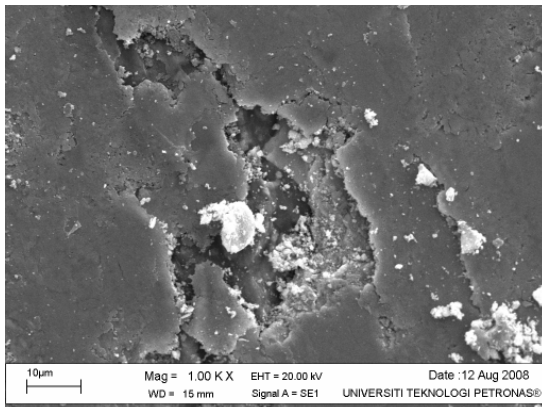


Figure 4.19 SEM micrograph shows friction layer consist of patch covered by another patch (Pad-1, 3 MPa, 600 rpm)

4.2.2. Effect of Sliding Speed to Coefficient of Friction

Another set of experiment was conducted in order to investigate the effect of sliding speed to the frictional characteristic of the sample materials. The friction characteristics of sample material under different sliding speeds and constant contact pressure are shown in Figure 4.20 to Figure 4.22.

Basically, similar friction behavior to the previous set of experiment was shown by Pad-1 (Figure 4.20). Similar general curve shape as shown in Figure 4.9 was observed. However at slowest speed (300 rpm), duration of stage II and stage III was found a bit longer then the other. Furthermore, sliding speed seemed to accelerated the occurrence of stage I – stage III at faster speed. Thus, it is postulate that sliding speed much affects to duration of each stage. Effect of sliding speed to friction variation was found differ from contact pressure. The friction variation seems to be rougher with the increasing of sliding speed. In addition, stick slip phenomena revealed at the highest sliding speed.

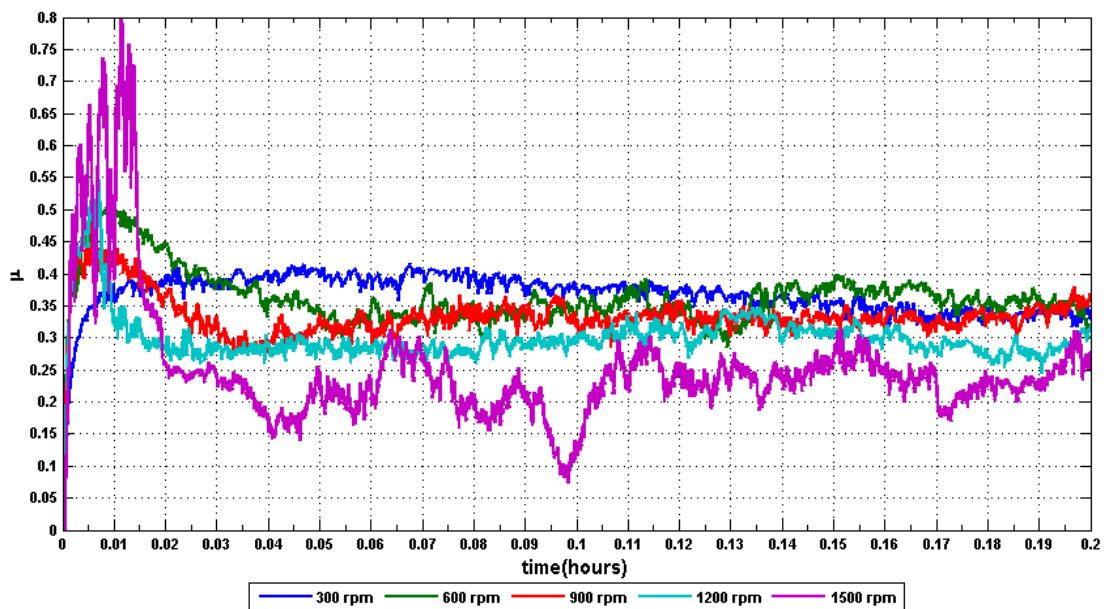


Figure 4.20 Effect of sliding speed to friction characteristic of Pad-1

The friction characteristic of Pad-2 under different sliding speed is presented in Figure 4.21. Duration and occurrence of each stage seem to be affected by sliding speed. Sliding speed tends to accelerate the occurrence of stage II and III. At speed 300 rpm and 600 rpm, it show similar general curve as Figure 4.11(a). At speed 900 rpm, similar friction curve to Figure 4.11(c) was observed. Furthermore, at speed 1200 and 1500 rpm, stage II and stage III are clearly visible and friction curve has a similar shape as shown in Figure 4.9(a). Unlike Pad-1, increasing of sliding speed seems to smoothing the friction variation and in addition, stick-slip behavior occurred at the lowest sliding speed (300 rpm).

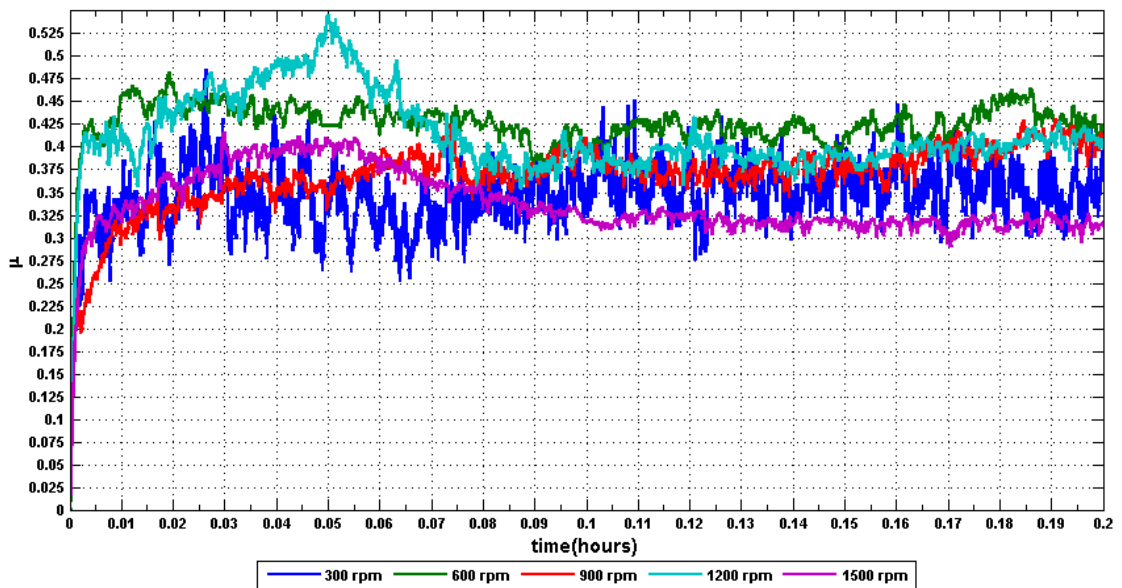


Figure 4.21 Effect of sliding speed to friction characteristic of Pad-2

The friction characteristic of Pad-3 under different sliding speed is presented in Figure 4.22. There are three friction curve observed. At the lowest speed (300 rpm), a similar friction curve to Figure 4.13(c) was observed. At speed 600 rpm and 1200 rpm, a similar friction curve in the Figure 4.9(a) was observed. Finally, a similar friction curve in the Figure 4.11(a) was observed at speed 900 rpm and 1500 rpm and a stick slip behavior occurred at sliding speed 1500 rpm. Friction variation seems to be smoother with incremental of speed except at the highest speed.

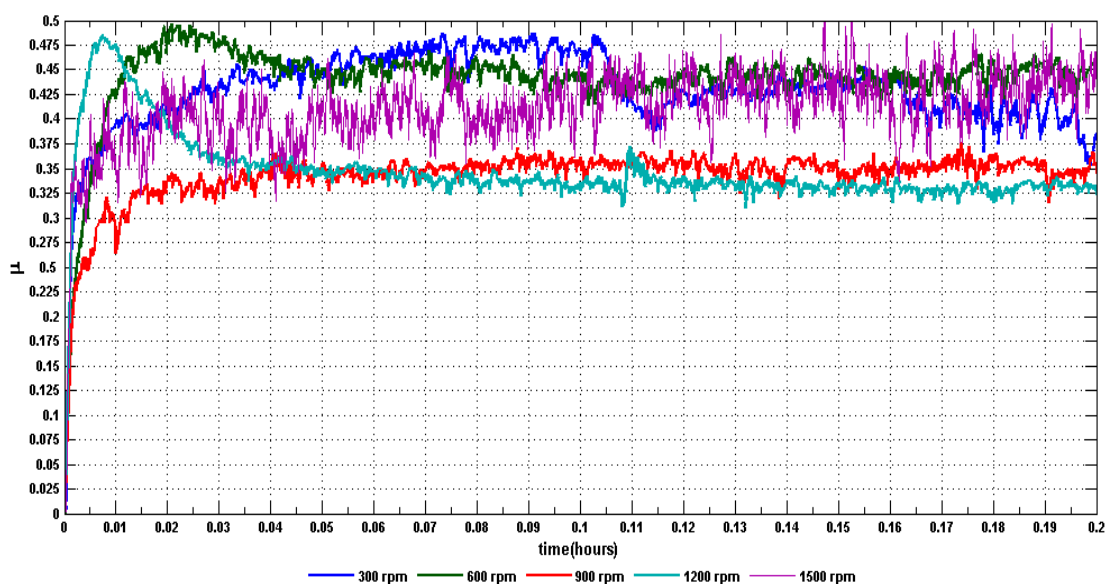


Figure 4.22 Effect of sliding speed to friction characteristic of Pad-3

As the sliding speed was increased, the frequency of the asperities brought to contact increased as well. As a consequence, rapid plastic deformation will take place as well as adhesion and the formation of wear debris will be accelerated. Fatigue effect also more intense due to this frequent contact of the asperities. In addition, frictional heating also increase due to more kinetic energy converted to be heat with incremental of speed [1, 7, 65].

At the highest sliding speed (1500 rpm), Pad-1 and Pad-3 show stick slip behavior. This phenomenon is possibly due to the increasing of periodic tearing of the friction layer. SEM micrograph of Pad-1 and Pad-3 at sliding speed 1500 rpm shows several patches cover on another patch after rubbing process (Figure 4.23). This occurrence may be due to high flash temperature which accelerate the thermal degradation of the resin and subsequently intensify adhesion and bond fracture on the contact surface.

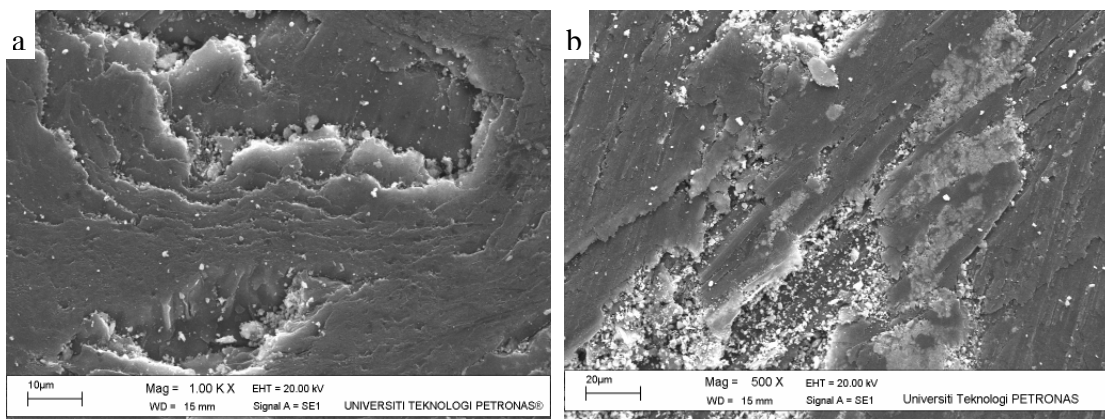


Figure 4.23 SEM micrograph of plateau on contact surface at high sliding speed (1500 rpm, 1 MPa); (a) Pad-1, and (b) Pad-3

In contrary, stick slip occurred at the lowest speed of Pad-2 (300 rpm) was possibly associated with lower frictional heating which result in less thermal degradation of high organic content. At temperature lower than the chemical decomposition temperature of the binding agent and its constituent materials, intensive mechanical deformation of the superficial layers occur initially [100]. This phenomenon can be explained by using schallamach waves theory as shown in Figure 4.24 [101, 102].

In the early stage of sliding with uniform contact applied pressure, shear throughout the body of the soft binder. However, the contact pressure is reduced at the rear of contact, which cause the binder to slip first at the rear. This slipping alters the stress state in the binder. The contact pressure that is in front of the slipped region is reduced until the rear of slipped region. Slip then occurs in this region, which then alters the contact pressure further ahead. A wave of slip occurs and moves forward at about 10 times the sliding speed. With continued sliding, standing waves are established, which often have frequencies in the audible range. It also can produce periodic sinking of fine particle into the rather soft layer followed by its climbing out of the impression and settling into the subsequent one [88]

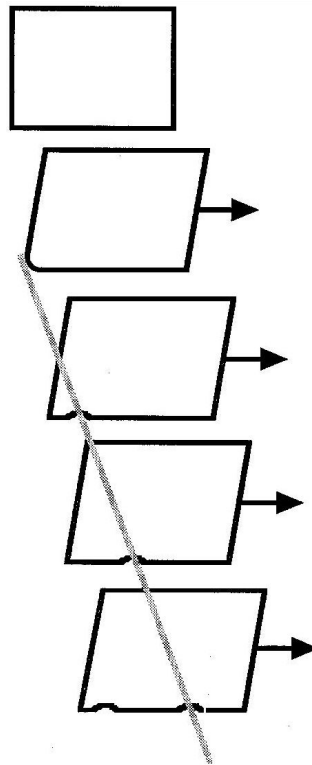


Figure 4.24 Skechth of schallmach waves during sliding [102]

4.2.3. Effect of Relative Humidity to Coefficient of Friction

Friction characteristics of Pad-1 at different relative humidity (RH) are shown in Figure 4.25. It is observed that humidity has a stabilizing effect on Pad-1. At low humidity, the friction curve has stage V before reaching the steady state condition

again (similar shape to Figure 4.9(b)). When the relative humidity was increased, a similar curve shapes as Figure 4.9(a) was observed.

Friction characteristic of Pad-2 at different relative humidity are shown in Figure 4.26. Humidity seems to produce rougher friction variation and there were two friction curve observed. At lower RH, the curve shape was found to be similar as Figure 4.11(a) while at medium and high RH, the curve has similar shape as Figure 4.11(c).

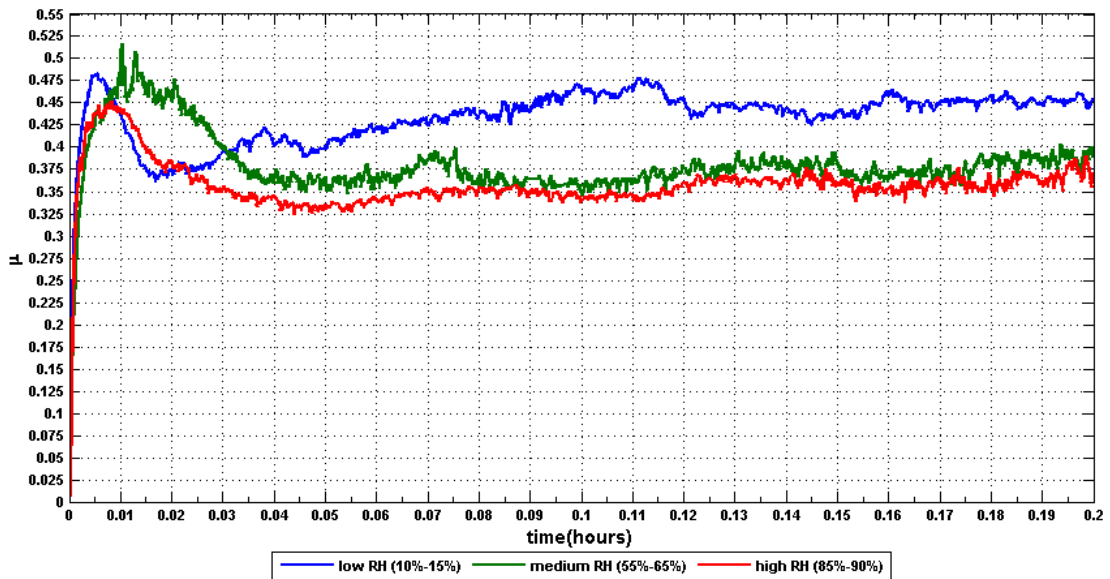


Figure 4.25 Effect of relative humidity to COF of Pad-1

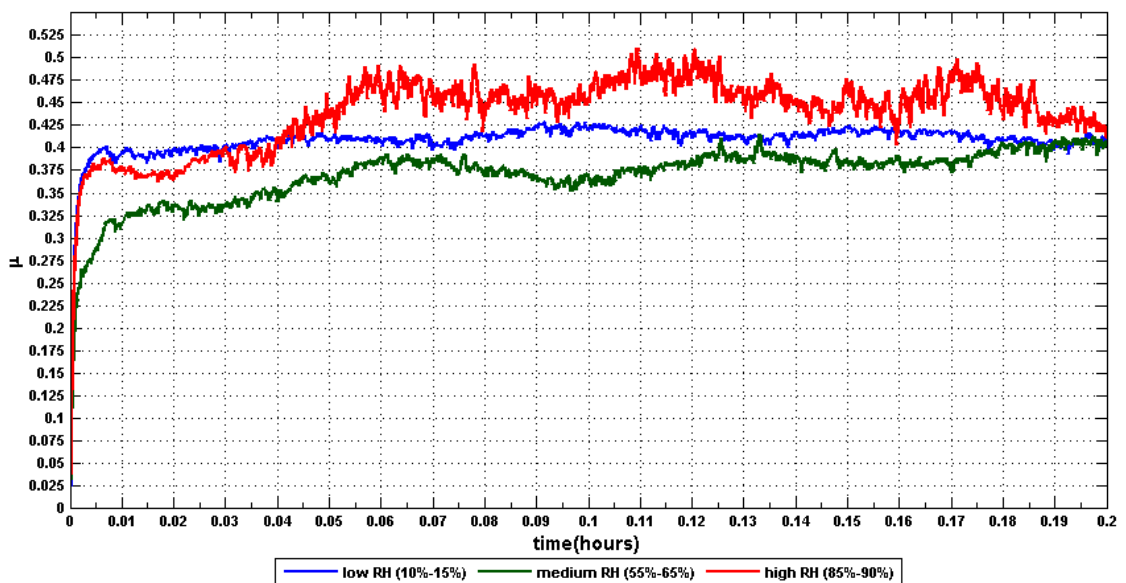


Figure 4.26 Effect of relative humidity to COF of Pad-2

Friction characteristic of Pad-3 at different relative humidity are shown in Figure 4.27. There two friction curve observed. At lower RH, the curve was found to be similar as Figure 4.13(b) while at medium and high RH, the curve has similar shape as Figure 4.13(c).

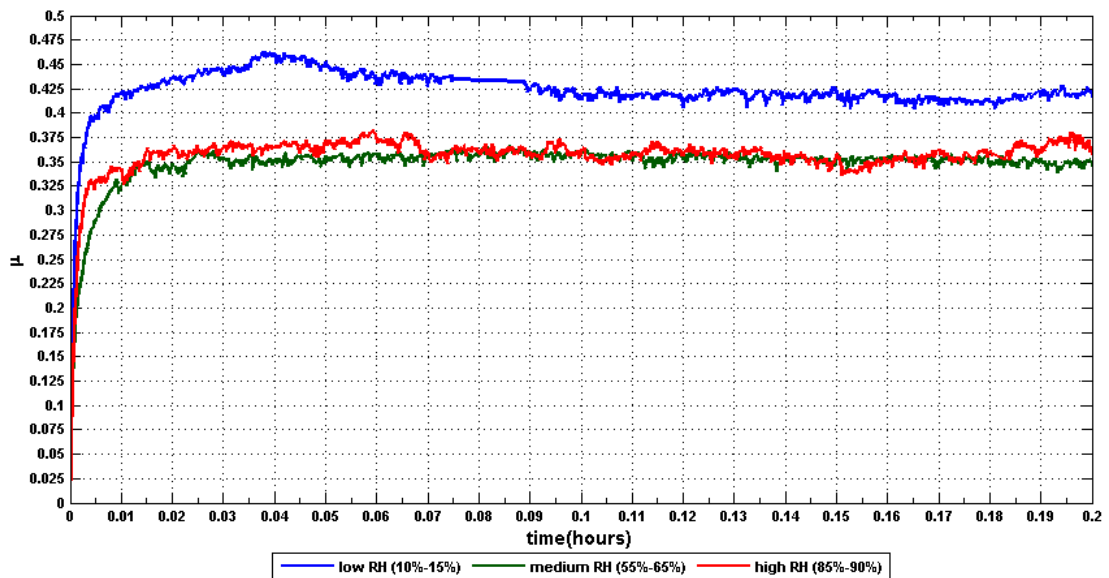


Figure 4.27 Effect of relative humidity to COF of Pad-3

Frictional behavior differences of the sample at different RH are considered much related to the formation of friction layer, frictional heat and porosity. Porosity of the samples is detailed in Appendix C. High porosity related to capability of friction material to absorb moisture and moreover a lower porosity able to causes increasing of heat accumulation [33].

The stabilization effect of friction in Pad-1 is thought much related to ability of moisture to maintain the layer [103]. Figure 4.28 depict feature of Pad-1 surface at different humidity. Smoother friction layer surface was observed at higher humidity (Figure 4.28). EDX analysis of Pad-1 at different relative humidity is shown in Table 4.8. Significant increasing of O and S with humidity was found imply the possibility of sulfur oxide influence the friction layer formation in Pad-1.

Contrary to Pad-1, friction variation of Pad-2 became rougher with relative humidity. This behavior possibly due to low porosity which resulted in less moisture absorbed and low friction layer stability. This factor also considered related to high

content of fillers in this sample. Fillers in general are inert material, which is not affected by various friction conditions [73], but it also could act as anti blocking material that entraps air and voids to reduce adhesion/sticking of the friction layers, thus lowering the interlayer blocking (adhesive) force [104]. This factor influenced to tendency of stage V to occur due to intense destruction of the friction layer at high RH environment while stable friction layer relatively easily formed at lower RH. SEM micrograph of the Pad-2 show less friction layer formed at high RH (Figure 4.29).

At low humidity, Pad-3 shows high coefficient of friction. The coefficient of friction decreased when the humidity was increased to medium level. When the humidity was further increased to a higher level, similar coefficient of friction was observed. In addition, the friction variation was observed quite stable at each relative humidity as well (Figure 4.22). This behavior is probably due to abrasive material contained in the Pad-3 material that has increased the generation of friction layers by acting as powdered lubricant to reduce the friction [10]. At low humidity, several ploughing mark was visually observed at the surface while at the higher humidity the symptom visually reduced. Figure 4.30 show Pad-3 surface after sliding at different relative humidity and Table 4.10 show EDX analysis on the elemental composition of the layer.

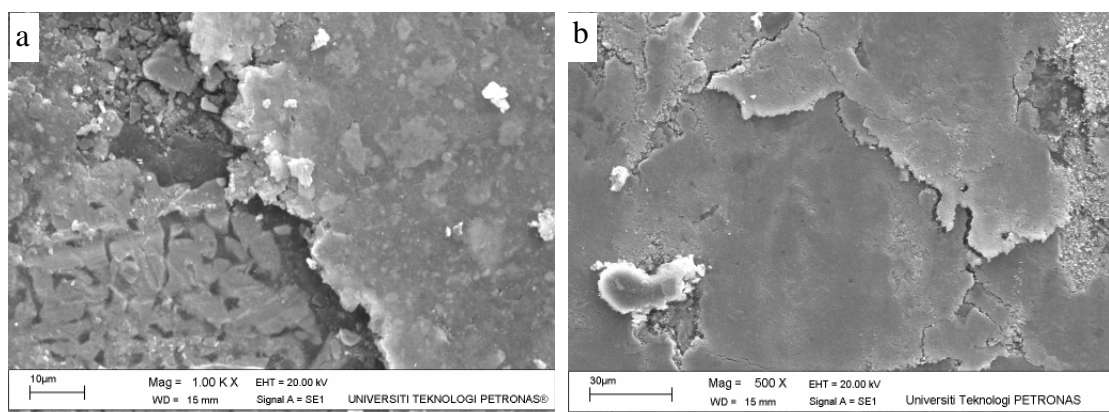


Figure 4.28 SEM micrograph of Pad-1 surface rubbing at different RH; (a) low RH, (b) medium RH, and (c) high RH

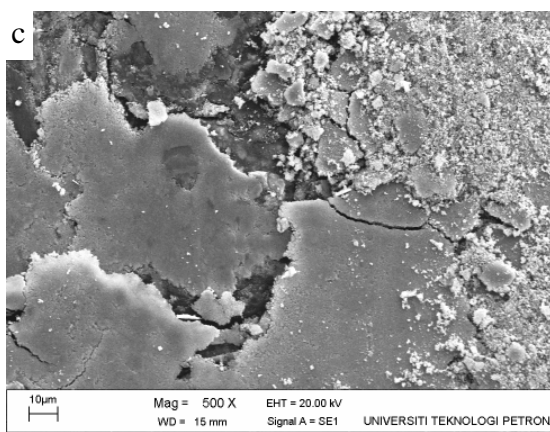


Figure 4.28 SEM micrograph of Pad-1 surface rubbing at different RH; (a) low RH, (b) medium RH, and (c) high RH (*Continue*)

Table 4.8 EDX analysis of Pad-1 at different experimental humidity

Low RH (10 -15 %)			Medium RH (55 – 65 %)			High RH (85 – 90%)		
Element	Weight (%)	Atomic (%)	Element	Weight (%)	Atomic (%)	Element	Weight (%)	Atomic (%)
C K	29.51	51.51	C K	12.49	26.98	C K	14.4	29.6
O K	23.02	30.16	O K	26.82	43.48	O K	29.05	44.83
Al K	1.03	0.80	Al K	1.36	1.31	Al K	1.31	1.2
Si K	0.88	0.66	Si K	4.04	3.73	Si K	1.54	1.36
S K	0.70	0.46	S K	0.87	0.70	S K	0.95	0.73
Fe K	42.04	15.78	Fe K	47.96	22.28	Fe K	46.91	20.74
Ba L	1.61	0.25	Ba L	5.81	1.10	Ba L	3.33	0.6
Zn K	1.20	0.39	Ca K	0.65	0.42	Zn K	2.22	0.84
						Co K	0.27	0.11
Totals	100		Totals	100.00		Totals	100	

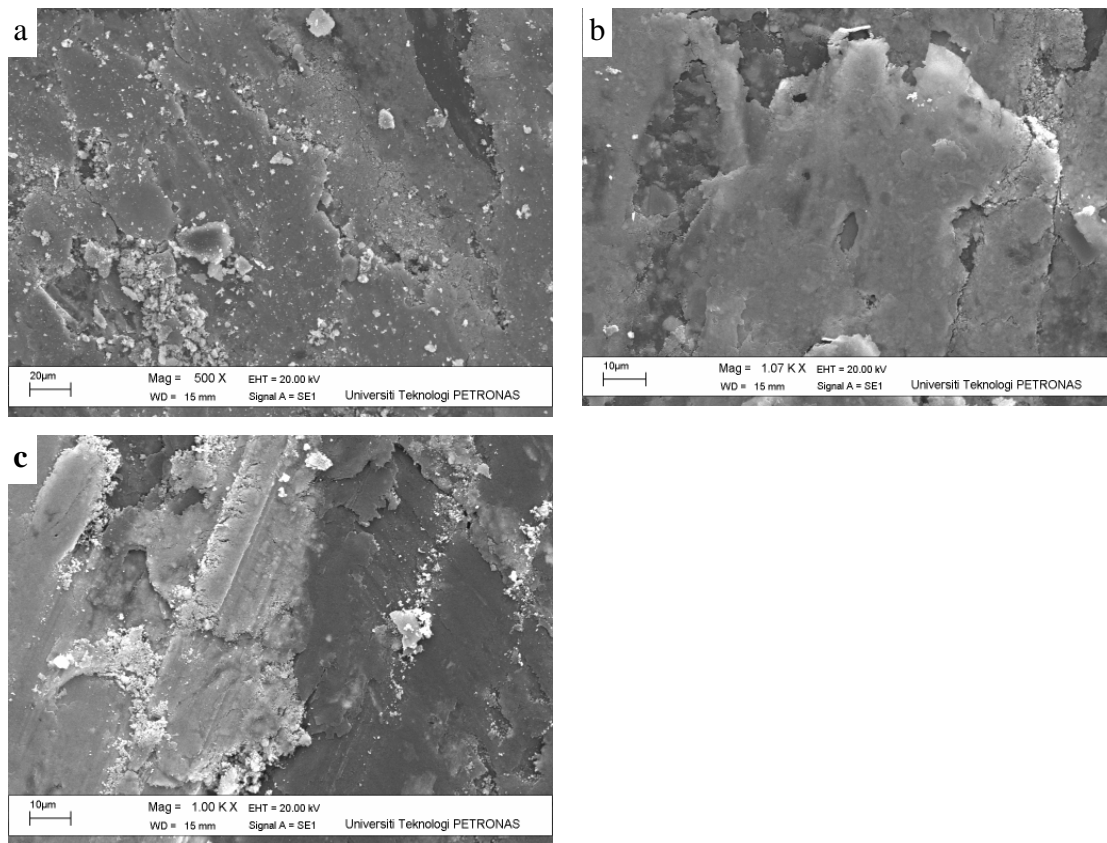


Figure 4.29 SEM micrograph of Pad-2 surface rubbing at different RH; (a) low RH, (b) medium RH, and (c) high RH

Table 4.9 EDX analysis of Pad-2 at different experimental humidity

Low RH (10 -15 %)			Medium RH (55 – 65 %)			High RH (85 – 90%)		
Weight (%)	Atomic (%)	Element	Weight (%)	Atomic (%)	Element	Weight (%)	Atomic (%)	Element
C K	25.31	46.8	C K	23.11	43.91	C K	16.68	35.46
O K	23.76	32.98	O K	21.48	40.46	O K	26.93	40.48
Al K	0.79	0.65	Al K	0.76	0.53	Al K	1.08	0.97
Si K	1.55	1.23	Si K	1.47	0.98	Si K	2.61	2.24
S K	0.7	0.49	S K	1.07	1.2	S K	0.77	0.57
Ca K	0.67	0.37	Ca K	0.55	0.26	Ca K	0.59	0.35
Fe K	41.7	16.59	Fe K	46.47	11.32	Fe K	44.18	19.03
Ba L	5.51	0.89	Ba L	5.09	1.34	Ba L	5.16	0.9
Totals	100		Totals	100		Totals	100	

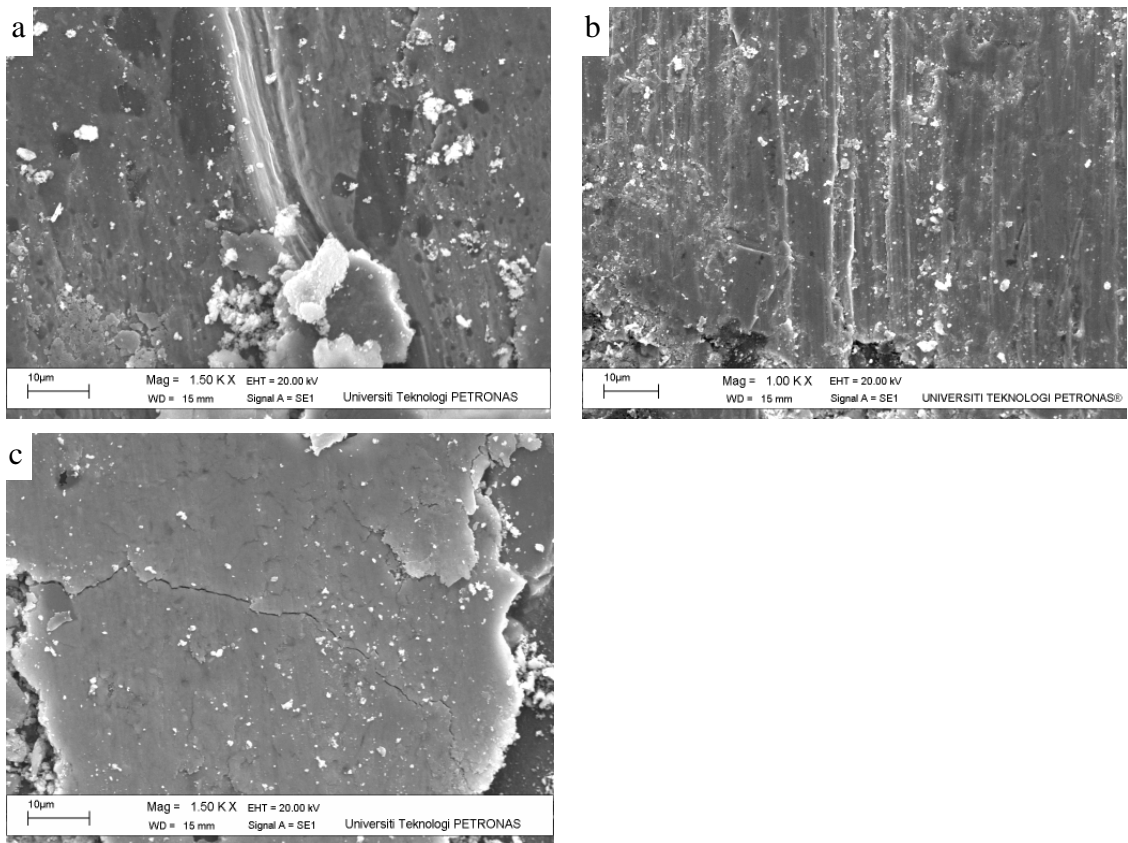


Figure 4.30 SEM micrograph of Pad-3 surface rubbing at different RH; (a) low RH, (b) medium RH, and (c) high RH

Table 4.10 EDX analysis of Pad-3 at different experimental humidity

Low RH (10 -15 %)			Medium RH (55 – 65 %)			High RH (85 – 90%)		
Weight (%)	Atomic (%)	Element	Weight (%)	Atomic (%)	Element	Weight (%)	Atomic (%)	Element
C K	8.33	16.13	C K	13.32	27.97	C K	35.54	55.77
O K	35.58	51.74	O K	28.91	45.58	O K	25.53	30.08
Al K	4.88	4.21	Si K	2.89	2.59	Al K	1.57	1.10
Ca K	6.19	3.59	Ca K	0.87	0.55	Ca K	0.92	0.43
Fe K	32.09	13.37	Fe K	46.73	21.11	Fe K	26.44	8.93
Si K	11.00	9.11	S K	1.43	1.12	S K	1.29	0.76
Mg K	1.94	1.86	Ba L	5.86	1.08	Ba L	5.44	0.75
						Si K	3.26	2.19
Totals	100.00		Totals	100.00		Totals	100.00	

4.3. Effect of Test Parameters to Wear

4.3.1. Effect of Contact Pressure to Wear

Figure 4.31 shows the effect of contact pressure to wear. Wear of the sample is shown in term of average weight losses. Generally wear of the samples show increase with incremental of contact pressure by two trends, linearly and exponentially.

Pad-2 is found as the most wear resistant sample among the others and Pad-3 is the least resistant. Even though several researchers still could not find significant effect of porosity and hardness to wear for friction materials [105, 106, 107], it seems that hardness and porosity may affect wear of these materials (see Appendix C). Hardness is considered related to its resistance to plastic deformation, whilst porosity is associated to heat accumulation [33].

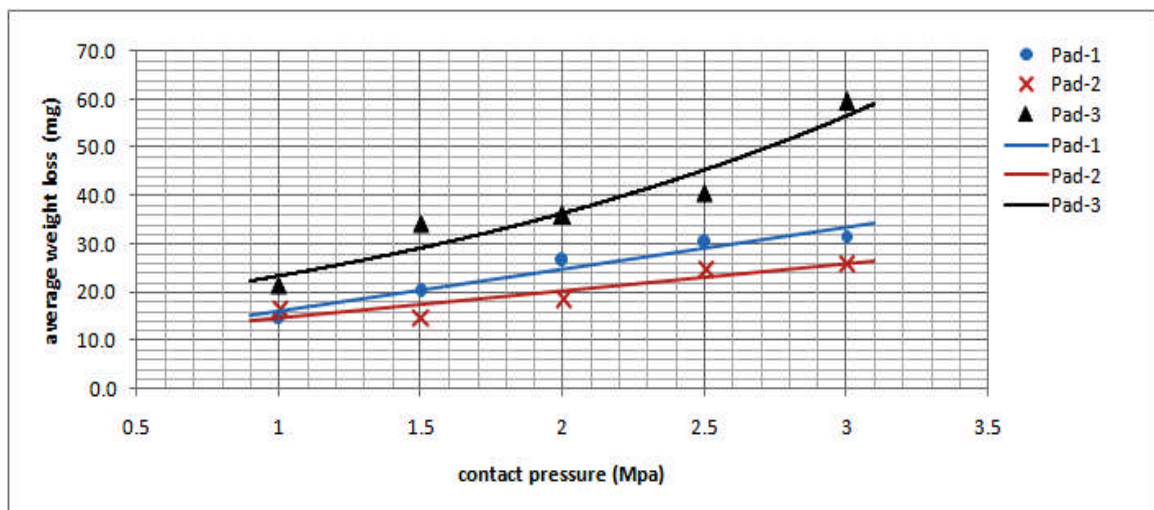


Figure 4.31 Effects of contact pressure to wear

The increase applied contact pressure was found to increase wear as well. It is hypothesized to be related with the increasing of plastic deformation of the contact asperities. As the contact pressure increased, more asperities will be brought to real contact situation. Since the rubbing process involving shear mechanism, if the friction defined as force to shearing the real contact, thus a double contact pressure will have an effect on doubling the real contact area as well as double friction force [56]. This plastic deformation consequently sheared off the asperities and the more asperities brought in real contact the more acceleration of plastic deformation will occur. This in

turn will increase adhesion and generation of wear debris. Both of adhesion and generation of wear debris is much affect on the formation of the third body layer.

The formation of wear debris is also attributed to the increasing of the penetration of a rather hard material on the contact surface. The deeper penetration of the harder material into the softer material will cause more cutting action and removal of the softer material, and thus more wear debris is produced.

By analyzing friction variation from the friction curves above, the tendency of wear mode can be postulated as well. At 1 MPa, the tendency of fiber pull out or sudden surface fracture seems often to happen on Pad-1 and Pad-2, while tendencies of transfer or seizure seemed dominantly happen. It also observed several sudden increase of friction at Pad-1 and Pad-2. This sudden increase is mainly caused by three body abrasions during this process [90].

Figure 4.32 show several type of the wear debris found after the rubbing process. From this micrograph, it can be postulated that different wear process were taken place during the rubbing process. Fiber pull-out, micro-cutting, transfer and fracture are the dominant wear process found during the braking. Short fiber features as shown in Figure 4.32 (a) suggested that the fiber has been pulled out from the bulk material. Flake debris as shown in Figure 4.32 (b) and (c) was formed due to adhesion and delaminating process which is mainly caused by subsurface cracks [108]. Spall debris as shown in Figure 4.32(d) may come up from fracture. Plough mark and embedded hard particles as shown in Figure 4.30 above suggest abrasion was taken place.

4.3.2. Effect of Sliding Speed to Wear

Figure 4.33 shows the effect of sliding speed to wear. Similar to effect of contact pressure, wear of the sample generally increasing with the incremental of sliding speed by two trends, linearly and exponentially. Similar to previous finding, Pad-2 is the most resistant with changing of sliding speed while Pad-1 shows the lowest resistant at different sliding speed.

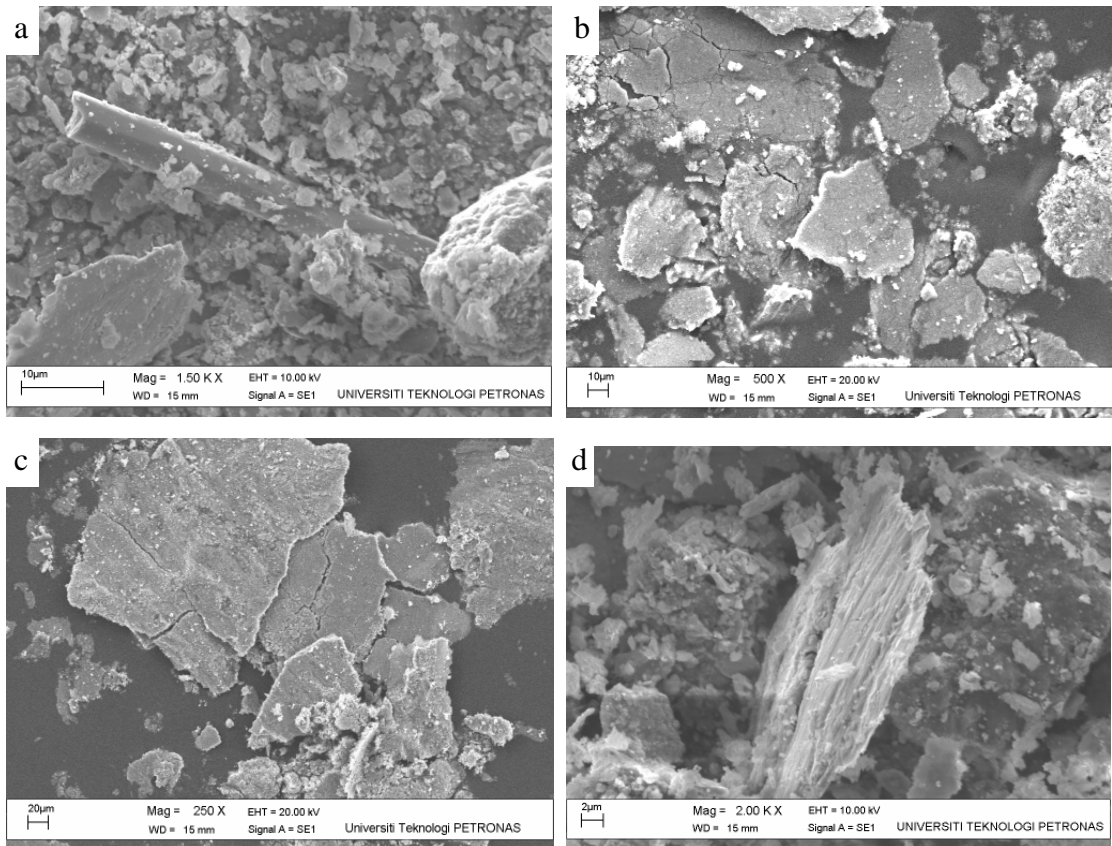


Figure 4.32 SEM micrograph of several types of wear debris collected from samples, (a) fiber pulled out type, (b) Flake debris type, (c) Flake debris type with bigger size, (d) spall debris type

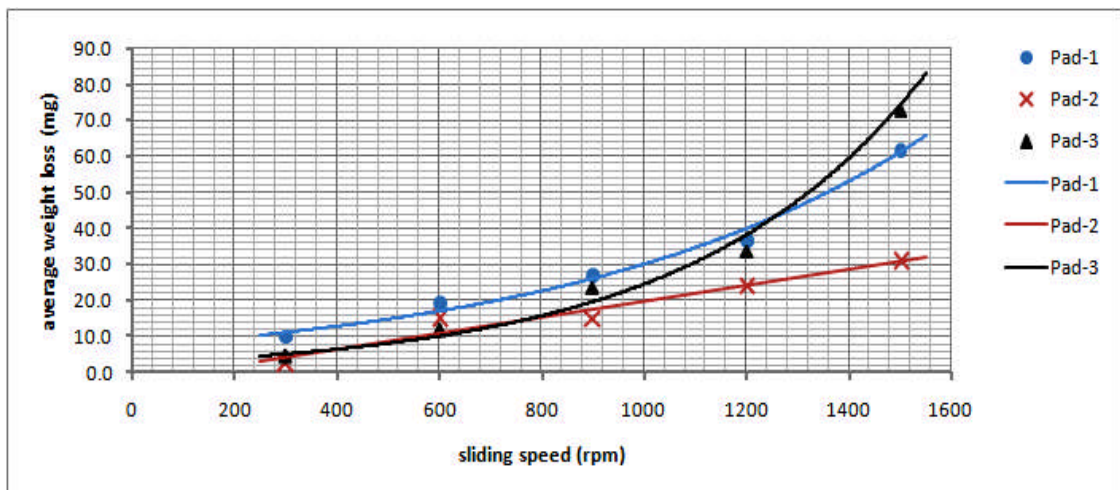


Figure 4.33 Effects of sliding speed to wear

As the sliding speed was increased, the frequency of the asperities brought to contact increased as well. As a consequence, a rapid plastic deformation will take place as well as adhesion and the formation of wear debris will be accelerated. The

fatigue effects and frictional heating may intensify wear too. At higher speed, fatigue effect and frictional heating are intensified causing strong surface damage in the form of fiber pull-outs and extensive fiber and matrix fracture. High speeds also intensify the debris removal by centrifugal force avoiding the formation of protective layer [109].

Increasing velocity increases the wear rate, which in turn roughens the surface and raises the plowing and cutting contribution to friction [88]. Surface profile of the sample after sliding is shown in Appendix M. It was found the significant roughening surface with increasing sliding speed only shown by Pad-3. This factor possibly influenced by composition, hardness, and wear mechanism. Pad-3 is postulated to be dominantly consisting of abrasive material, thus the possibility of plowing and cutting action to relative soft surface become more intense.

4.3.3. Effect of Relative Humidity to Wear

The effect of relative humidity to wear is illustrated in Figure 4.34. It was found that wear of Pad-1 and Pad-2 decreased with increasing relative humidity. The decrease of wear of Pad-1 with decreasing RH is thought due the reaction between the solid lubricants and air moisture, which accelerated the formation of friction layer. When a stable friction film is formed at the surface, a stable coefficient of friction and low wear rates can be maintained [51]. EDX analyses of Pad-1 at different RH suggest possible influence of sulfur oxide in the formation of the friction layer (Table 4.8). Another possible reason to this behavior is possibly due to air moisture trapped in the pores and penetrated deep enough to maintain the moisture layer [103]. High hardness and low porosity are possibly related to decreasing trend of wear for Pad-2. At low RH, moisture trapped not sufficient enough to reduce heat accumulated. On the other hand, higher RH is possible able to reduce heat accumulation which in turn reduce wear.

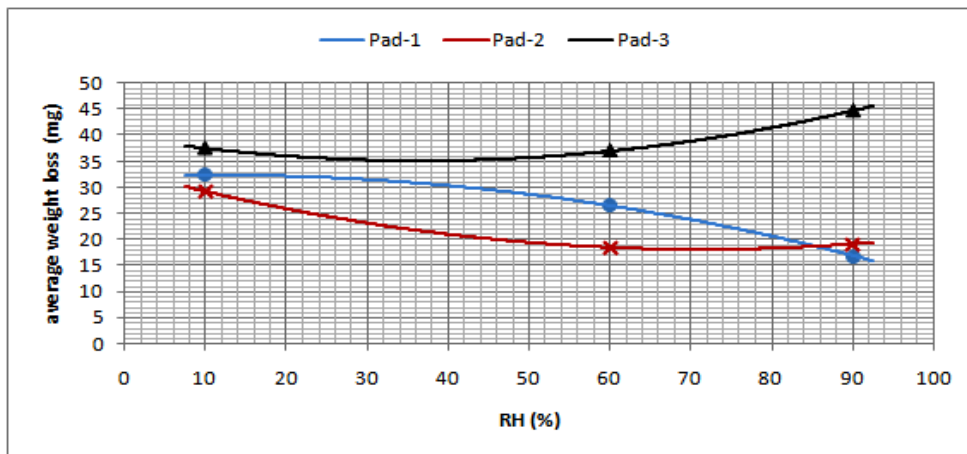


Figure 4.34 Effect of relative humidity to wear

Wear of Pad-3 increased with increasing relative humidity. The increase of wear of Pad-3 with relative humidity is thought to be due to high abrasive content of the material that actively abrade the softer part, which increased the generation of the friction layer. Moreover, SEM micrographs of Pad-3 at different RH suggest transition of abrasive to delamination mechanism was possibly take place which in turn intensify wear (Figure 4.30).

4. 4. Morphology of Worn Surface

As the result of sliding friction, the changes on the surface morphology can be observed and could be used to postulate the wear mechanism in the rubbing process. The mechanisms of the wear on the samples were occurred not in a single mechanism but rather combination of several wear mechanism. These wear mechanisms were found to be exist concurrently during rubbing process.

Adhesive wear mechanism was seemed to be dominant mechanism to cause wear on the samples. Adhesion mechanism can be noticed from the appearance of micro plateaus or scuffed surface due to adhesion of the sheared contact asperities to other location. It also can be noticed from newly developed layer at the countersurface (see section 4.5). Figure 4.35 – Figure 4.40 show several symptom of adhesion mechanism.

This adhesion form patch or else form wear particles that flow again along the contact surface and initiate the formation of other patches at other location. When the

contact pressure was increased, more friction layer was smeared at the surface and severe adhesion was taken place. At the higher contact pressure, especially Pad-1, delamination mechanism was found. Delamination wear is a wear mechanism where flake like debris is removed from the surface parallel to the wear surface, mimicking delamination as the sliding proceeds [68]. Figure 4.41 – Figure 4.43 show several symptoms of delamination mechanism on the worn surface of the sample. Flake debris as been shown in Figure 4.32(b) and (c) also imply the existence of adhesion and delamination mechanism.

Figure 4.44 – Figure 4.49 show several abrasive mechanisms at different contact pressure and speed. Abrasive wear symptom can be identified from surface scratch or groovy cut indicating hard particles cut and or ploughed the contact surface. This phenomenon imply that abrasive content as well as the wear debris were actively abraded the surface during sliding, which in turn increased the gripping and furthermore initiate formation of friction layer.

Figure 4.50 – Figure 4.54 show several fatigue mechanisms at different sample, contact pressure and speed. This mechanism can be identified from surface or subsurface crack, striation and spall on the surface.

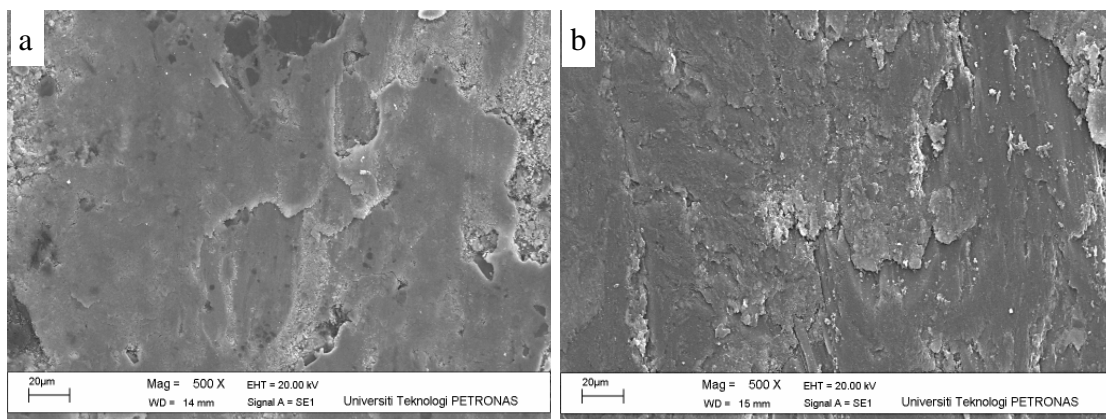


Figure 4.35 Adhesive wear feature on Pad-1 at different contact pressure; (a) 1 MPa, (b) 1.5 MPa, (c) 2 MPa, (d) 2.5 MPa, (e) 3 MPa

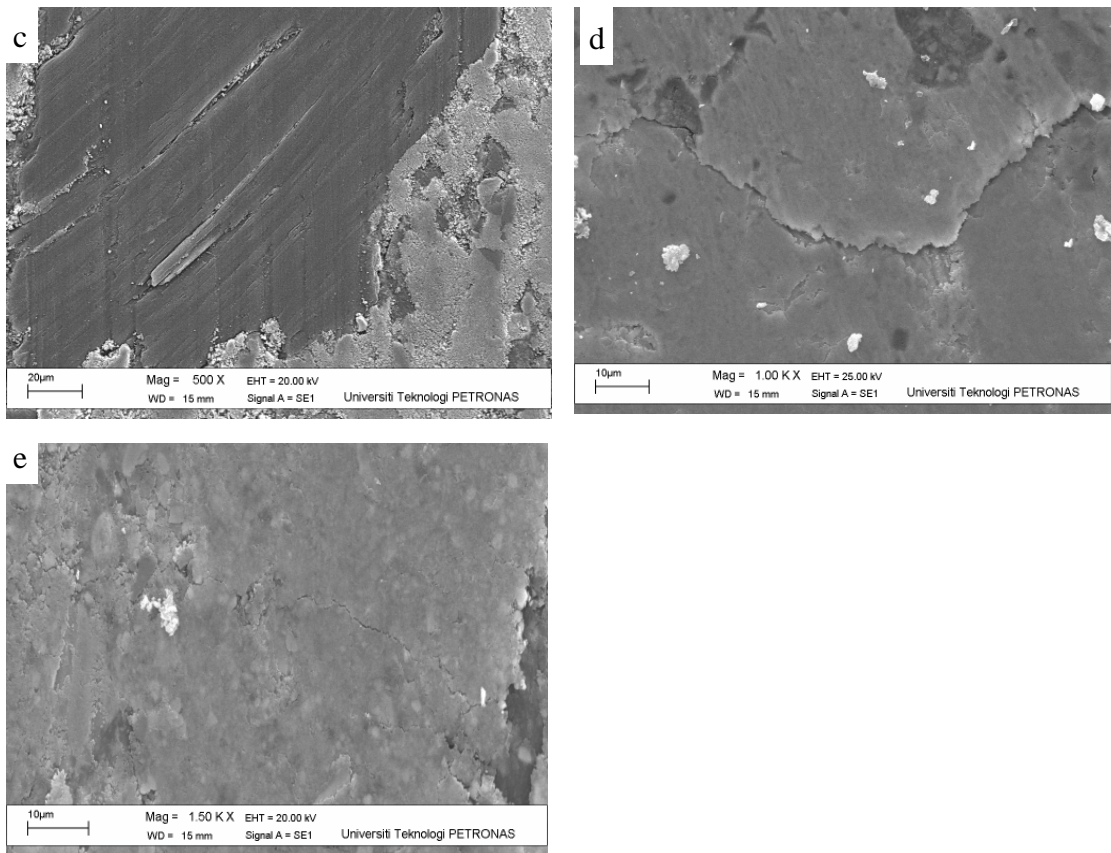


Figure 4.35 Adhesive wear feature on Pad-1 at different contact pressure; (a) 1 MPa, (b) 1.5 MPa, (c) 2 MPa, (d) 2.5 MPa, (e) 3 MPa (*continued*)

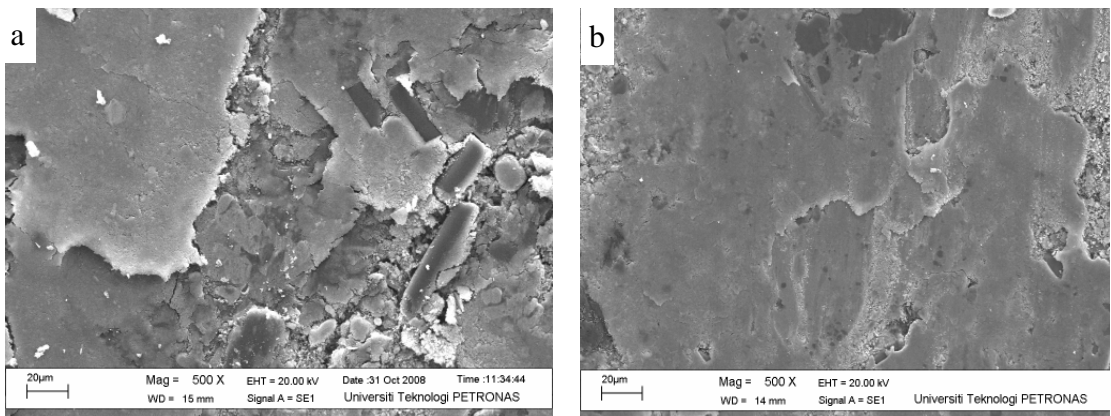


Figure 4.36 Adhesive wear feature on Pad-1 at different sliding speed; (a) 300 rpm, (b) 600 rpm, (c) 900 rpm, (d) 1200 rpm, (e) 1500 rpm

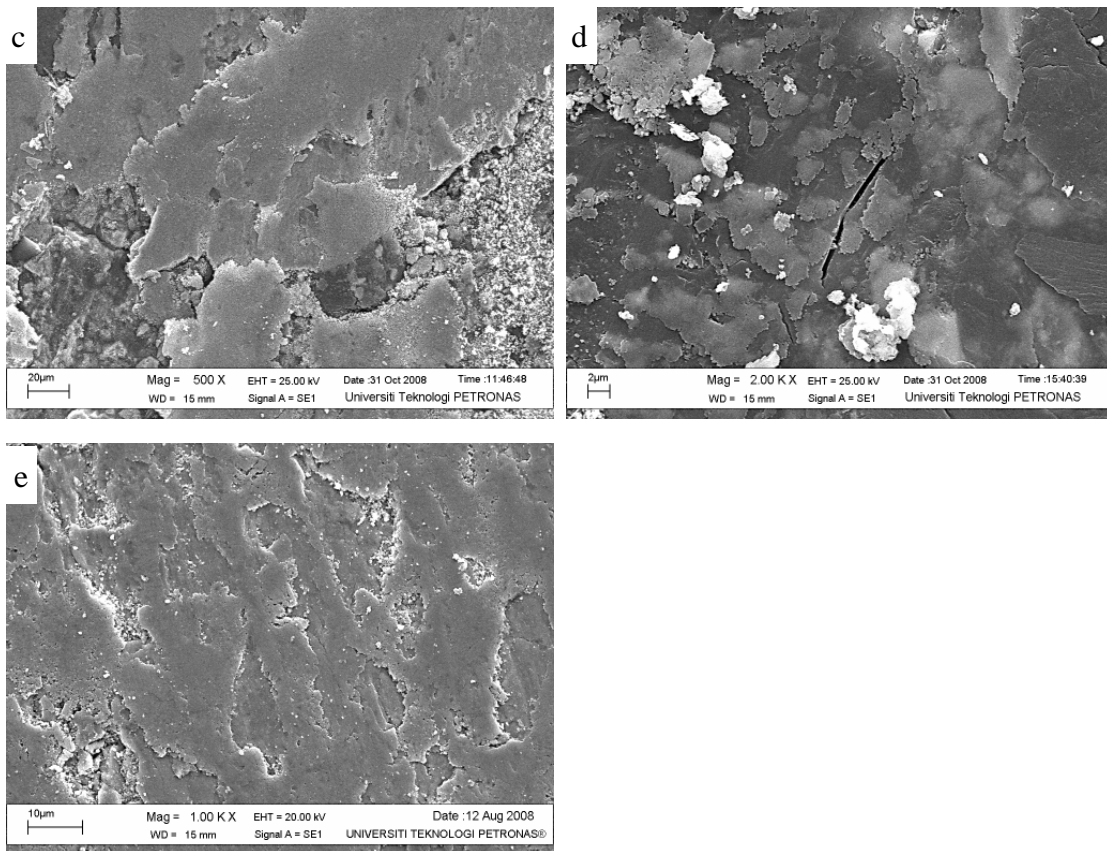


Figure 4.36 Adhesive wear feature on Pad-1 at different sliding speed; (a) 300 rpm, (b) 600 rpm, (c) 900 rpm, (d) 1200 rpm, (e) 1500 rpm (*continued*)

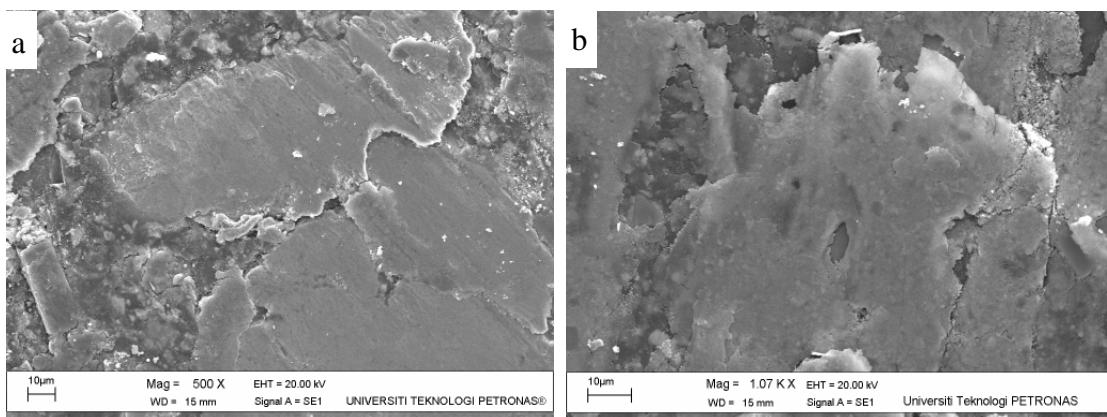


Figure 4.37 Adhesive wear feature on Pad-2 at different contact pressure; (a) 1 MPa, (b) 1.5 MPa, (c) 2 MPa, (d) 2.5 MPa, (e) 3 MPa

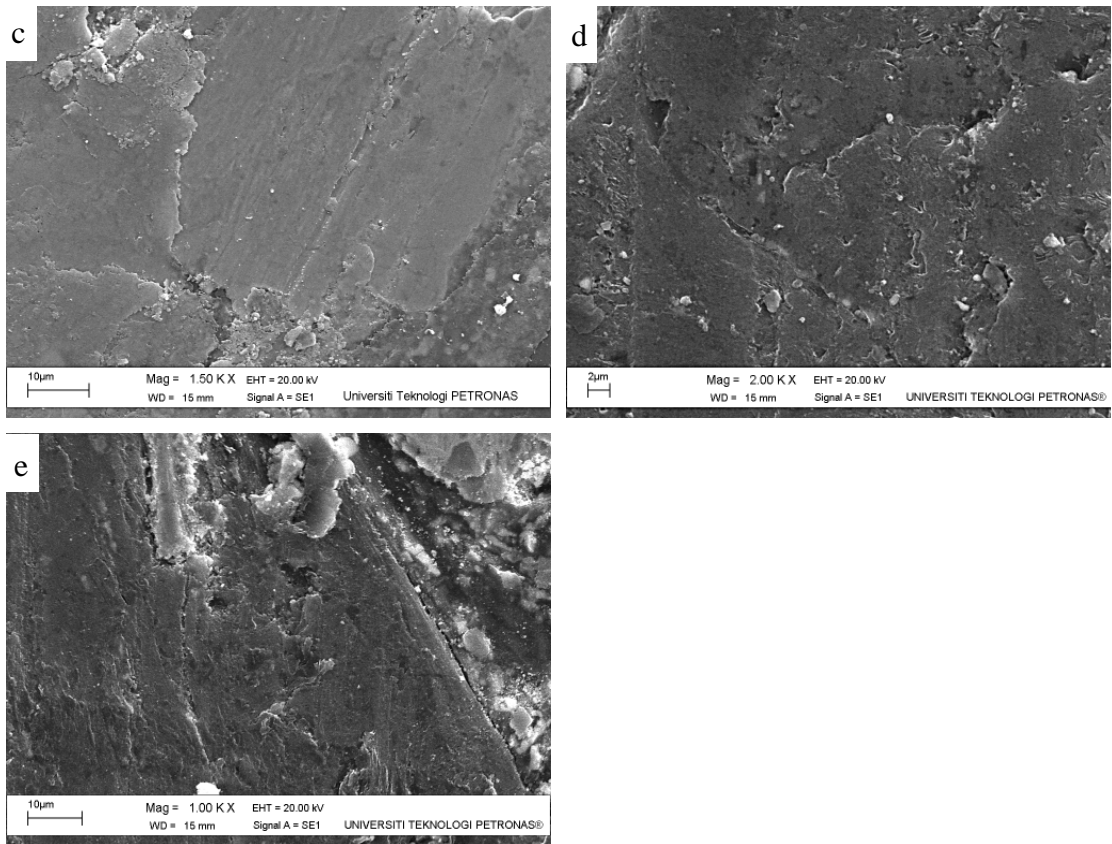


Figure 4.37 Adhesive wear feature on Pad-2 at different contact pressure;
(a) 1 MPa, (b) 1.5 MPa, (c) 2 MPa, (d) 2.5 MPa, (e) 3 MPa (*continued*)

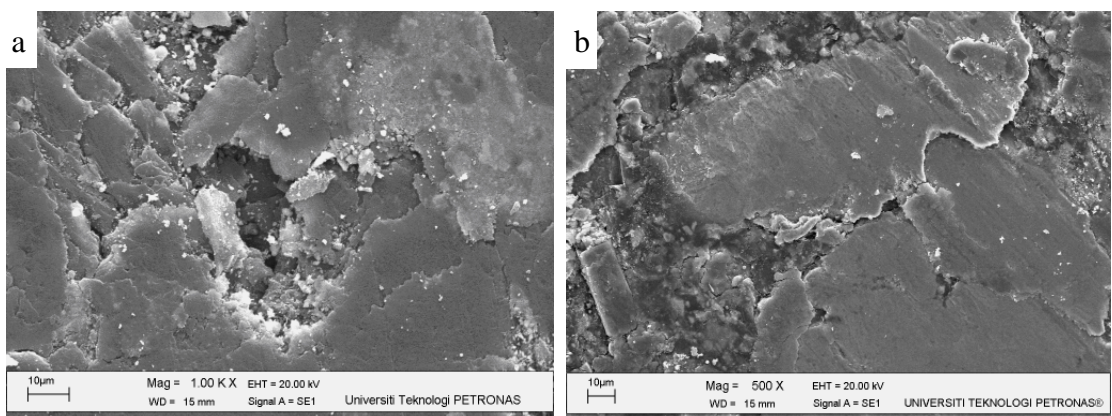


Figure 4.38 Adhesive wear feature on Pad-2 at different sliding speed;
(a) 300 rpm, (b) 600 rpm, (c) 900 rpm, (d) 1200 rpm, (e) 1500 rpm

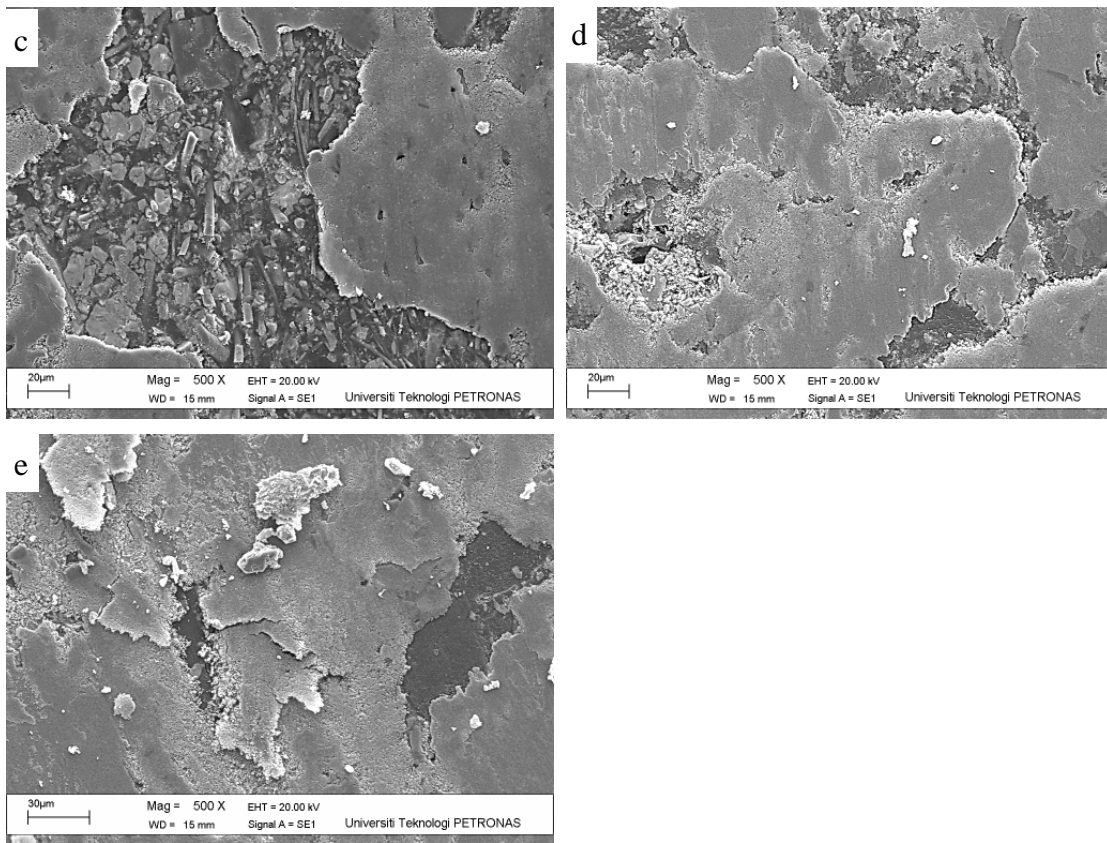


Figure 4.38 Adhesive wear feature on Pad-2 at different sliding speed; (a) 300 rpm, (b) 600 rpm, (c) 900 rpm, (d) 1200 rpm, (e) 1500 rpm (*continued*)

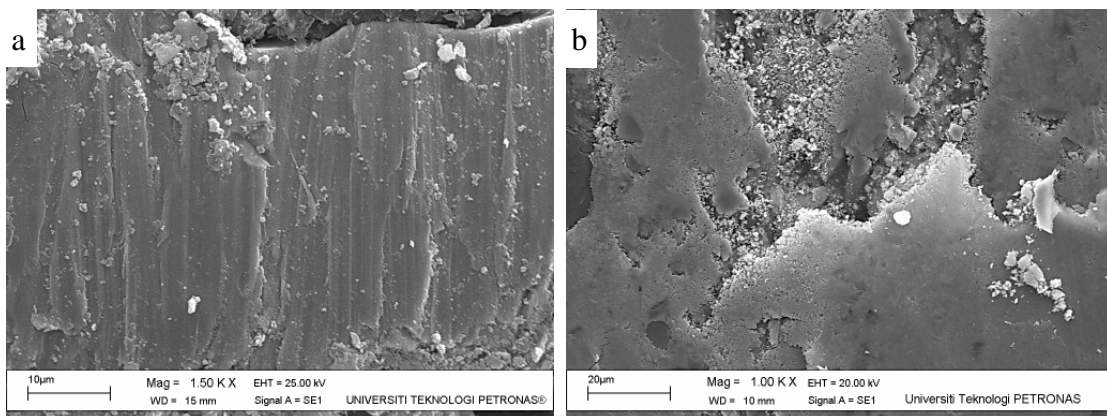


Figure 4.39 Adhesive wear feature on Pad-3 at different contact pressure; (a) 1 MPa, (b) 1.5 MPa, (c) 2 MPa, (d) 2.5 MPa, (e) 3 MPa

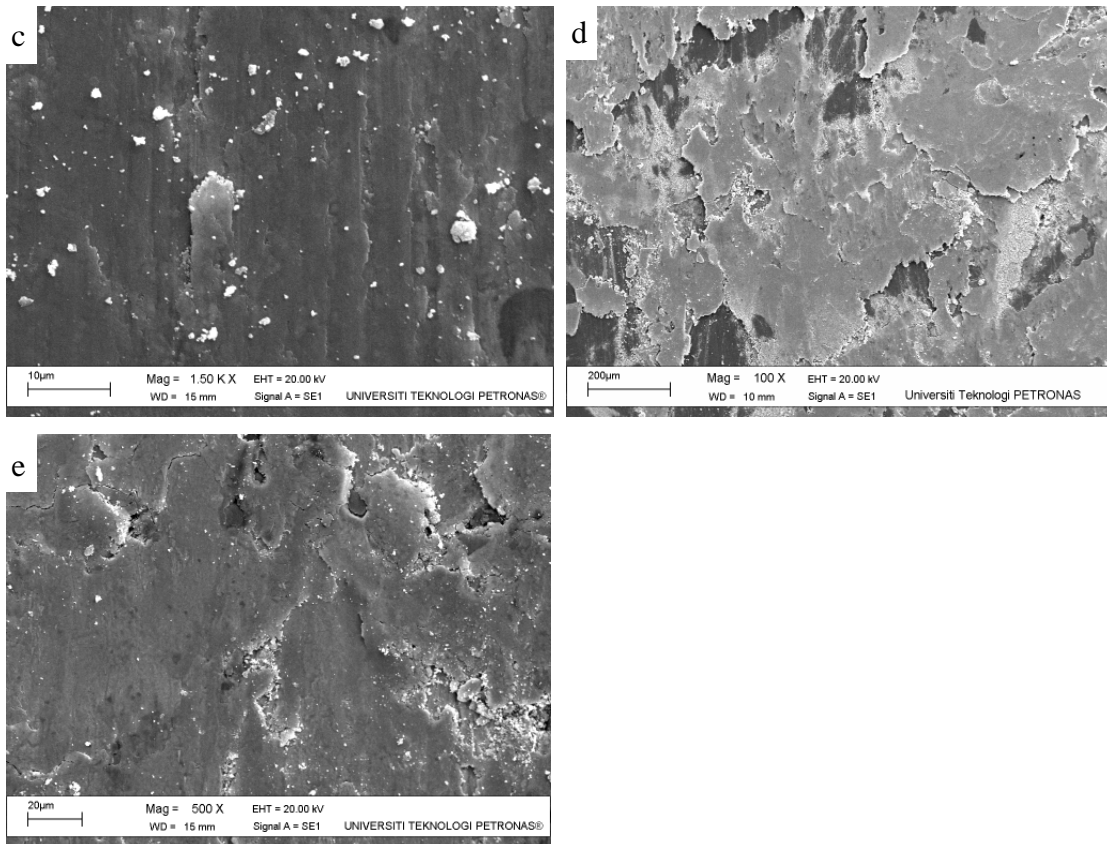


Figure 4.39 Adhesive wear feature on Pad-3 at different contact pressure;
(a) 1 MPa, (b) 1.5 MPa, (c) 2 MPa, (d) 2.5 MPa, (e) 3 MPa (*continued*)

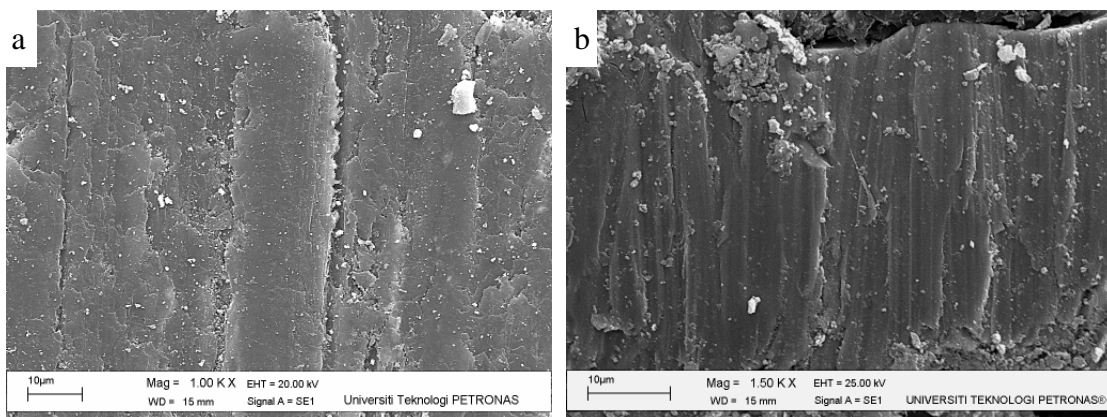


Figure 4.40 Adhesive wear feature on Pad-3 at different sliding speed;
(a) 300 rpm, (b) 600 rpm, (c) 900 rpm, (d) 1200 rpm, (e) 1500 rpm

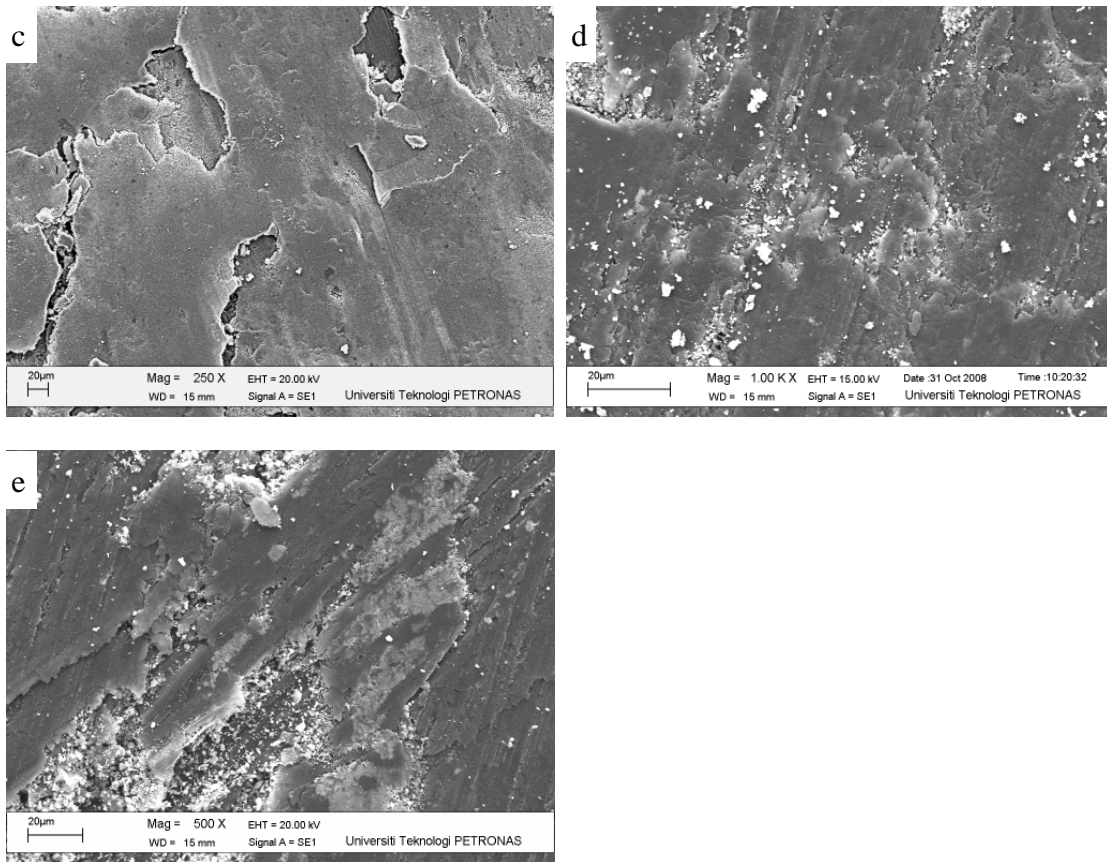


Figure 4.40 Adhesive wear feature on Pad-3 at different sliding speed; (a) 300 rpm, (b) 600 rpm, (c) 900 rpm, (d) 1200 rpm, (e) 1500 rpm (*continued*)

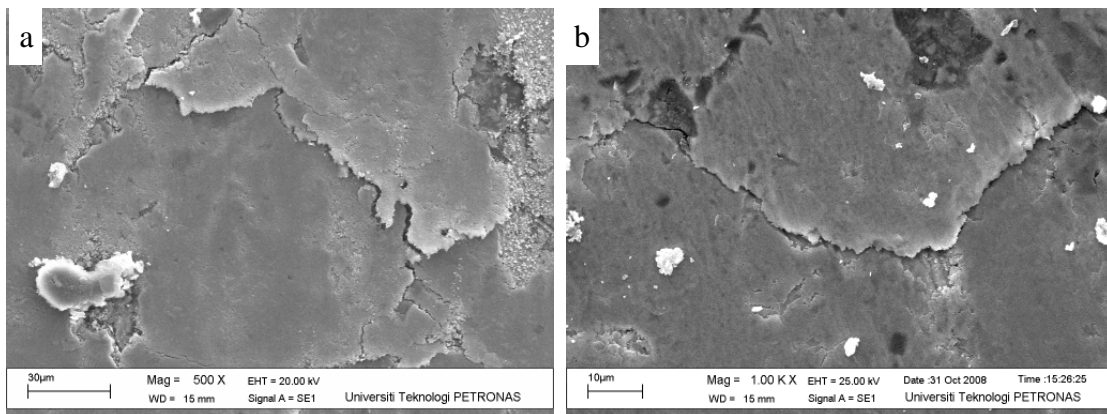


Figure 4.41 Delamination wear feature on Pad-1; (a) 2 MPa, (b) 2.5 MPa, and (c) 3 MPa

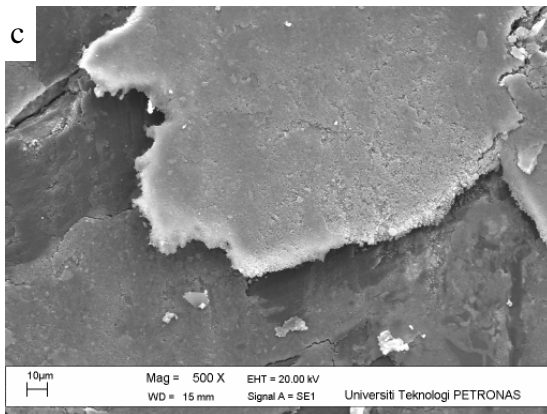


Figure 4.41 Delamination wear feature on Pad-1; (a) 2 MPa, (b) 2.5 MPa, and (c) 3 MPa (*continued*)

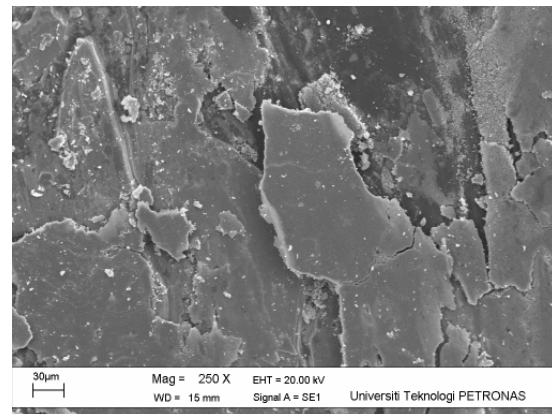


Figure 4.42 Delamination wear feature on Pad-2 at 2 MPa

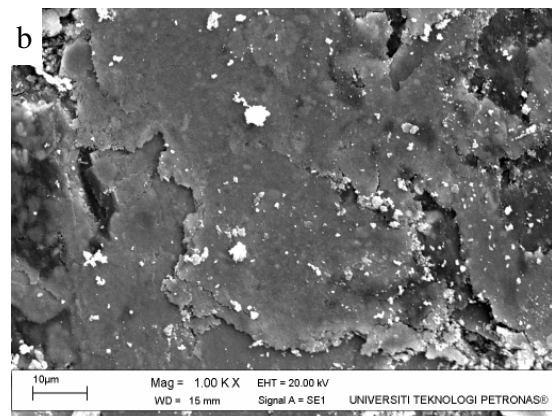
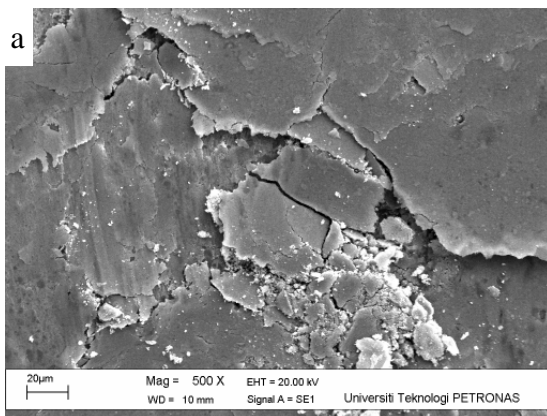


Figure 4.43 Delamination wear feature on Pad-3 at different contact pressure; (a) 2.5 MPa, (b) 3 MPa

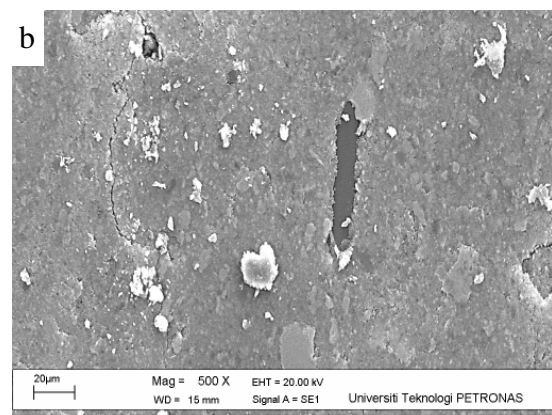
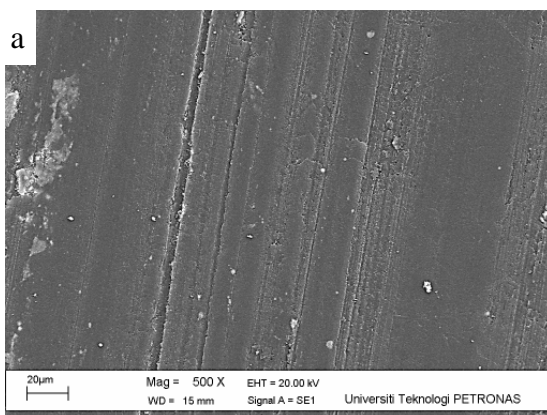


Figure 4.44 Abrasive wear feature on Pad-1 at different contact pressure; (a) 1 MPa, (b) 3 MPa

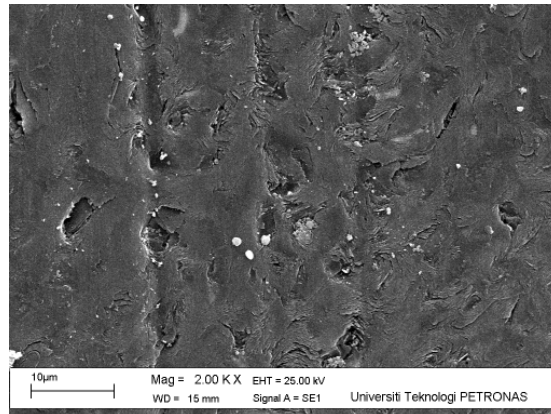


Figure 4.45 Abrasive wear feature on Pad-1 at 900 rpm

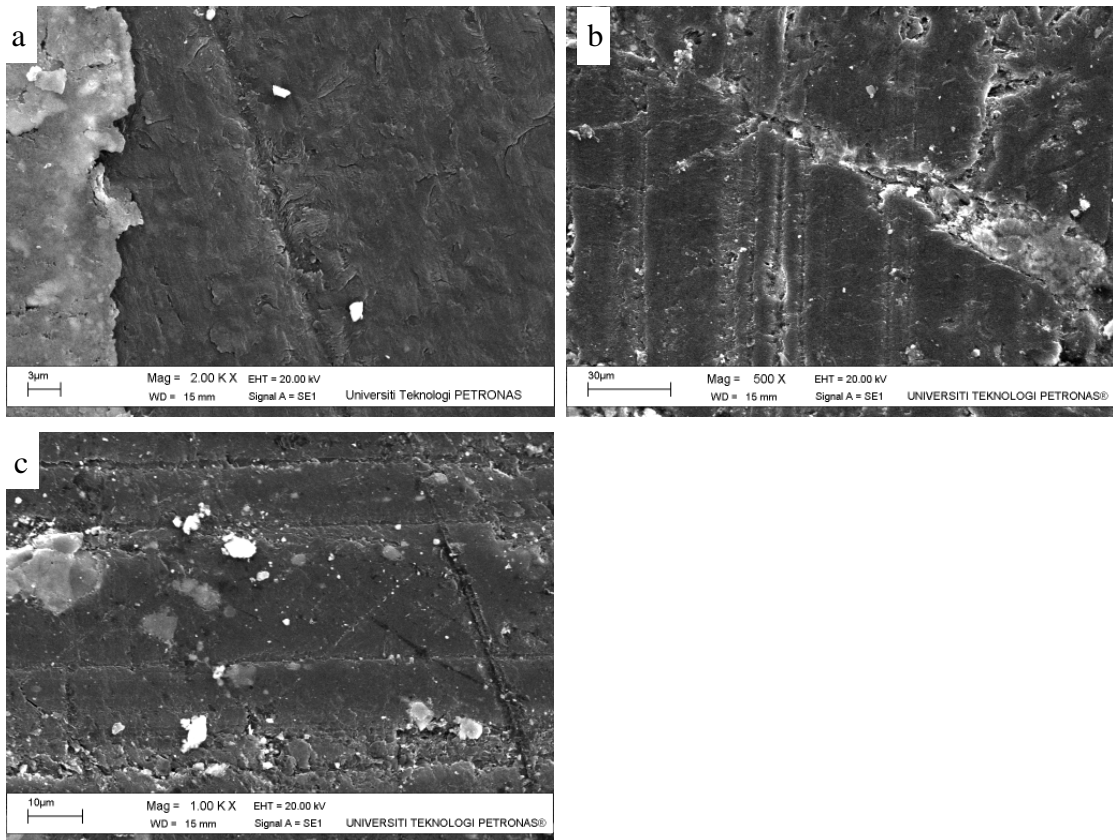


Figure 4.46 Abrasive wear feature on Pad-2 at different contact pressure; (a) 1 MPa, (b) 2.5 MPa, (c) 3 MPa

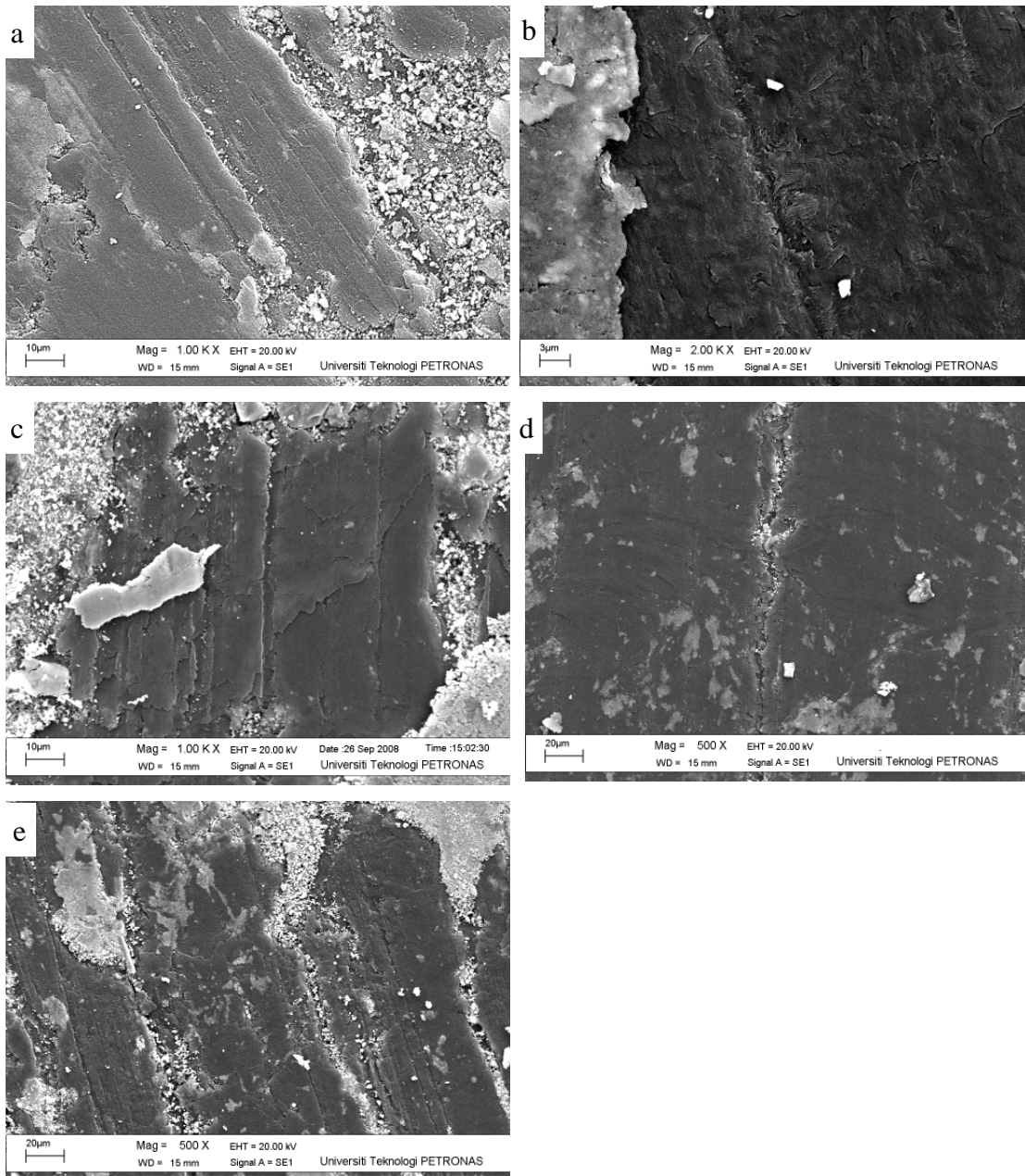


Figure 4.47 Abrasive wear feature on Pad-2 at different sliding speed; (a) 300 rpm, (b) 600 rpm, (c) 900 rpm, (d) 1200 rpm, (e) 1500 rpm

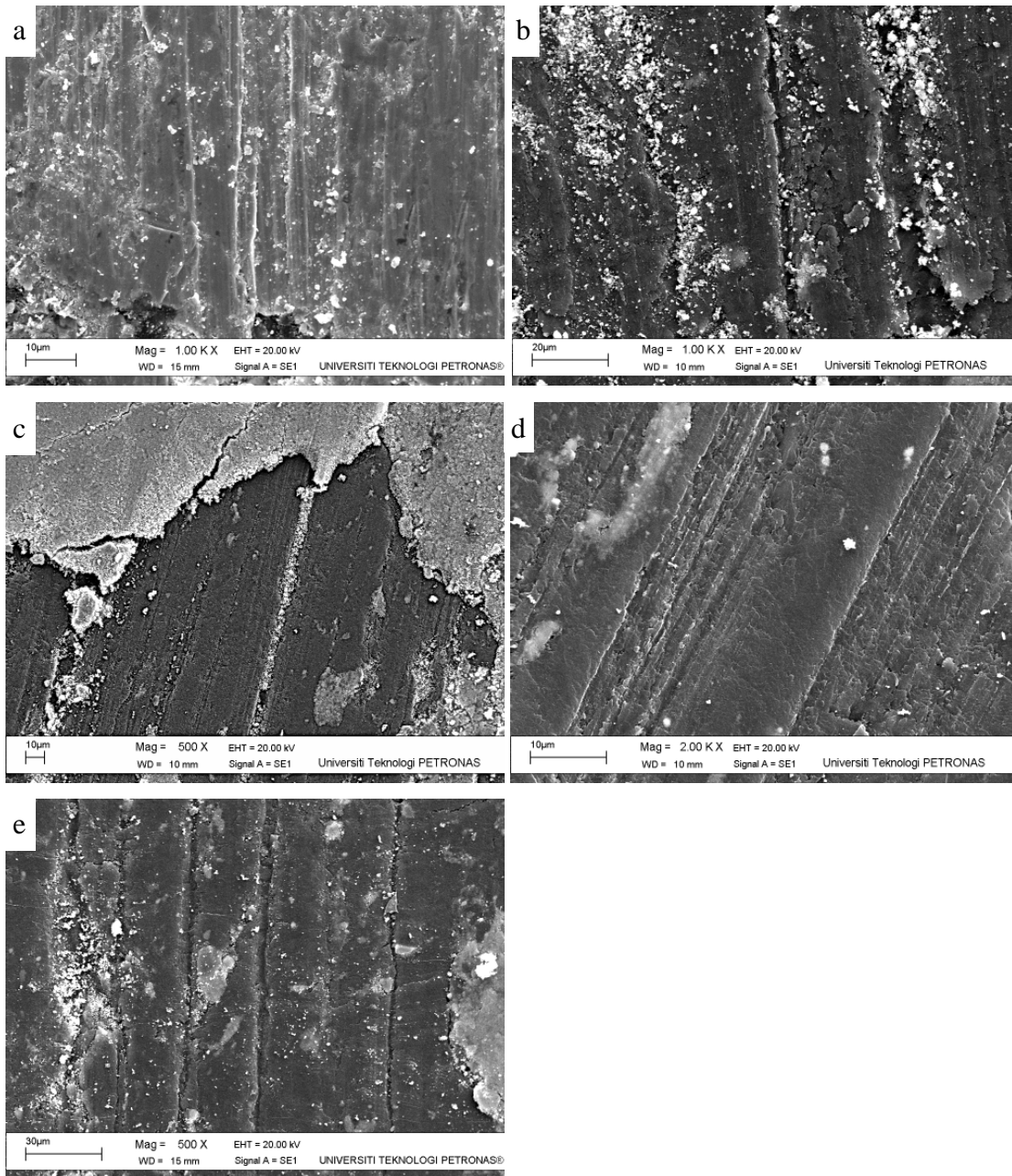


Figure 4.48 Abrasive wear feature on Pad-3 at different contact pressure; (a) 1 MPa, (b) 1.5 MPa, (c) 2 MPa, (d) 2.5 MPa, (e) 3 MPa

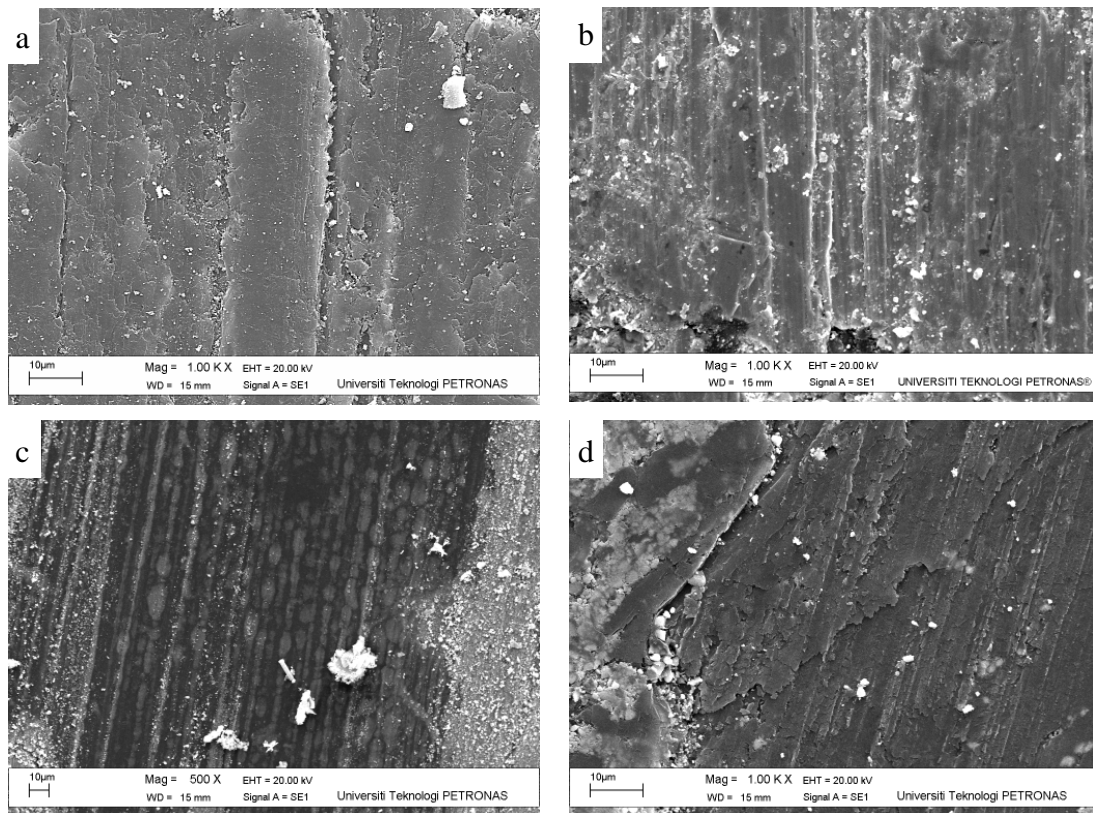


Figure 4.49 Abrasive wear feature on Pad-3 at different sliding speed; (a) 300 rpm, (b) 600 rpm, (c) 1200 rpm, (d) 1500 rpm

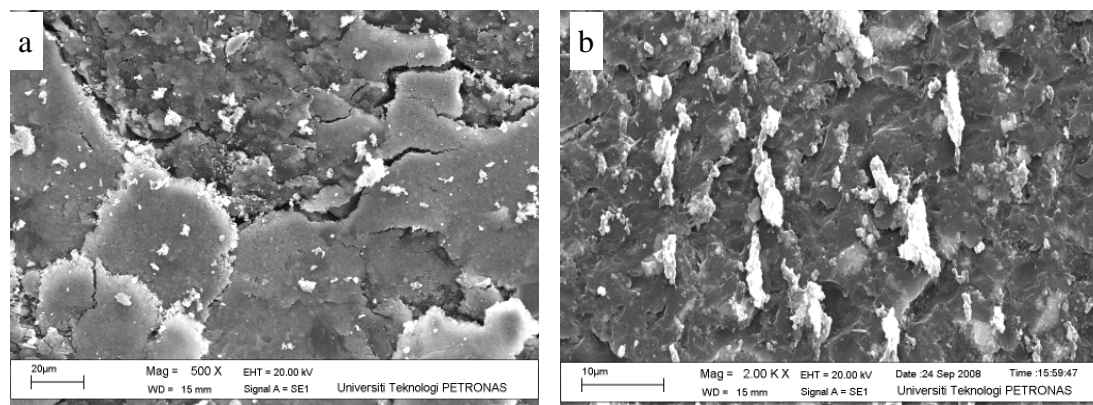


Figure 4.50 Fatigue wear feature on Pad-1 at different contact pressure; (a) 1 MPa, (b) 1.5 MPa, (c) 2 MPa, (d) 2.5 MPa

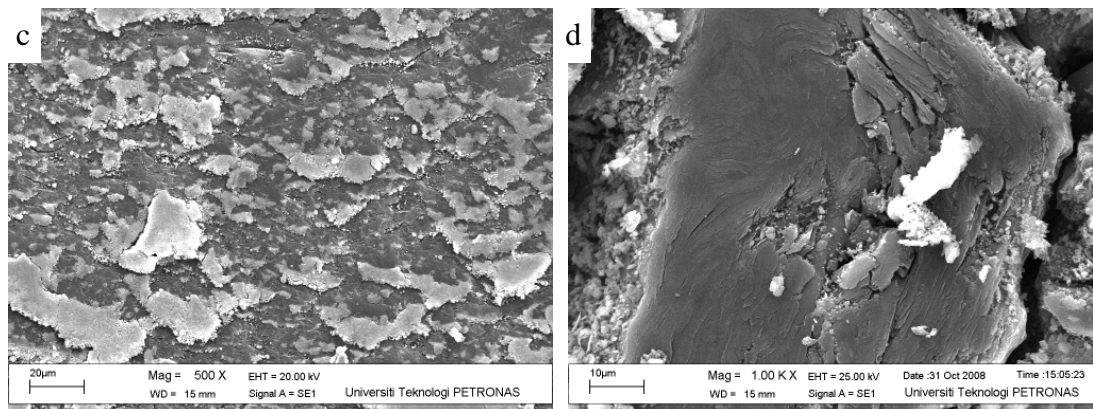


Figure 4.50 Fatigue wear feature on Pad-1 at different contact pressure; (a) 1 MPa, (b) 1.5 MPa, (c) 2 MPa, (d) 2.5 MPa (*continued*)

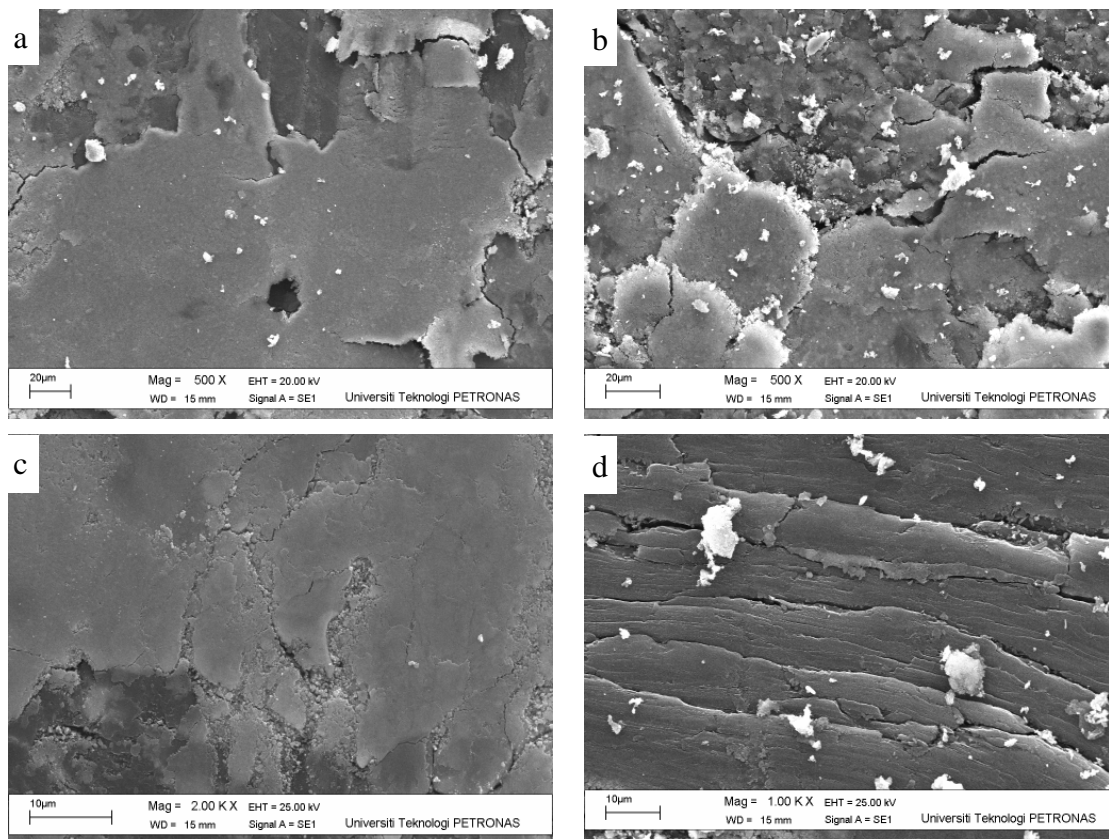


Figure 4.51 Fatigue wear feature on Pad-1 at different sliding speed; (a) 300 rpm, (b) 600 rpm, (c) 900 rpm, (d) 1200 rpm, (e) 1500 rpm

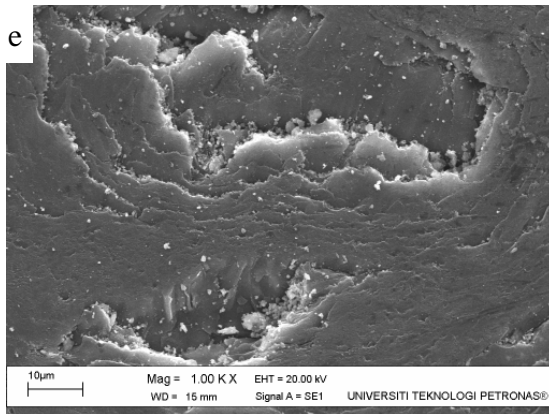


Figure 4.51 Fatigue wear feature on Pad-1 at different sliding speed; (a) 300 rpm, (b) 600 rpm, (c) 900 rpm, (d) 1200 rpm, (e) 1500 rpm (*continued*)

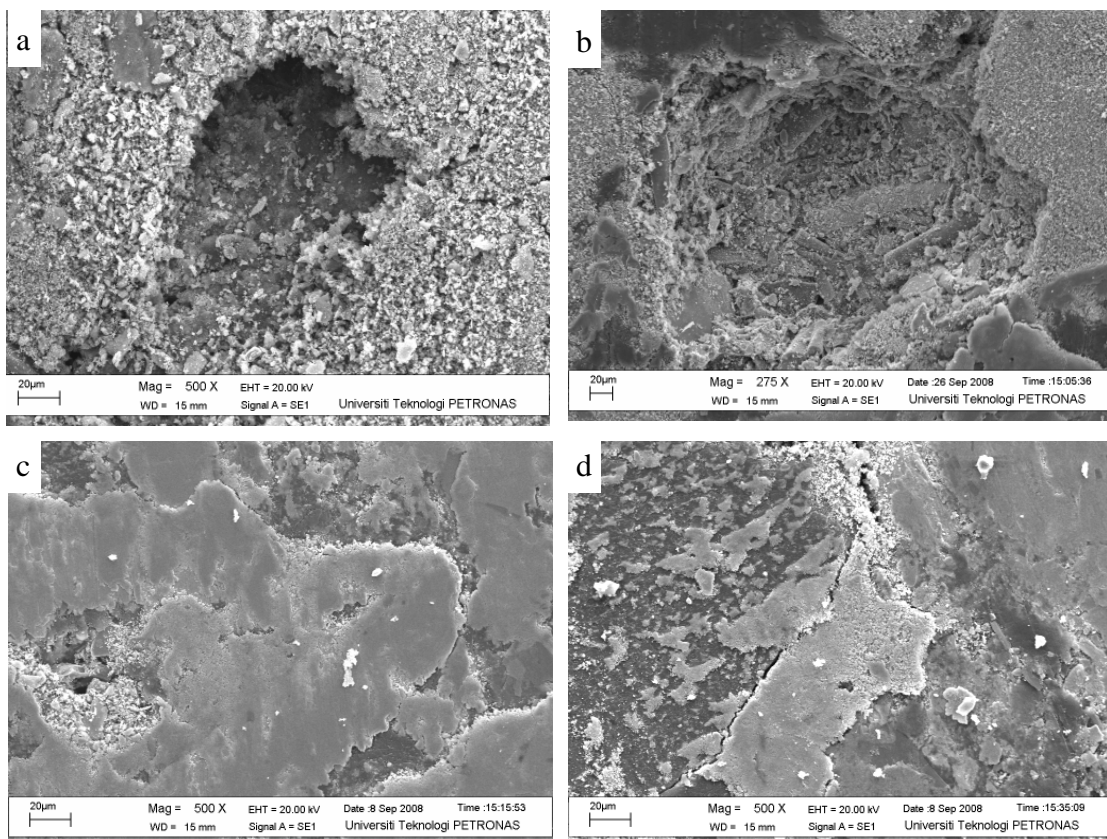


Figure 4.52 Fatigue wear feature on Pad-2; (a) 300 rpm, (b) 900 rpm, (c) 1200 rpm, (d) 1500 rpm

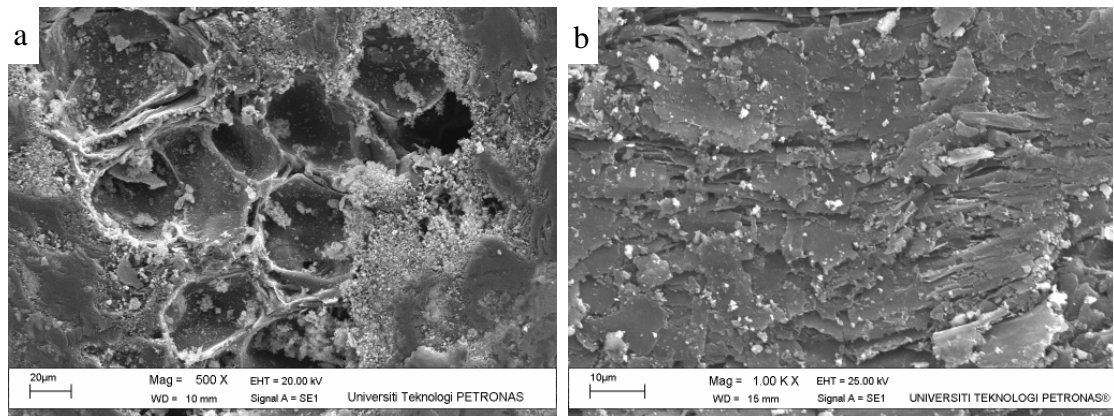


Figure 4.53 Fatigue wear feature on Pad-3 at different load; (a) 1.5 MPa, (b) 2 MPa

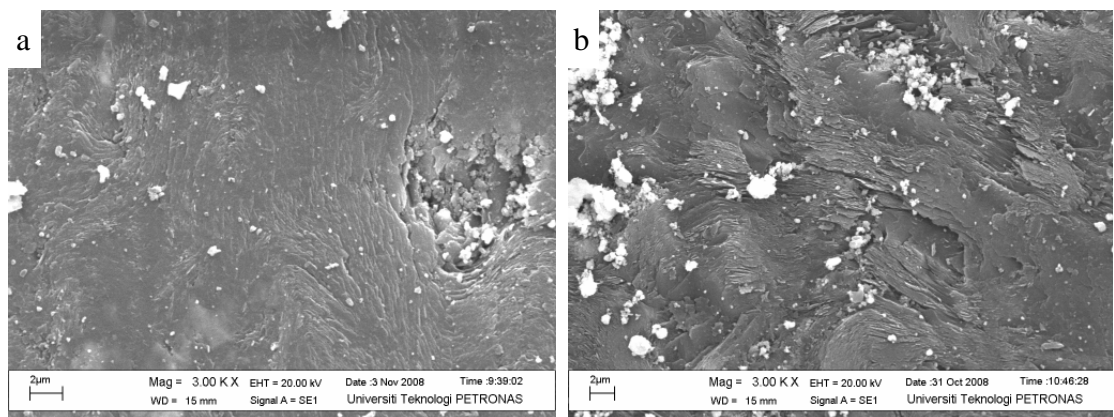


Figure 4.54 Fatigue wear feature on Pad-3 at different sliding speed (a) 300 rpm, (b) 900 rpm

The severe adhesion and delamination mechanism at the high contact pressure could be the possible reason for the increasing of wear rate and decreasing of COF. Similar finding by Talib and Azhari stated that delamination mechanism started earlier when the applied contact pressure was increased [68]. Severe adhesion and delamination mechanism phenomenon may be happened due to this process; at initial stage, the contact area was small at any given moment. With the increasing frictional heating, most organic constituents produced an oily degradation product which condensed nearby as miniature droplets. When the rubbing contact zone included these droplets, they smeared, along with fine particulate debris, transform into platelets. The platelets were seen to flow through the shearing action at the interface toward the trailing edge of the lining. Some of the platelets eventually adhered to the

countersurface and were swept away from the trailing edge of the lining. When the sliding condition provide low lining wear rates, these platelets then reenter the contact zone at the leading edge of the lining and again flowed toward the trailing edge. Occasionally these platelets exited the side of the lining specimen. When the lining wear rates were high the percentage of platelets which exited laterally, or did not reenter the leading edge, increased [110]. This phenomenon is due to the tangential force which may entrap and pressurized the gaseous decay product of the organic component (pyrolysis product). The occurrences of several flat wear particles confirm the formation of surface layers. During frictional contact, some fibers may be detached from the surface and adhesion also may detach large chips of filler material (Figure 4.32).

More hard particles and compacted debris spread over the surface may also has to be considered for its role in increasing the friction and wear. Figure 4.44, Figure 4.46, and Figure 4.48 indicates more cutting action happen due to increasing of applied load which result in the increasing of wear. The ability of contact pressure to penetrate the contact asperities is considered to affect wear. It is thought that increasing contact pressure will cause deeper penetration of the harder material into the softer material. As result, the more cutting action and removal of the softer material will occur and more wear debris will be produced.

Fatigue wear also seemed to be often occurred with the increasing of sliding speed for pad-1. This factor could be related to high organic content and frictional heating effect. In other sample (Pad-2 and Pad-3), fatigue effect found on relative low contact pressure and sliding speed. Similar finding by Talib dan Azhari stated that fatigue wear usually will predominate and the adhesive wear will dominate as the load increased [68].

4.5. Generation of Friction Layer

The sliding action between the brake pad sample and the gray cast iron pin generates the development of friction layer on both mating surfaces. In this work, the generation of the friction layer was investigated on the worn pin as well. After rubbing and sliding action, a dark grey colored layer was observed covering the

rubbing surfaces of both pin and pad material. The SEM micrograph shows that the grounding grooves were no longer visible and the worn surface has been covered the by friction layer as shown in Figure 4.55. The layer indicates that there was material transferred from the pad to pin during the sliding process. In order to observe the friction layer, a cross sectional image was captured by tilting the position of the specimen to 40° from the normal position. Figure 4.56 shows that a rather thin layer which has been transferred compacted and smeared on the pin surface can be observed by this technique.

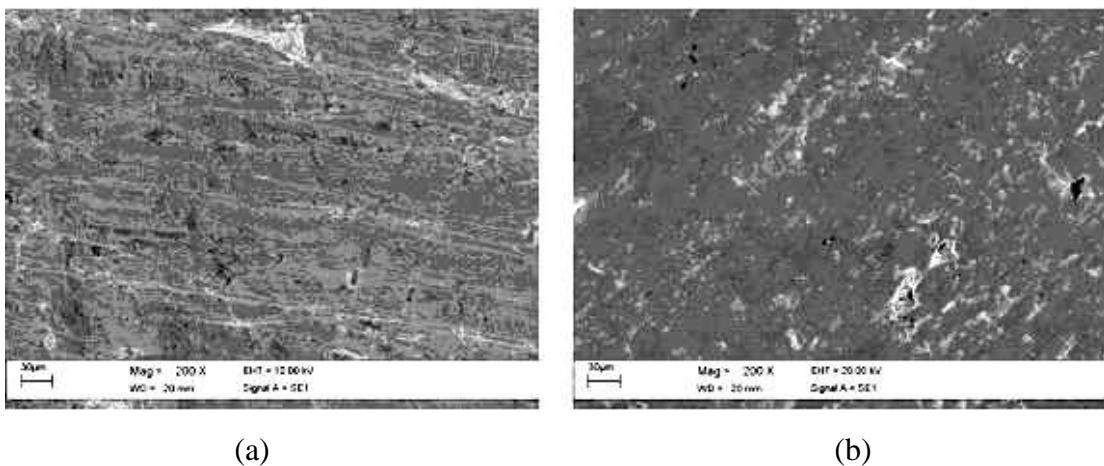


Figure 4.55 Micrograph of pin surface; (a) the rough groove on the surface before tribological test, (b) formation of transfer layer after tribological test

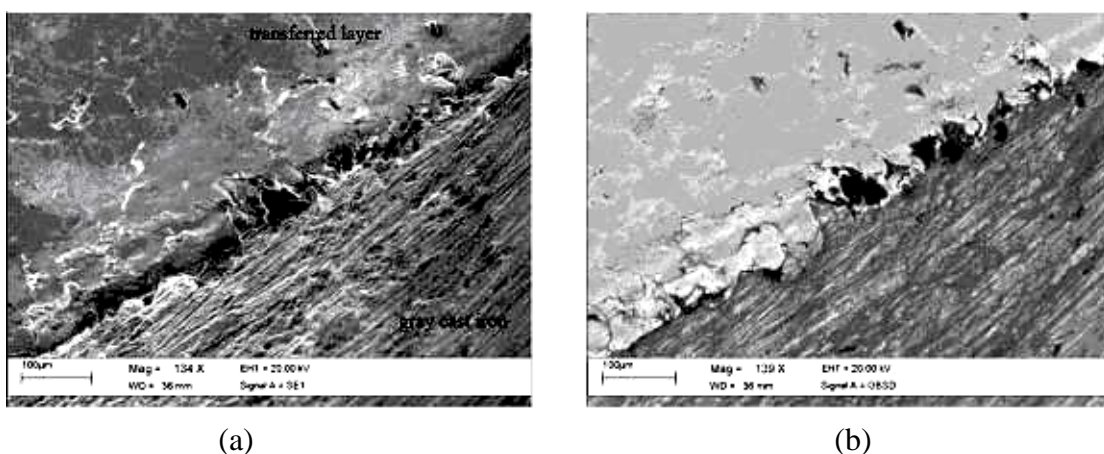
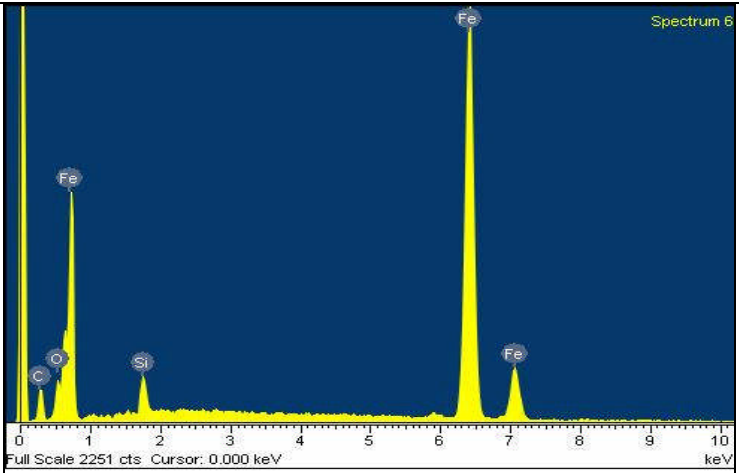


Figure 4.56 Micrograph showing transfer layer has been generated on the pin surface using; (a) secondary electron and (b) backscattered electron

EDX analysis was conducted in order to investigate the elements that had adhered on the pin by comparing the composition of the pin before and after the tribological test. The initial composition of the gray cast iron pin investigated with EDX analysis is shown in Table 4.11.

Table 4.11 Initial elements and EDX spectra of gray cast iron pin

gray cast iron		
Element	Weight %	Atomic %
C K	14.41	39.93
O K	5.14	10.69
Si K	2.48	2.93
Fe K	77.97	46.45
Totals	100	100



When the gray cast iron pin slid against Pad-1, several additional elements were found on the surface. The result of SEM-EDX analysis of the gray cast iron pin after slid against Pad-1 is presented in Table 4-12. Significant changes to peak height of O, C and Fe were observed, in addition, elements such as Al, S, and Ba had been observed as well. It was also observed that C has reduced by 9 %-wt and Fe has reduced by 15 %-wt, while O had been added by 21 %-wt.

The result of SEM-EDX analysis of the gray cast iron pin after sliding against the Pad-2 is presented in Table 4.13. Some additional elements such as Mg, Al, S, Ca, and Ba were observed after the gray cast iron pin has been rubbed against the Pad-2. The significant changes in the amount of C, O, and Fe are also observed. As can be observed from Table 4.13, C has been reduced by 5.99 %-wt. and Fe by 17.84 %-wt. from initial condition. On the other hand, O has been increased by 19.13 %-wt. to the surface while no significant change in Si is observed.

Copper was the only additional element found when the pin was sliding against Pad-3. The changes in the amount of C, O, and Fe are also observed. As can be observed from Table 4.14, C has been reduced from 14.41 %-wt to 4.45 %-wt and

Fe was reduced from 77.97 %-wt to 65.34 %-wt. On the other hand, 5.14 %-wt of O at initial condition was increased to 26.99 %-wt after sliding against Pad-3

Table 4-12 Elements and EDX spectra of gray cast iron pin after sliding with Pad-1

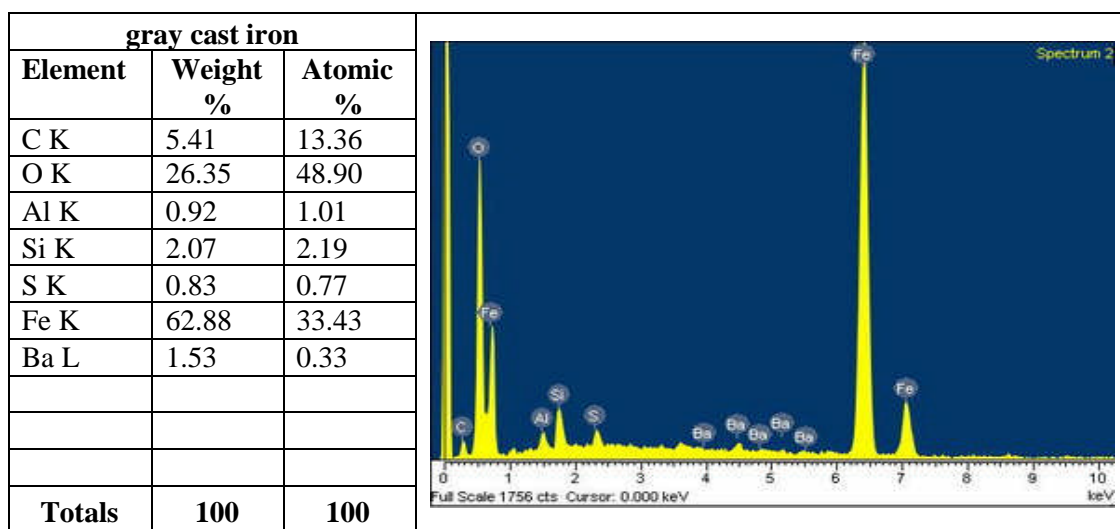
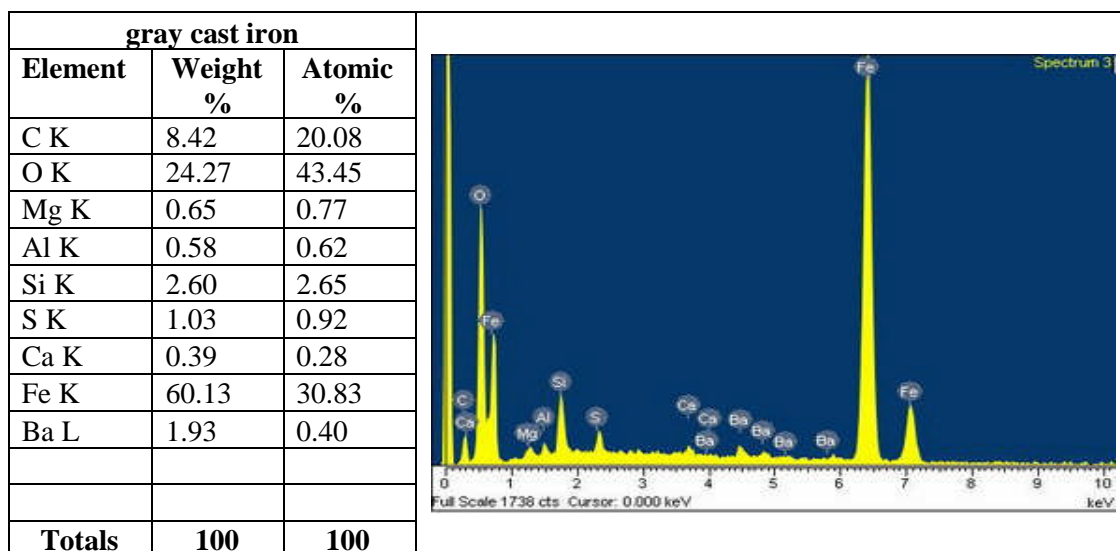
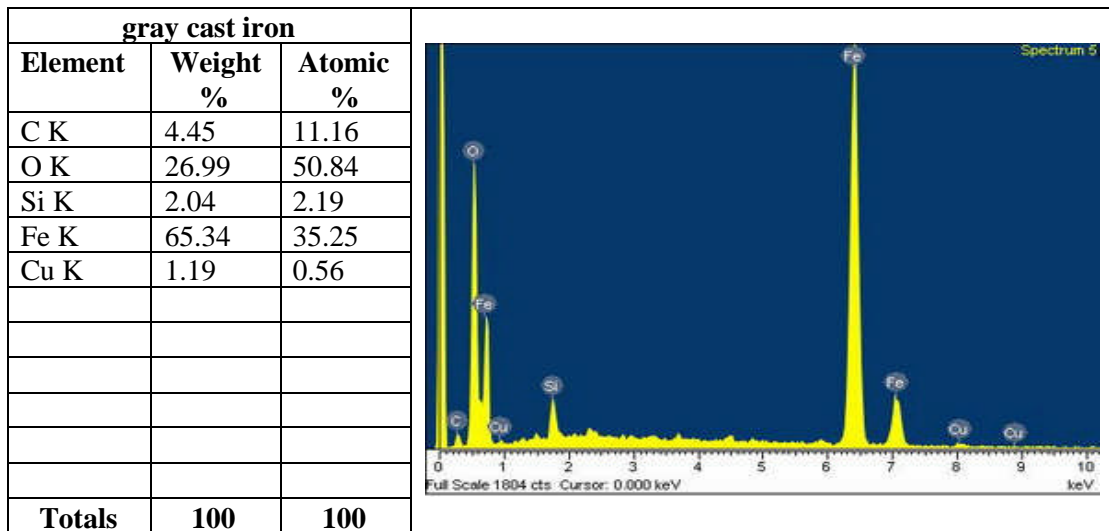


Table 4.13 Elements and EDX spectra of gray cast iron pin after sliding with Pad-2



Tabel 4.14 Elements and EDX spectra of gray cast iron pin after sliding with Pad-3

The additional new elements as shown by SEM-EDX analysis indicate that material transfer from brake pad materials to cast iron pin surface took place during sliding. This process generates the development of transfer layer at the pin surface. The increasing amount of O and decreasing amount of Fe suggests that the transfer layers mainly consist of iron oxides. The SEM-EDX results also suggest that the composition of friction layer depends on the composition of brake pad materials. Appendix N shows the elemental compositions of the gray cast iron pin before and after test.

A similar observation was also recorded by Phillip *et.al* in [3] and Gudmand-Høyer *et.al* in [35]. They found several compounds at the disc surface which originally exist in the pad. In addition, Cho *et.al* [48] stated that at low temperature the transfer layer is formed by mechanical attrition and simultaneous attachment of wear debris from friction material onto the gray iron disc surface. Furthermore, Oesterle *et.al* [38] concluded that the compact friction layer is comprised of nanocrystalline microstructure and exist at the surface of both mating surfaces. They also added in their conclusion that the mechanical mixing and oxidation plays a major role during debris production and friction layer formation.

CHAPTER FIVE

CONCLUSIONS

Friction and wear testing has been conducted on three semi metallic brake pad material for light rail transit application: Pad-1, Pad-2, and Pad-3. The results of the test show that the friction characteristics of each sample are influenced by contact pressure, sliding speed and relative humidity. The friction characteristic, however, show six general shape which the changes from one shape to another was also affected by test parameters. This factor is thought associated with composition and mechanical properties of the sample.

The friction process between mating samples is concluded as follows: (i) rapid increased at the initial stage was due to the increasing interaction of the encountered asperities, contact area and adhesion as well as abrasion of hard particles to the softer part of the sample surface, (ii) because of continuous process of deformation, adhesion, and abrasion; the increasing of friction will continuously taken place until reaching a maximum COF where the maximum interfacial adhesion, plastic deformation, and wear particles entrapment is reached, (iii) coefficient of friction then decreased due to degradation of organic content, formation of fine friction layer at the interfacial contact and most asperities tip have been sheared, (iv) a steady state friction was reached due to formation of well developed and stable friction layer, (v) destruction of the previous well developed friction layer by wear particles which then initiate the formation of other stable friction layer. The presence of the above process is postulated due to the process of plastic deformation of friction layer and thermal degradation of the sample.

Contact pressure and sliding speed were found influence the duration of the friction processes. This occurrence is most possibly influence by composition and thermal degradation of the organic component in the sample. In addition, relative humidity was found to affect the friction fluctuation stability. This is related to formation of the friction layer which affected by composition and porosity of the sample.

Wear of the samples were found increase with contact pressure and sliding speed. The increase of wear with pressure is postulated due to the increasing of plastic deformation on the contact asperities. This plastic deformation consequently sheared off the asperities and the more asperities brought in real contact the more acceleration of plastic deformation will occur. This in turn will increase adhesion and generation of wear debris. More cutting action and removal of the softer material due to a deeper penetration of harder material into the softer material with increasing contact pressure could be another source of increasing of wear rate. The increasing wear to sliding speed is postulate related to increasing shear frequency of the asperities. Rapid plastic deformation will take place due to this action, which in turn could roughen the surface and raises the plowing and cutting action. Moreover, adhesion and the formation of wear debris will be accelerated. The other factor could be associated with increasing of fatigue effects and frictional heating. At higher speed, fatigue effect and frictional heating are intensified causing strong surface damage in the form of fiber pull-outs and extensive fiber and matrix fracture. High speeds also intensify the debris removal by centrifugal force avoiding the formation of protective layer

Wear of Pad-1 and Pad-2 were found decrease with relative humidity but wear of Pad-3 increase with humidity. This behavior is possibly associated with ability of sample to trap moisture and reduce frictional heating which affected by composition, hardness and porosity of the sample.

Surface morphology had revealed combination of several wear mechanism; (i) adhesive wear, (ii) abrasive wear, (iii) fatigue wear, and (iv) delamination wear. However, adhesive and fatigue mechanism was found as the dominant wear mechanism. These mechanisms were found in the sample under all contact pressures and sliding speeds.

In the study on the worn surface morphology, SEM can be used to provide the information on the microstructural changes (microcrack, wear mechanism, topography) on the investigated surface. However this technique could not provide the bulk microstructure such as strain, dislocation, nucleation and propagation of microcrack, third body, and fatigue, wear morphology. Thus, a combination SEM, transmission electron microscopy and focused ion beam (FIB) is recommended to be

used in the study of; (i) friction layer composition, (ii) friction layer thickness, (iii) dislocation and crack propagation. The knowledge on the bulk and subsurface could be shed greater understanding on the microstructural changes of the sample worn surfaces.

In the present work, the study tribological tests were performed under different contact pressures, sliding speed and relative humidity. It would be interesting to study and gain more information on the tribological properties of friction materials by varying the other testing parameters (sliding time, surface temperature) and test conditions (wet, oily, surface roughness) in the future.

REFERENCES

1. Jang, H., J. J. Lee, S. J. Kim, and K.Y. Jung, *The Effect of Solid Lubricants on Friction Characteristics*, SAE technical paper no. 982235, Society of Automotive Engineers, 1998.
2. Jang, H. and S. J. Kim, The effects of antimony trisulfide (Sb_2S_3) and zirconium silicate (ZrSiO_4) in the automotive brake friction material on friction characteristics. *Wear*, 2000, 239, 229–236.
3. Filip, P., Z. Weiss, and D. Rafaja, On friction layer formation in polymer matrix composite materials for brake applications, *Wear*, 2002, 252, 189–198.
4. Filip, P., L. Kovarik, and M. A. Wright, Automotive brake lining characterization, SAE technical paper no. 973024, Society of Automotive Engineers, 1997, 41–61.
5. Desplanques, Y., O. Roussette, G. Degallaix, R. Copin, and Y. Berthier, Analysis of tribological behavior of pad–disc contact in railway braking; Part 1. Laboratory test development, compromises between actual and simulated tribological triplets, *Wear*, 2007, 262, 582–591.
6. Eriksson, M., F. Bergman, and S. Jacobson, On nature of tribological contact in automotive brakes, *Wear*, 2002, 252, 26–36.
7. Rhee, S. K., *Friction Coefficient of Automotive Friction Materials – Its Sensitivity to Load, Speed, and Temperature*, SAE technical paper no. 740415, Society of Automotive Engineers, 1974.
8. Pogosian, A. K. and N. A. Lambarian, Estimation of wear for some asbestos-reinforced friction materials, *Wear*, 1973, 23, 3–7.
9. Castelli, V., Friction, *Marks' Standard Handbook for Mechanical Engineering*, McGraw Hill, 1999.
10. Blau, P. J., R. L. Martin, M. H. Weintraub, H. Jang, and W. Donlon, *Frictional Behavior of Automotive Brake Materials Under Wet and Dry Conditions*, Oak Ridge National Laboratory, 1996.
11. Orthwein, W. C., *Clutches and Brakes: Design and Selection*, Second Edition, Marcel Dekker Inc., USA, 2004.

12. Bushan, B., *Introduction to Tribology*. John Wiley & Son Inc, New York, 2002.
13. Blau, P. J., The significance and use of the friction coefficient, *Tribology International*, 2001, 34, 585–591.
14. Budinski, K. G., and M. K. Budinski, *Engineering Materials; Properties and Selection*, Pearson Education, 2002.
15. Czichos, H., System approach to wear problems, *Wear Control Handbook*, American Society of Mechanical Engineers, 1980.
16. Czichos, H., Basic tribological parameters, *ASM Handbook Vol. 18; Friction, Lubrication, and Wear Technology*, ASM International, 1998.
17. Mahmoud, K. R. M., *Theoretical and Experimental Investigations on New Adaptive Duo Servo Drum Brake with High and Constant Brake Shoe Factor*, Dr.-Ing Dissertation, Universität Paderborn, 2005.
18. Limfert, R., *Brake Design and Safety*, Society of Automotive Engineering, Warrendale, 1999.
19. Talib, R. J., *Penelitian Morfologi Haus Permukaan Serta Pukul Bahan Geseran Automotif*, PhD Thesis, Universiti Kebangsaan Malaysia, 2001.
20. Talib, R. J., Friction material test procedure, *Brake Pad & Disc Materials*, UPENA UiTM, Shah Alam, 2007.
21. Sutantra, I. N., *Teknologi Otomotif; Teori dan Aplikasinya*, Surabaya, 2001.
22. Anderson, A. E., Friction and wear of automotive brakes, *ASM Handbook Vol. 18; Friction, Lubrication, and Wear Technology*, ASM International, 1998.
23. Chan, D., and G.W. Stachowiak. Review of automotive brake friction materials, *Proc. Institution Mech. Engineers Vol. 218 part D: Journal of Automobile Engineering*, 2004, 953-966.
24. Gardziella, A., L. A. Pilato, and A. Knop, *Phenolic Resins; Chemistry, Applications, Standardization, Safety and Ecology*, Springer-Verlag, Berlin, 2000.
25. Watson, C. and T. Millshap, *Friction Material; From Prototype to Production*, SAE technical paper no.1999-01-3389, Society of Automotive Engineers, 1999.

26. Nicholson, G., *Facts about friction; 100 years of brake lining and clutch facings*, P&W Enterprises Inc., Croydon, 1995.
27. Blau, P. J., *Composition, Function, and Testing of Friction Brake Materials and Their Additives*, Oak Ridge National Laboratory, Tennessee, 2001.
28. Selamat, M. S., Overview on friction materials, *Brake Friction Materials*, UPENA UiTM, Shah Alam, 2006.
29. Anderson, A.E., Brake system performance; effects of fiber types and concentration, *Proceeding of Fibers in Friction Materials Symposium*, The Asbestos Institute, 2–49 , 1987.
30. Kim, S.J. and H. Jang, Friction characteristics of non-asbestos organic (NAO) and low-steel materials: the comparative study, *KSTLE International Journal*, 2000, Vol. 1 No. 1, 1–7.
31. Liu, T. and S. K. Rhee, High temperature wear of semi metallic disk brake pads, *Wear*, 1978, 46, 213–218.
32. Jacko, M. G., P. H. S. Tsang, and S. K. Rhee, Automotive friction materials evaluation during the past decade, *Wear*, 1984, 100, 503–515.
33. Kim, S. J. and H. Jang, Friction and wear of friction material containing two different phenolic resins reinforced with aramid pulp, *Tribology International* 2000, 33, 477–484.
34. Kim, S.J., M.H. Cho, D.S. Lim, H. Jang, Synergetic effects of aramid pulp and potassium titanate whiskers in the automotive friction material, *Wear*, 2001, 251, 1484–1491.
35. Gudman-Høyer, L., A. Bach, G. T. Nielsen, and P. Morgen, Tribological properties of automotive disc brakes with solid lubricants, *Wear*, 1999, 232, 168–175.
36. Lu, Y., A combinational approach for automotive friction materials: Effects of ingredients on friction performance, *Composites Science and Technology*, 2006, 66, 591 –598.
37. Rhee, S. K., Wear mechanism for asbestos-reinforced automotive friction materials, *Wear*, 1974, 29, 391–393.
38. Rhee, S. K., High temperature wear of asbestos reinforced friction materials, *Wear*, 1976, 37, 291–197.

39. Jang, H., K. Ko, S. J. Kim, R. H. Basch, and J. W. Fash, The effect of metal fibers on the friction performance of automotive brake friction materials, *Wear*, 2004, 256, 406–414.
40. Bijwe, J. and M. Kumar, Optimization of steel wool contents in non-asbestos organic (NAO) friction composites for best combination of thermal conductivity and tribo-performance, *Wear*, 2007, 263, 1234–1248.
41. Cho, M. H., S. J. Kim, D. Kim, and H. Jang, Effects of ingredients on tribological characteristics of a brake lining: an experimental case study. *Wear*, 2005, 258, 1682–1687.
42. Shibata, K., A. Goto, S. Yoshida, Y. Azuma, and K. Nakamura, *Development of Brake Friction Material*, SAE technical paper no. 930806, Society of Automotive Engineers, 1993.
43. Cho, M. H., E. G. Bae, H. Jang, G. Jeong, D. Kim, and C. Choi, *The role of raw material ingredients of brake linings on the formation of transfer film and friction characteristics*, SAE technical paper no. 2001-01-3130, Society of Automotive Engineers, 2001.
44. Oestermeyer, G. P., On the dynamics of friction coefficient, *Wear*, 2003, 254, 852–858.
45. Boz, M. and A. Kurt, The effect of Al_2O_3 on the friction performance of automotive brake friction materials, *Tribology International*, 2007, 1167–1169.
46. Lu, Y., A combinatorial approach for automotive friction materials: combined effects of ingredients on friction performance, *Polymer Composites*, 2002, 23(5), 814–823.
47. Österle, W., A. Dimitrev, I. Urban, Characterization of up to date brake friction materials, *Proceedings of the International Workshop on Advances in Asbestos-free Friction Composites*, Indian Institute of Technology, 2006, 21–35.
48. Cho, M. H., K. H. Cho, S. J. Kim, D. Kim, and H. Jang, The role of transfer layers on friction characteristics in the sliding interface between friction materials against gray cast iron brake disc, *Tribology Letters*, 2005, 20(2), 101–108.

49. Jacko, M. G., P. H. S. Tsang, and S. K. Rhee, Wear debris compaction and friction film formation of polymer composites, *Wear*, 1989, 133, 23–38.
50. Oesterle, W, I Urban, Friction layer and friction films on PMC brake pads, *Wear*, 2005, 257, 215 – 226.
51. Godet, M., The third body approach: a mechanical view of wear, *Wear*, 1984, 100, 437–452.
52. Österle, W. and I. Urban, Third body formation on brake pads and rotors, *Tribology International*, 2006, 39, 401 – 408.
53. Österle, W., H. Kloß, I. Urban, and A. I. Dmitriev, Towards better understanding of brake friction material, *Wear*, 2007, 263, 1189 – 1201.
54. Eriksson, M., F. Bergman, and S. Jacobson., Surface characterization of brake pad after running under silent and squealing condition, *Wear*, 1999, 232, 163–167.
55. Eriksson, M. and S. Jacobson, Tribological surface of organic brake pad, *Tribology International*, 2000, 33, 817–827.
56. Eriksson, M., *Friction and contact phenomena of disc brakes related to squeal*, PhD Dissertation, ACTA Universitatis Upsaliensis, Uppsala, 2000.
57. Hammerström, L., *Mechanism and Phenomena in Braking and Gripping*, PhD Dissertation, ACTA Universitatis Upsaliensis, Uppsala, 2006.
58. Östermeyer, G. P., Friction and wear of brake system, *Forschung im Ingenieurwesen*, 2001, 66, 267–272.
59. Östermeyer, G. P., and M. Müller, Dynamic interaction of friction and surface topography in brake system, *Tribology International*, 2006, 39, 370–380.
60. Rigney, D. A., and J. P. Hirth, Plastic deformation and sliding friction of metals, *Wear*, 1979, 53, 345 – 370.
61. Rhee, S. K., Wear equation for polymers sliding against metal surfaces, *Wear* 1970, 16, 431 – 435.
62. Rhee, S. K., Wear mechanism at low temperature for metal-reinforced phenolic resins, *Wear*, 1973, 23, 261 – 265.
63. Rhee, S. K., Wear of metal-reinforced phenolic resin, *Wear*, 1971, 18, 471 – 477.

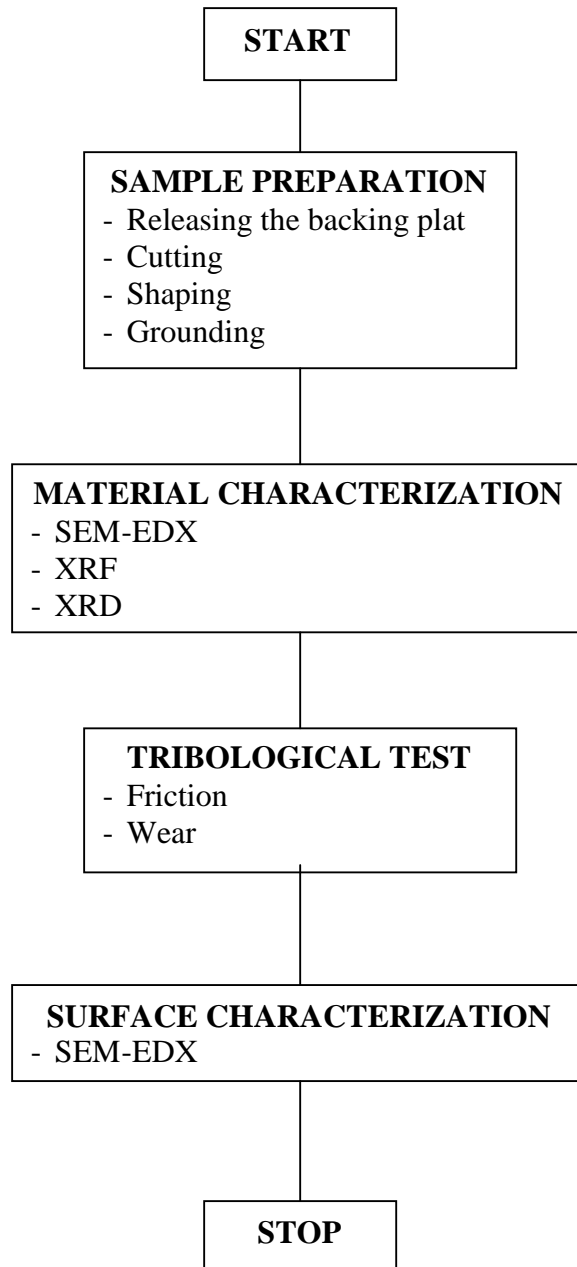
64. Egglestone, D., Automotive Friction Material, *EURAC Technical Bulletin 00010433*, 2000.
65. Kato, K., and K. Adachi, Wear Mechanism, *Modern Tribology Handbook vol. 1: Principles of Tribology*, CRC Press, New York, 2001.
66. David, N.V, M. N. Berhan, and Darius G. S., Thermal characteristics of novel brake friction material for light rail transit application, *Brake Friction Materials*, UPENA UiTM, Shah Alam, 2006.
67. Jacko, M. G., Physical and chemical changes of organic disc pads in service, *Wear*, 1978, 46, 163–175.
68. Talib, R.J. and C. H. Azhari, Wear mechanism of semi-metallic friction materials, *Advances in materials processing vol.1*, Institute of Materials, Malaysia, 2003.
69. Tanaka, K., S. Ueda, and N. Noguchi, Fundamental studies on the brake friction of resin-based friction materials, *Wear*, 1973, 23, 349–365.
70. Blau, P. J., and J. C. McLaughlin, Effects of water films and sliding speed on the frictional behavior of truck disc brake materials. *Tribology International*, 2003, 36, 709–715.
71. Satapathy, B. K., and J. Bijwe, Wear data analysis of friction materials to investigate the simultaneous influence of operating parameters and compositions, *Wear*, 2004, 256, 797–804.
72. Eriksson, M., A. Lundqvist, and S. Jacobson, A study of the influence of humidity on the friction and squeal generation of automotive brake pads, *Proceedings of the Institution of Mechanical Engineers*, 2001, 215(3), 329–334.
73. Kim, S. J., J. Y. Lee, and H. Jang, Effect of humidity on friction characteristics of automotive friction materials, *KSTLE International Journal*, 2001, 2(2), 150–153.
74. Czichos, H., Design of Friction and Wear Experiments, *ASM Handbook Vol. 18; Friction, Lubrication, and Wear Technology*, ASM International, 1998.
75. Lab report XRD S8, *Quantitative Analysis of Geological Sample: Combined XRD-XRF analysis*, Bruker Advanced X-Ray Solution, 2006.

76. Adam H., Akramin M.Z., Berhan M.N, and Darius G.S, The XRD analysis of brake friction material formulations, *Brake Pad & Disc Materials*, UPENA UiTM, Shah Alam, 2007.
77. Kato, H., *Sliding Wear of Nitrided Steels*, PhD thesis, Department of Materials Technology, Brunel University, 1993.
78. Karaveli, K., *Tribological Properties of a Tightly Woven Carbon/Carbon Composite*, MSc thesis, Middle East Technical University, Turkey, 2005.
79. Mosleh, M., P. J. Blau, and D. Dumitrescu, Characteristics and morphology of wear particles from laboratory testing of disk brake materials, *Wear*, 2004, 256, 1128–1134.
80. Elliott, D. M., J. Fisher, and D. T. Clark, Effect of counterface surface roughness and its evolution on the wear and friction of PEEK and PEEK-bonded carbon fibre composite on stainless steel, *Wear*, 1998, 217, 288–296.
81. Prasad, K.V.R., M.V. Shankar, G.N. Subbanna, and K.B.R. Varma, Principles of scanning electron microscope (SEM) for structural characterization, *Handbook of Advanced Material Testing: Material Engineering vol. 9*, Marcell-Dekker, New York, 1995.
82. Saleh, M.H., Z. Meh, and R.J. Talib, Characterization of brake pad materials by scanning electron microscope, *Brake Pad & Disc Materials*, UPENA UiTM, Shah Alam, 2007.
83. Selamat, M. S., M. A. Selamat, M. Mustapha, Y. M. Junus, M. I. Ishak, and B. Meh, Development of friction materials for light rail transit, *Brake Friction Materials*, UPENA UiTM, Shah Alam, 2006.
84. Österle, W, M. Griepentrog, Th. Gross, and I. Urban, Chemical and microstructural changes induced by friction and wear of brakes, *Wear*, 2001, 251, 1469-1476.
85. Berhan, M.N., Darius G.S., David N.V., Adam H., and Akramin M.Z., Thermal analysis of brake pad material formulation, *Brake Pad & Disc Materials*, UPENA UiTM, Shah Alam, 2007.
86. Roslani, N., Eliasidi A. O, and R. J. Talib, TGA of brake friction materials before and after road performance test, *Brake Pad & Disc Materials*, UPENA UiTM, Shah Alam, 2007.

87. Berhan, M. N., Darius G. S., David N.V, S. A. Abdullah, M. Z. Bahrom, and Z. Mohamad, *TG/DTG Analysis of Different Formulation of Brake Friction Materials*, 2nd Malaysian Brake Friction Materials Colloquium, UiTM, 2004.
88. Blau, P. J., *Friction Science and Technology*, Marcell Dekker, Inc. New York 1996.
89. Czichos, Horst, Presentation of friction and wear data, *ASM Handbook Vol. 18; Friction, Lubrication, and Wear Technology*, ASM International, 1998.
90. Blau, P. J., Interpretation of the friction and wear break-in behavior of metals in sliding contact, *Wear*, 1981, 71, 29-43.
91. Bowden, F.P, Introduction to the Discussion: The Mechanism of Friction, *Proceedings of the Royal Society of London. Series A, Mathematical and Physical Sciences*, 1952, 212 (1111), 440-449.
92. Holinski, R., Fundamental of dry friction and some practical examples, *Industrial Lubrication and Tribology*, 2001, 53 (2), 61–65.
93. Hee, K.W. and P. Filip, Performance of ceramic enhanced phenolic matrix brake lining materials for automotive brake linings, *Wear*, 2005, 259, 1088 – 1095.
94. Mutlu, I, O. Eldogan, and F. Findik, Tribological properties of some phenolic composites suggested for automotive brakes, *Tribology International*, 2005, 39, 317 – 325.
95. Starczewski, L., J. Szumniak, Mechanism of transferring matter in a friction process in a tribology system: polymeric composite-metal, *Surface and Coating Technology*, 1998, 100-101, 33–37.
96. Kim, S.J. M.H. Cho, R. H. Basch, J. W. Fash, and H. Jang, Tribological properties of polymer composites containing barite (BaSO_4) or potassium titanate ($\text{K}_2\text{O} \cdot 6(\text{TiO}_2)$), *Tribology Letters*, 2004, 7(3).
97. Archard, J.F, Contact and Rubbing of Flat Surface, *Journal of Applied Physics*, 1953, 24 (8), 981-988.
98. Burwell, J.T. and C.D. Strang, On the Empirical Law of Adhesive Wear, *Journal of Applied Physics*, 1953, 23(1), 18-28.
99. Jacko, M.G., P. H. S. Tsang, S. K. Rhee, Wear debris compaction and friction film formation of polymer composites, *Wear*, 1989, 133 (1), 23 -38.

100. Scieszka, S. F., Tribological phenomena in steel composite brake material friction pairs, *Wear*, 1980, 64, 367-378.
101. Schallamach, A., A theory of dynamic rubber friction, *Wear*, 1963, 6, 375.
102. Ludema, K.C., Friction, *Modern Tribology Handbook vol.1*, CRC Press, New York, 2001.
103. Godfrey, D., Diagnosis of Wear Mechanisms, *Wear Control Handbook*, American Society of Mechanical Engineers, 1980.
104. Patel, S. H., Surface Property Modifiers, *Functional Fillers for Plastics*, Edited by M. Xanthos, Wiley.VCH Verlag GmbH & Co. KGaA, Weinheim, German, 2005.
105. Junus, M. Y., M. I. Ishak, M. S. Selamat, Correlation between physical properties with friction and behavior of LRT brake pad, *Brake Friction Materials*, UPENA UiTM, Shah Alam, 2006.
106. Talib, R. J, M. S. Shaari, W. M. A. W. Ibrahim, S. Kemin, and R. Kasiran, Properties enhancement of indigenously developed brake pad for light rail transit, *Brake Friction Materials*, UPENA UiTM, Shah Alam, 2006.
107. Othman, E. A., W. M. A. W. Ibrahim, R. J. Talib, Correlation of friction and wear with hardness properties of friction material, *Brake Friction Materials*, UPENA UiTM, Shah Alam, 2006.
108. Rigney, D. A., L. H. Chen, and M.G. S. Taylor, Wear process in sliding system, *Wear*, 1984, 100, 195–219.
109. Gomes, J.R., O. M. Silva, C. M. Silva, L. C. Pardini, R. F. Silva, The effect of sliding speed and temperature on the tribological behavior of carbon–carbon composites, *Wear*, 2001, 249, 240 – 245.
110. Anderson, A.E., Wear of Brake Materials, *Wear Control Handbook*, The American Society of Mechanical Engineers, New York, 1980

APPENDIX A
EXPERIMENTAL FLOW CHART



APPENDIX B

ASTM G-99

Designation: G 99 – 95a (Reapproved 2000)*¹

Standard Test Method for Wear Testing with a Pin-on-Disk Apparatus¹

This standard is issued under the fixed designation G 99; the number immediately following the designation indicates the year of original adoption or, in the case of revision, the year of last revision. A number in parentheses indicates the year of last reapproval. A superscript epsilon (ϵ) indicates an editorial change since the last revision or reapproval.

*¹ Note—Editorial corrections were made throughout in May 2000.

1. Scope

1.1 This test method describes a laboratory procedure for determining the wear of materials during sliding using a pin-on-disk apparatus. Materials are tested in pairs under nominally non-abrasive conditions. The principal areas of experimental attention in using this type of apparatus to measure wear are described. The coefficient of friction may also be determined.

1.2 The values stated in SI units are to be regarded as standard.

1.3 *This standard does not purport to address all of the safety concerns, if any, associated with its use. It is the responsibility of the user of this standard to establish appropriate safety and health practices and determine the applicability of regulatory limitations prior to use.*

2. Referenced Documents

2.1 ASTM Standards:

E 122 Practice for Choice of Sample Size to Estimate a Measure of Quality for a Lot or Process²

E 177 Practice for Use of the Terms Precision and Bias in ASTM Test Methods²

E 178 Practice for Dealing with Outlying Observations²

G 40 Terminology Relating to Wear and Erosion³

2.2 *Other Standard:*⁴

DIN-50324 Testing of Friction and Wear

3. Summary of Test Method

3.1 For the pin-on-disk wear test, two specimens are required. One, a pin with a radiused tip, is positioned perpendicular to the other, usually a flat circular disk. A ball, rigidly held, is often used as the pin specimen. The test machine causes either the disk specimen or the pin specimen to revolve about the disk center. In either case, the sliding path is a circle on the disk surface. The plane of the disk may be oriented

either horizontally or vertically.

NOTE 1—Wear results may differ for different orientations.

3.1.1 The pin specimen is pressed against the disk at a specified load usually by means of an arm or lever and attached weights. Other loading methods have been used, such as, hydraulic or pneumatic.

NOTE 2—Wear results may differ for different loading methods.

3.2 Wear results are reported as volume loss in cubic millimetres for the pin and the disk separately. When two different materials are tested, it is recommended that each material be tested in both the pin and disk positions.

3.3 The amount of wear is determined by measuring appropriate linear dimensions of both specimens before and after the test, or by weighing both specimens before and after the test. If linear measures of wear are used, the length change or shape change of the pin, and the depth or shape change of the disk wear track (in millimetres) are determined by any suitable metrological technique, such as electronic distance gaging or stylus profiling. Linear measures of wear are converted to wear volume (in cubic millimetres) by using appropriate geometric relations. Linear measures of wear are used frequently in practice since mass loss is often too small to measure precisely. If loss of mass is measured, the mass loss value is converted to volume loss (in cubic millimetres) using an appropriate value for the specimen density.

3.4 Wear results are usually obtained by conducting a test for a selected sliding distance and for selected values of load and speed. One set of test conditions that was used in an interlaboratory measurement series is given in Table 1 and Table 2 as a guide. Other test conditions may be selected depending on the purpose of the test.

3.5 Wear results may in some cases be reported as plots of wear volume versus sliding distance using different specimens for different distances. Such plots may display non-linear relationships between wear volume and distance over certain portions of the total sliding distance, and linear relationships over other portions. Causes for such differing relationships include initial "break-in" processes, transitions between regions of different dominant wear mechanisms, etc. The extent of such non-linear periods depends on the details of the test system, materials, and test conditions.

3.6 It is not recommended that continuous wear depth data

¹ This test method is under the jurisdiction of ASTM Committee G02 on Wear and Erosion and is the direct responsibility of Subcommittee G02.40 on Non-Abrasive Wear.

Current edition approved Nov. 10, 1995. Published January 1996. Originally published as G 99-90. Last previous edition G 99-95.

² *Annual Book of ASTM Standards*, Vol 14.02.

³ *Annual Book of ASTM Standards*, Vol 03.02.

⁴ Available from Bouth Verlag GmbH, Burggrafenstrasse 6, 1000 Berlin 30, Germany.

APPENDIX B

ASTM G-99 (CONTINUE)

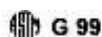


TABLE 1 Characteristics of the Interlaboratory Wear Test Specimens

Note 1—See Note 4 in 10.4 for information.

	Composition (weight%)	Microstructure	Hardness (HV 10)	Roughness ^a	
				R_a (mean) (μm)	R_a (mean) (μm)
Steel ball (100 Cr6) (AISI 52 100) ^b Diameter 10 mm	1.35 to 1.65 Cr ← 0.95 to 1.10 C 0.15 to 0.35 Si 0.25 to 0.45 Mn	martensitic with minor carbides and austenite	838 ± 21	0.100	0.010
Steel disc (100 Cr6) (AISI 52 100) ^c Diameter 40 mm	← <0.030 P ← <0.030 S	martensitic with minor carbides and austenite	852 ± 14	0.052	0.113 ^d
Alumina ball, diameter = 10 mm ^d	← 95 % Al ₂ O ₃ (with addi- tives of TiO ₂ MgO and ZnO)	equi-granular alpha alumina with very minor secondary phases	1610 ± 101 (HV 0.2)	1.365	0.123
Alumina disc, diameter = 40.6 mm ^d	←		1569 ± 144 (HV 0.2)	0.868	0.041

^a Measured by stylus profilometry. R_z is maximum peak-to-valley roughness. R_a is arithmetic average roughness.

^b Standard ball-bearing balls (SKF).

^c Standard spacers for thrust bearings (INA).

^d Manufactured by Compagnie Industrielle des Ceramiques Electroniques, France.

TABLE 2 Results of the Interlaboratory Tests^a

Note 1—See Note 4 in 10.4.

Note 2—Numbers in parentheses refer to all data received in the tests. In accordance with Practice E 178, outlier data values were identified in some cases and discarded, resulting in the numbers without parentheses. The differences are seen to be small.

Note 3—Values preceded by ± are one standard deviation.

Note 4—Between eleven and twenty laboratories provided these data.

Note 5—Calculated quantities (for example, wear volume) are given as mean values only.

Note 6—Values labeled “NM” were found to be smaller than the reproducible limit of measurement.

Note 7—A similar compilation of test data is given in DIN-50324.

Results (ball) (disk)	Specimen Pairs			
	Steel-steel	Alumina-steel	Steel-alumina	Alumina-alumina
Ball wear scar diameter (mm)	2.11 ± 0.27 (2.11 ± 0.27)	NM	2.08 ± 0.35 (2.03 ± 0.41)	0.3 ± 0.06 (0.3 ± 0.06)
Ball wear volume (10 ⁻³ mm ³)	198 (198)	—	196 (109)	0.08 (0.08)
Number of values	102 (102)	—	60 (64)	56 (59)
Disk wear scar width (mm)	NM	0.64 ± 0.12 (0.64 ± 0.12)	NM	NM
Disk wear volume (10 ⁻³ mm ³)	—	480 (490)	—	—
Number of values	—	60 (60)	—	—
Friction coefficient	0.60 ± 0.11	0.76 ± 0.14	0.60 ± 0.12	0.41 ± 0.08
Number of values	109	75	64	76

^a Test conditions: $F = 10 \text{ N}$; $v = 0.1 \text{ ms}^{-1}$; $T = 23 \text{ }^\circ\text{C}$; relative humidity range 12 to 76 %; laboratory air; sliding distance 1000 m; wear track (nominal) diameter = 32 mm; materials: steel = AISI 52 100; and alumina = $\alpha\text{-Al}_2\text{O}_3$.

obtained from position-sensing gages be used because of the complicated effects of wear debris and transfer films present in the contact gap, and interferences from thermal expansion or contraction.

4. Significance and Use

4.1 The amount of wear in any system will, in general, depend upon the number of system factors such as the applied load, machine characteristics, sliding speed, sliding distance, the environment, and the material properties. The value of any wear test method lies in predicting the relative ranking of material combinations. Since the pin-on-disk test method does not attempt to duplicate all the conditions that may be experienced in service (for example; lubrication, load, pressure, contact geometry, removal of wear debris, and presence of corrosive environment), there is no assurance that the test will predict the wear rate of a given material under conditions differing from those in the test.

5. Apparatus

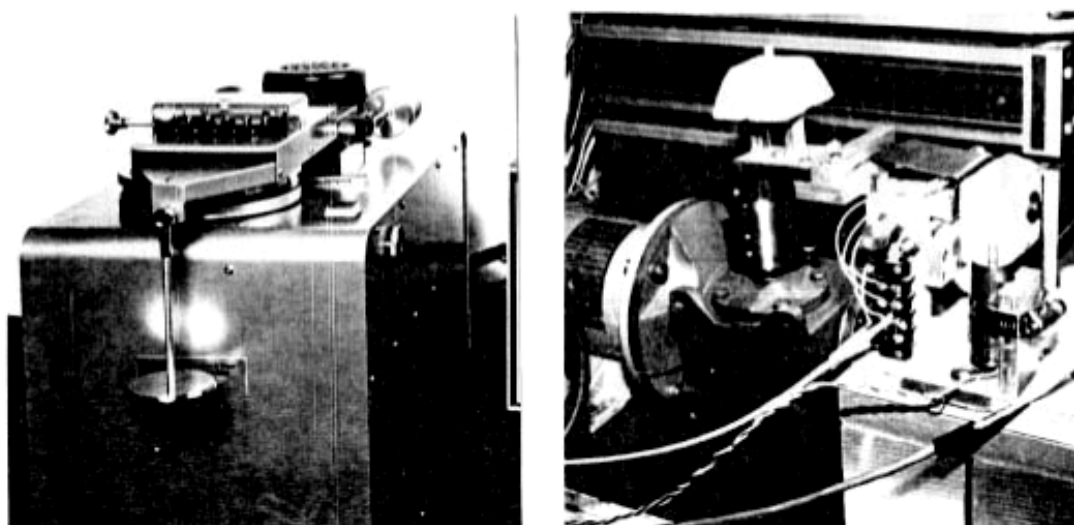
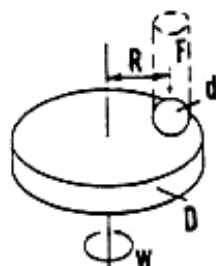
5.1 *General Description*—Fig. 1 shows a schematic drawing of a typical pin-on-disk wear test system, and photographs of two differently designed apparatuses.⁵ One type of typical system consists of a driven spindle and chuck for holding the revolving disk, a lever-arm device to hold the pin, and attachments to allow the pin specimen to be forced against the revolving disk specimen with a controlled load. Another type of system loads a pin revolving about the disk center against a stationary disk. In any case the wear track on the disk is a

⁵ A number of other reported designs for pin-on-disk systems are given in “A Catalog of Friction and Wear Devices,” American Society of Lubrication Engineers (1973). The sole source of supply of commercially built machines known to the committee at this time is Falex Corp., 1020 Airpark Dr., Sugar Grove, IL 60554. If you are aware of alternative suppliers, please provide this information to ASTM Headquarters. Your comments will receive careful consideration at a meeting of the responsible technical committee, ¹ which you may attend.

APPENDIX B

ASTM G-99 (CONTINUE)

G 99



Note: 1— F is the normal force on the pin, d is the pin or ball diameter, D is the disk diameter, R is the wear track radius, and w is the rotation velocity of the disk.

FIG. 1 (a) Schematic of pin-on-disk wear test system. (b) Photographs of two different designs.

circle, involving multiple wear passes on the same track. The system may have a friction force measuring system, for example, a load cell, that allows the coefficient of friction to be determined.

5.2 Motor Drive—A variable speed motor, capable of maintaining constant speed ($\pm 1\%$ of rated full load motor speed) under load is required. The motor should be mounted in such a manner that its vibration does not affect the test. Rotating speeds are typically in the range 0.3 to 3 rad/s (60 to 600 r/min).

5.3 Revolution Counter—The machine shall be equipped with a revolution counter or its equivalent that will record the number of disk revolutions, and preferably have the ability to shut off the machine after a pre-selected number of revolutions.

5.4 Pin Specimen Holder and Lever Arm—In one typical system, the stationary specimen holder is attached to a lever arm that has a pivot. Adding weights, as one option of loading, produces a test force proportional to the mass of the weights applied. Ideally, the pivot of the arm should be located in the plane of the wearing contact to avoid extraneous loading forces

due to the sliding friction. The pin holder and arm must be of substantial construction to reduce vibrational motion during the test.

5.5 Wear Measuring Systems—Instruments to obtain linear measures of wear should have a sensitivity of 2.5 μm or better. Any balance used to measure the mass loss of the test specimen shall have a sensitivity of 0.1 mg or better; in low wear situations greater sensitivity may be needed.

6. Test Specimens and Sample Preparation

6.1 Materials—This test method may be applied to a variety of materials. The only requirement is that specimens having the specified dimensions can be prepared and that they will withstand the stresses imposed during the test without failure or excessive flexure. The materials being tested shall be described by dimensions, surface finish, material type, form, composition, microstructure, processing treatments, and indentation hardness (if appropriate).

6.2 Test Specimens—The typical pin specimen is cylindrical or spherical in shape. Typical cylindrical or spherical pin

APPENDIX B

ASTM G-99 (CONTINUE)



specimen diameters range from 2 to 10 mm. The typical disk specimen diameters range from 30 to 100 mm and have a thickness in the range of 2 to 10 mm. Specimen dimensions used in an interlaboratory test with pin-on-disk systems are given in Table 1.

6.3 *Surface Finish*—A ground surface roughness of 0.8 μm (32 $\mu\text{in.}$) arithmetic average or less is usually recommended.

NOTE 3—Rough surfaces make wear scar measurement difficult.

6.3.1 Care must be taken in surface preparation to avoid subsurface damage that alters the material significantly. Special surface preparation may be appropriate for some test programs. State the type of surface and surface preparation in the report.

7. Test Parameters

7.1 *Load*—Values of the force in Newtons at the wearing contact.

7.2 *Speed*—The relative sliding speed between the contacting surfaces in metres per second.

7.3 *Distance*—The accumulated sliding distance in meters.

7.4 *Temperature*—The temperature of one or both specimens at locations close to the wearing contact.

7.5 *Atmosphere*—The atmosphere (laboratory air, relative humidity, argon, lubricant, etc.) surrounding the wearing contact.

8. Procedure

8.1 Immediately prior to testing, and prior to measuring or weighing, clean and dry the specimens. Take care to remove all dirt and foreign matter from the specimens. Use non-chlorinated, non-film-forming cleaning agents and solvents. Dry materials with open grains to remove all traces of the cleaning fluids that may be entrapped in the material. Steel (ferromagnetic) specimens having residual magnetism should be demagnetized. Report the methods used for cleaning.

8.2 Measure appropriate specimen dimensions to the nearest 2.5 μm or weigh the specimens to the nearest 0.0001 g.

8.3 Insert the disk securely in the holding device so that the disk is fixed perpendicular ($\pm 1^\circ$) to the axis of the resolution.

8.4 Insert the pin specimen securely in its holder and, if necessary, adjust so that the specimen is perpendicular ($\pm 1^\circ$) to the disk surface when in contact, in order to maintain the necessary contact conditions.

8.5 Add the proper mass to the system lever or bale to develop the selected force pressing the pin against the disk.

8.6 Start the motor and adjust the speed to the desired value while holding the pin specimen out of contact with the disk. Stop the motor.

8.7 Set the revolution counter (or equivalent) to the desired number of revolutions.

8.8 Begin the test with the specimens in contact under load. The test is stopped when the desired number of revolutions is achieved. Tests should not be interrupted or restarted.

8.9 Remove the specimens and clean off any loose wear debris. Note the existence of features on or near the wear scar such as: protrusions, displaced metal, discoloration, microcracking, or spotting.

8.10 Remeasure the specimen dimensions to the nearest 2.5 μm or reweigh the specimens to the nearest 0.0001 g, as appropriate.

8.11 Repeat the test with additional specimens to obtain sufficient data for statistically significant results.

9. Calculation and Reporting

9.1 The wear measurements should be reported as the volume loss in cubic millimetres for the pin and disk, separately.

9.1.1 Use the following equations for calculating volume losses when the pin has initially a spherical end shape of radius R and the disk is initially flat, under the conditions that only one of the two members wears significantly:

$$\begin{aligned} \text{pin (spherical end) volume loss, mm}^3 & \quad (1) \\ &= \frac{\pi (\text{wear scar diameter, mm})^3}{64 (\text{sphere radius, mm})} \end{aligned}$$

assuming that there is *no significant disk wear*. This is an approximate geometric relation that is correct to 1 % for (wear scar diameter/sphere radius) < 0.3, and is correct to 5 % for (wear scar diameter/sphere radius) < 0.7. The exact equation is given in Appendix X1.

$$\begin{aligned} \text{disk volume loss, mm}^3 & \quad (2) \\ &= \frac{\pi (\text{wear track radius, mm}) (\text{track width, mm})^2}{6 (\text{sphere radius, mm})} \end{aligned}$$

assuming that there is *no significant pin wear*. This is an approximate geometric relation that is correct to 1 % for (wear track width/sphere radius) < 0.3, and is correct to 5 % for (wear track width/sphere radius) < 0.8. The exact equation is given in Appendix X1.

9.1.2 Calculation of wear volumes for pin shapes of other geometries use the appropriate geometric relations, recognizing that assumptions regarding wear of each member may be required to justify the assumed final geometry.

9.1.3 Wear scar measurements should be done at least at two representative locations on the pin surfaces and disk surfaces, and the final results averaged.

9.1.4 In situations where both the pin and the disk wear significantly, it will be necessary to measure the wear depth profile on both members. A suitable method uses stylus profiling. Profiling is the only approach to determine the exact final shape of the wear surfaces and thereby to calculate the volume of material lost due to wear. In the case of disk wear, the average wear track profile can be integrated to obtain the track cross-section area, and multiplied by the average track length to obtain disk wear volume. In the case of pin wear, the wear scar profile can be measured in two orthogonal directions, the profile results averaged, and used in a figure-of-revolution calculated for pin wear volume.

9.1.5 While mass loss results may be used internally in laboratories to compare materials of equivalent densities, this test method reports wear as volume loss so that there is no confusion caused by variations in density. Take care to use and report the best available density value for the materials tested when calculating volume loss from measured mass loss.

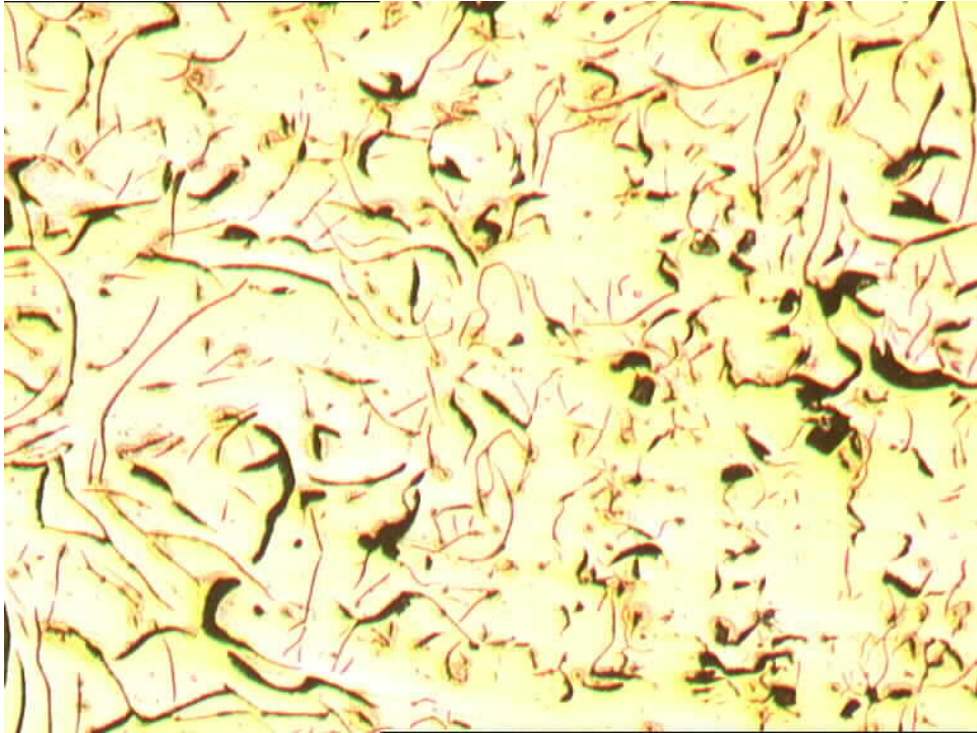
9.1.6 Use the following equation for conversion of mass loss to volume loss.

$$\text{volume loss, mm}^3 = \frac{\text{mass loss, g}}{\text{density, g/cm}^3} \times 1000. \quad (3)$$

APPENDIX C**PHYSICAL AND MECHANICAL PROPERTIES OF THE SAMPLES**

Sample	Hardness (HR _G)	Porosity (%)	Specific gravity	Surface roughness (μm)
Pad-1	68.2	12.9	3.29	2.173
Pad-2	97.0	7.86	2.76	2.837
Pad-3	67.3	9.82	2.64	2.397

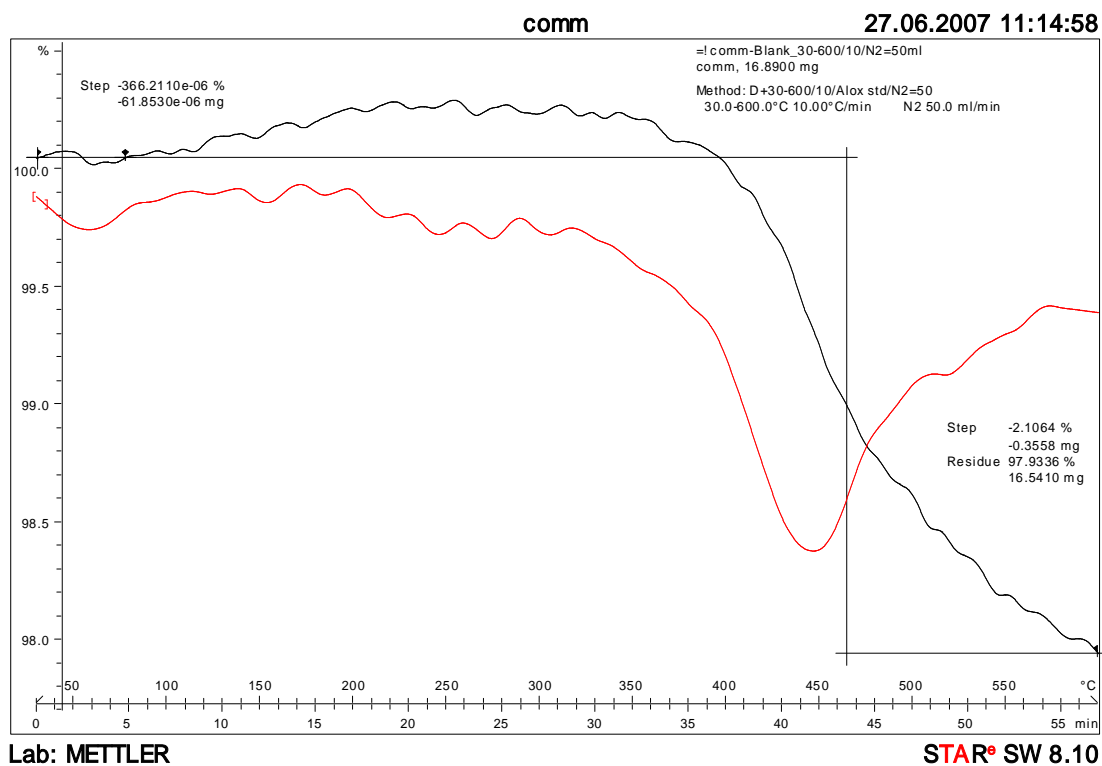
APPENDIX D
MICROSTRUCTURE OF THE GRAY CAST IRON PIN



Microstructure of gray cast iron pin

APPENDIX F

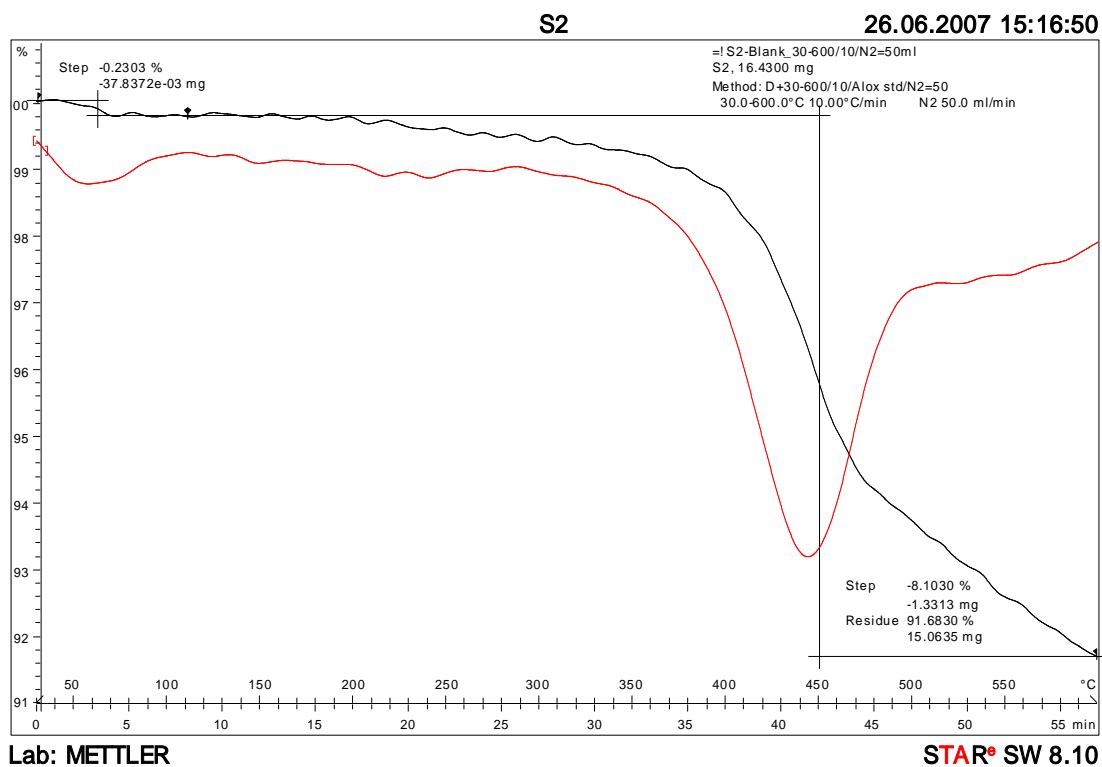
TGA RESULT OF THE SAMPLES, CONTINUED TO APPENDIX G



(a) TGA curve of Pad-1

APPENDIX G

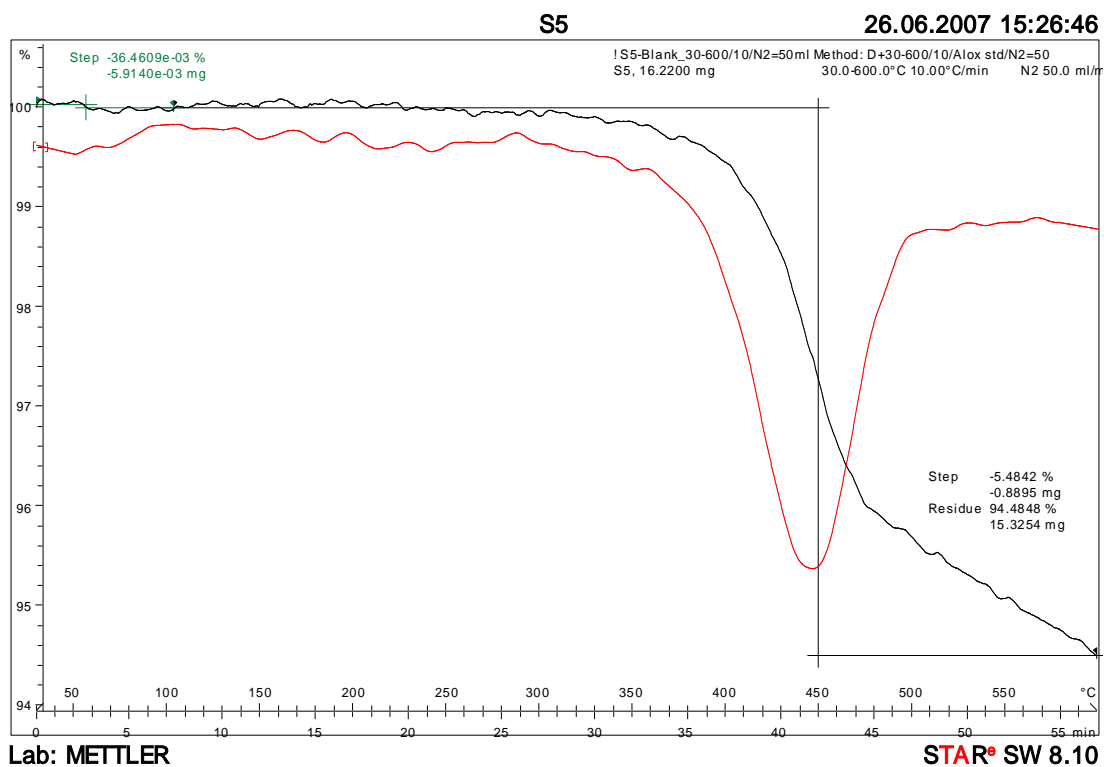
TGA RESULT OF THE SAMPLES, CONTINUED TO APPENDIX H



(b) TGA Curve of Pad-2

APPENDIX H

TGA RESULT OF THE SAMPLES, CONTINUED FROM APPENDIX G



(c) TGA Curve of Pad-3

APPENDIX I

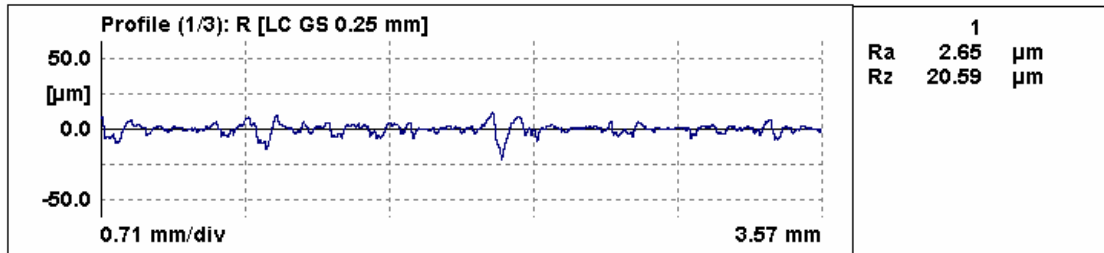
SUMMARY OF SAMPLE ELEMENTAL COMPOSITIONS DETECTED BY EDX/XRF/XRD TECHNIQUE

Pad - 1					Pad - 2					Pad - 3				
EDX		XRF		XRD	EDX		XRF		XRD	EDX		XRF		XRD
Element	% wt.	Compound	% wt.		Element	% wt.	Compound	% wt.		Element	% wt.	Compound	% wt.	
C K	62.75	-	-	carbon	C K	62.29	-	-	graphite	C K	59.35	-	-	carbon
O K	11.34	-	-	-	O K	16.08	-	-	-	O K	17.83	-	-	-
Mg K	1.23	MgO	0.423	-	Mg K	0.65	MgO	4.07	-	Mg K	0.58	MgO		-
Al K	0.32	Al ₂ O ₃	5.18	-	Al K	0.34	Al ₂ O ₃	2.09	-	Al K	0.96	Al ₂ O ₃	6.58	-
Si K	0.16	SiO ₂	5.15	quartz	Si K	0.84	SiO ₂	5.28	quartz	Si K	1.41	SiO ₂	9.31	quartz
S K	0.59	SO ₃	10.8	-	S K	0.6	SO ₃	6.3	-	S K	0.63	SO ₃	4.24	-
Fe K	20.77	Fe ₂ O ₃	65.8	hematite	Fe K	15.5	Fe ₂ O ₃	68.3	Hematite	Fe K	16	Fe ₂ O ₃	61	-
Ba L	2.83	BaO	4.12	barium sulphate	Ba L	3.14	BaO	9.81	barium sulphate	Ba L	2.39	BaO	7.38	-
		CuO	0.376	Brass			CuO			Cu L	0.43	CuO		copper thin sulphide
		ZnO	3.76	zinc sulphide			ZnO	3.76	-			ZnO	0.0275	-
		MnO	0.361	-			MnO	0.349	-			MnO	0.566	-
		CaO	1.64	-	Ca K	0.54	CaO	1.95	domolite, CaMg(CO ₃) ₂	Ca K	0.42	CaO	3.49	-
		Sb ₂ O ₃	0.92	antimony sulphide, Sb ₂ S ₃			Sb ₂ O ₃	-	-			Sb ₂ O ₃	-	-
		K ₂ O	0.436				K ₂ O	0.313				K ₂ O	0.266	
		Na ₂ O	0.431				Na ₂ O	0.381				Na ₂ O	0.352	
				Vermiculite, MgSi ₄ O ₁₀ (OH) ₂					vermiculite					vermiculite
				Wollastonite, CaSiO ₃					wollastonite					wollastonite

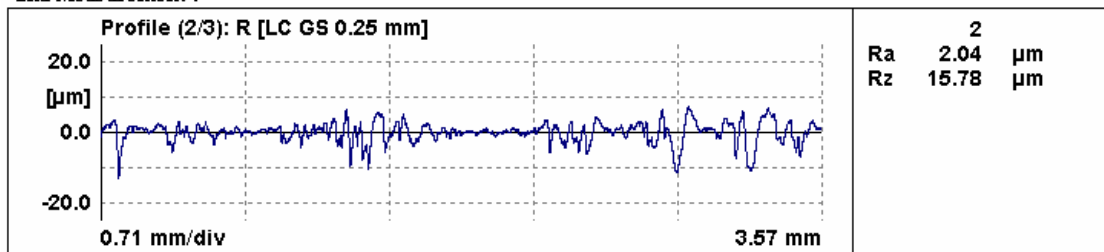
APPENDIX J

INITIAL SURFACE PROFILES OF THE SAMPLES, CONTINUED TO
APPENDIX K

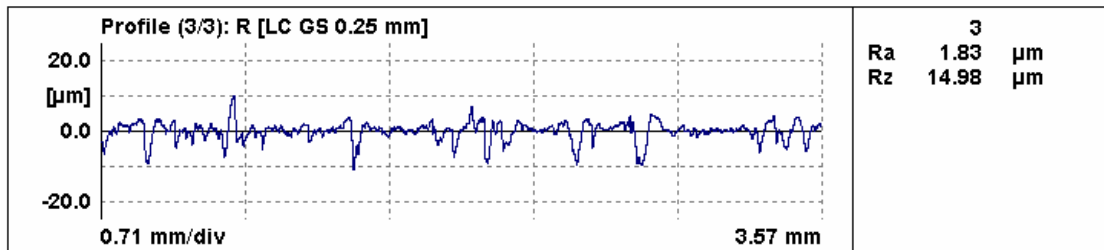
1st Measurement :



2nd Measurement :



3rd Measurement :

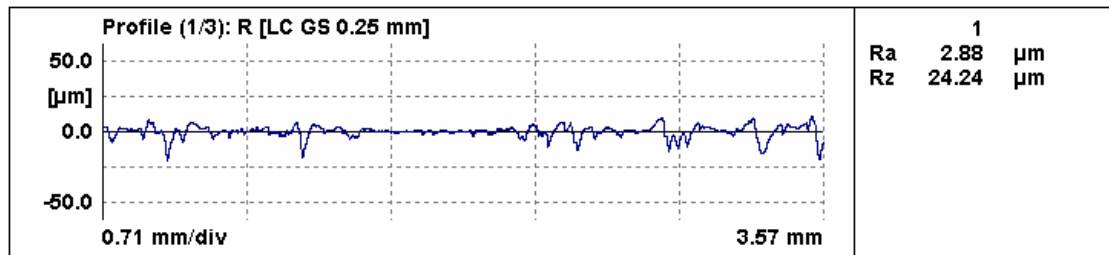


(a) Surface roughness of Pad-1

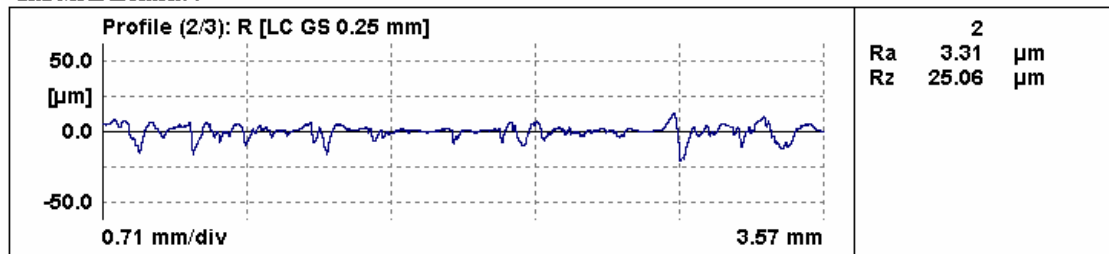
APPENDIX K

INITIAL SURFACE PROFILES OF THE SAMPLES, CONTINUED TO
APPENDIX L

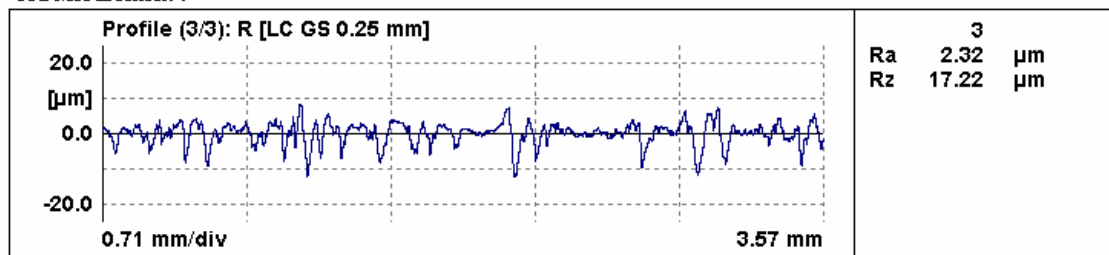
1st Measurement :



2nd Measurement :



3rd Measurement :

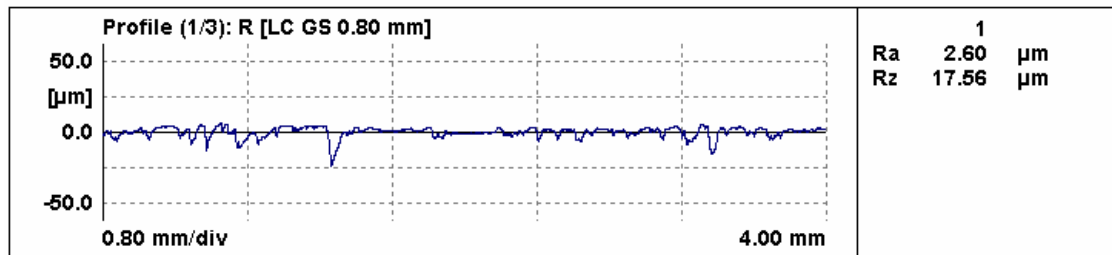


(b) Surface roughness of Pad-2

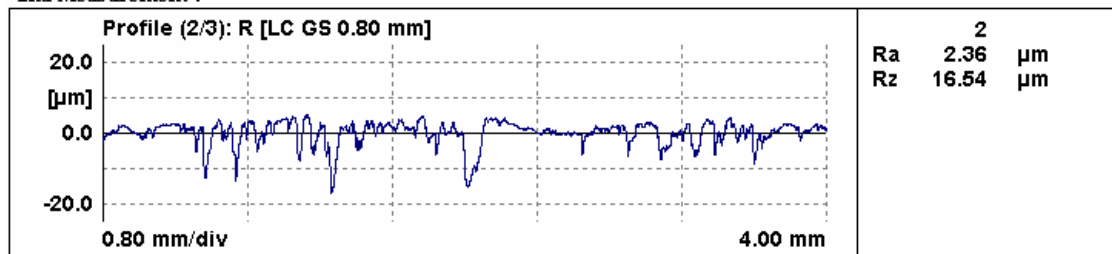
APPENDIX L

INITIAL SURFACE PROFILES OF THE SAMPLES, CONTINUED FROM
APPENDIX K

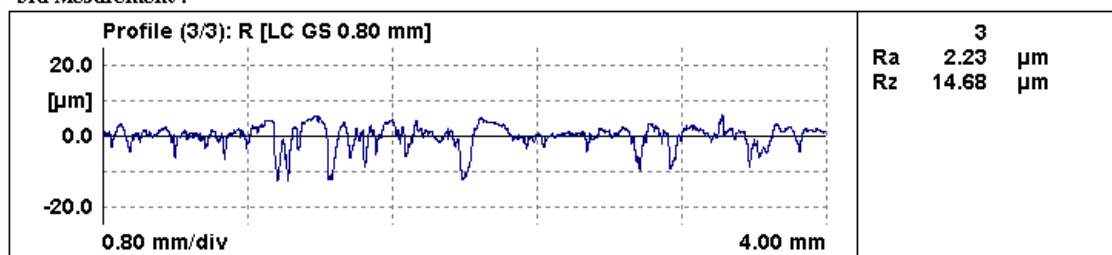
1st Measurement :



2nd Measurement :



3rd Measurement :



(c) Surface roughness of Pad-3

APPENDIX M

SURFACE ROUGHNESS OF THE SAMPLES BEFORE AND AFTER TEST

Load	Pad-1				Pad-2				Pad-3			
	1	2	3	average	1	2	3	average	1	2	3	average
Initial	2.65	2.04	1.83	2.173	2.88	3.31	2.32	2.837	2.6	2.36	2.23	2.397
1 MPa	0.99	1.54	1.15	1.227	1.85	0.89	1.6	1.447	1.73	0.43	1.41	1.19
1.5 MPa	1.25	1.67	0.95	1.29	1.84	1.67	0.62	1.377	2.27	2.14	1.04	1.817
2 MPa	1.58	1.56	1.64	1.593	1.27	0.93	1.11	1.103	1.53	1.93	1.91	1.79
2.5 MPa	0.93	0.81	1	0.913	1.52	0.97	1.69	1.393	0.65	0.41	0.48	0.513
3 MPa	0.4	0.63	0.92	0.65	2.14	1.18	3.38	2.233	0.74	0.53	0.93	0.733

Sliding Speed	Pad-1				Pad-2				Pad-3			
	1	2	3	average	1	2	3	average	1	2	3	average
Initial	2.65	2.04	1.83	2.173	2.88	3.31	2.32	2.837	2.6	2.36	2.23	2.397
300 rpm	1.07	1.34	1.06	1.157	1.45	0.99	0.65	1.030	2.02	0.67	0.56	1.083
600 rpm	0.99	1.54	1.15	1.227	1.85	0.89	1.6	1.447	1.73	0.43	1.41	1.190
900 rpm	1.87	1.92	0.96	1.583	1.46	1.94	1.43	1.610	1.03	2.45	1.86	1.780
1200 rpm	1.27	1.26	1.2	1.243	1.33	2.07	0.95	1.450	2.06	2.27	1.14	1.823
1500 rpm	1.81	1.09	2.18	1.693	1.97	0.77	1.21	1.317	2.85	2.66	3.38	2.963

